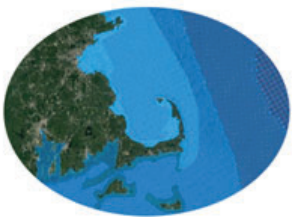

# Simulations of 2019 Hydrodynamics and Water Quality in the Massachusetts Bay System using the Bays Eutrophication Model

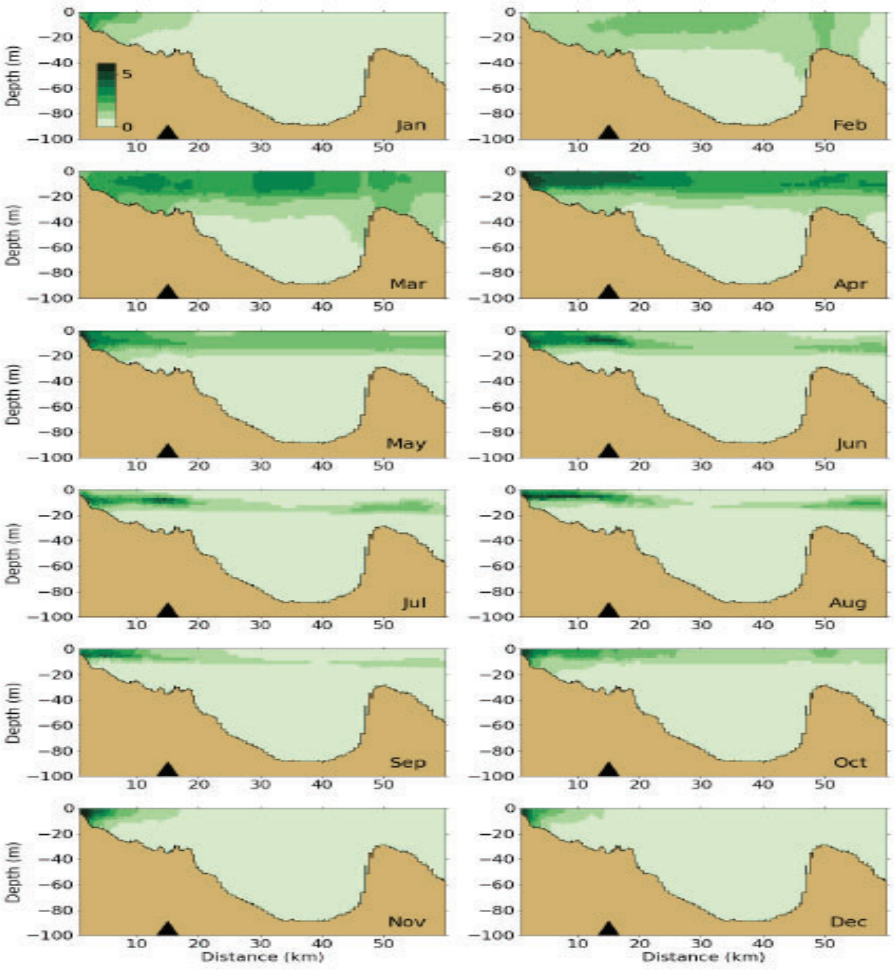


Massachusetts Water Resources Authority
Environmental Quality Department
Report 2022-07

**Citation:**

Deltares, 2022**. Simulations of 2019 Hydrodynamics and Water Quality in the Massachusetts Bay System using the Bays Eutrophication Model.** Boston: Massachusetts Water Resources Authority. Report 2022-07. 86 p.

MWRA Environmental Quality Department reports can be downloaded from http://www.mwra.com/harbor/enquad/trlist.html.

# Summary

**Background.** This report presents hydrodynamic and water quality model results for the Massachusetts Bays system (Massachusetts Bay, Cape Cod Bay, and Boston Harbor) during 2019. Treated effluent sent from the Massachusetts Water Resources Authority (MWRA) treatment plant through a 15 km (9.5 mi) long tunnel and released at an outfall offshore in Massachusetts Bay contains nutrients. Nutrients are necessary and important to support healthy and diverse marine ecosystems. However, excess nutrients can cause eutrophication, the overgrowth of phytoplankton (microscopic marine algae) which degrades water quality and can harm marine life by depleting oxygen when it decays. To address potential eutrophication and other concerns, MWRA maintains an extensive bay and harbor field monitoring program, which this modelling complements. The hydrodynamic model simulates temperature, salinity, and currents, and is the foundation for the water quality model, which simulates key eutrophication parameters including nutrients, chlorophyll (a measure of phytoplankton), and oxygen.

**Results for 2019.** Consistent with field observations, the model did not show effects of effluent on chlorophyll or oxygen, nor indications that eutrophication was occurring. The hydrodynamic results for 2019 agree well with available observations and capture the geographic and vertical structure, and temporal variability, of temperature and salinity distributions and density stratification, as well as tidal and non-tidal currents. The 2019 water quality simulation captured general patterns in observed seasonal variations, geographic distributions, and vertical structure for many variables. This included the late spring reduction in near-surface dissolved inorganic nitrogen (DIN) due to phytoplankton uptake, and its replenishment after mixing in fall due to cooling and storms. It also included seasonal dissolved oxygen variations, with peak values in spring at shallow depths due to colder water and phytoplankton growth, and late summer minima at depth where stratification inhibits reaeration by air-sea exchange. In addition to those more bay-wide patterns, in the model as in observations, DIN was elevated persistently within about 10 km (6 mi) of the outfall and intermittently as far as about 20 km (12 mi) away, mainly due to nitrogen from ammonium in the treated effluent. The model captured the observed vertical structure of this effluent influence, which reached the surface in winter months and remained at depth from about May through October when the bay was stratified.

As in observations, modeled stratification was stronger than typical due to an unusually strong river freshet in spring and warm summer surface temperatures. A large observed dinoflagellates bloom in late summer was not fully captured by the model, which simulated higher chlorophyll concentrations during the fall diatom bloom. This helps explain why the model under-predicted chlorophyll and particulate organic carbon during summer. Despite this, model results were mostly within ranges of past years, and the seasonal cycle of oxygen in the model was similar to a typical year, as observed.

Overall, the 2019 simulation supports the conclusions from field monitoring, that eutrophication was not a concern and bay-wide ecological function was not appreciably influenced by the outfall.

**Special study.** A scenario simulation otherwise identical to the main run had all nitrogen forms removed from the effluent. DIN declined within about 10-20 km of the outfall as expected. Phytoplankton decreased near the surface, and as a result more light reached a thin mid-depth layer below, causing phytoplankton there to increase. Shallow oxygen decreased due to less phytoplankton production and deep oxygen increased due to less settling organic matter. The phytoplankton and oxygen changes were weak so the influence on the ecosystem was minor.

# Contents

# List of Figures

# 1 Introduction

The Massachusetts Water Resources Authority (MWRA) has established a long-term monitoring program to evaluate the impact of its sewage treatment plant effluent on the water quality and ecosystem function of Massachusetts Bay, Cape Cod Bay, and Boston Harbor. The monitoring program primarily consists of a series of ongoing field observation surveys and includes complementary water quality modeling as required by the discharge permit. The water quality simulations are carried out using the Bays Eutrophication Model (BEM, Deltares, 2021). This report presents simulation results for the 2019 calendar year. The content of this report is derived from internal Deltares document ref. 11203379-005-ZKS-0004, dated 20 April 2022, except for Section 6 which is from internal Deltares document 11203379-008-ZKS-0013 dated 13 May 2022.

## 1.1 Background on oceanographic processes influencing water quality

Massachusetts Bay and Cape Cod Bay (Figure 1-1) comprise a temperate coastal embayment system. Readers unfamiliar with the geography and/or the current understanding of the physical and biological oceanographic processes characterizing the system are referred to the introductory summaries found in sections 1.2 and 1.3 of MWRA Technical Report 2011-13 (Zhao et al., 2012), in the annual MWRA water column monitoring reports (e.g., for calendar year 2020, Libby et al., 2021), and in references cited by them. (All MWRA Technical Reports, including those just cited, are available online at http://www.mwra.state.ma.us/harbor/enquad/trlist.html.) A brief summary follows here. In this subsection the focus is on processes and influences other than effluent from the MWRA outfall, which has been shown in past studies to have a minor system-wide effect.

System hydrodynamics are characterized by a persistent general circulation pattern driving the flow of offshore Gulf of Maine waters into Massachusetts Bay via the Western Maine Coastal Current off Cape Ann, then southward before returning offshore just to the north of Cape Cod, with a portion of the flow first passing through Cape Cod Bay to the south (Figure 1-1). Rough estimates of the water residence time are about a month based on the surface currents, somewhat longer at mid-depth or deeper, where currents are weaker, and also longer in Cape Cod Bay than in Massachusetts Bay. While this slow general circulation is important in determining long-term average transport pathways, superposed on it are stronger and more variable wind-driven currents, and oscillatory tidal motions. Temperatures follow the characteristic temperate seasonal pattern of minima in late winter and peaks in late summer. Salinities are freshest inshore and in the upper several meters; in addition to the influence of offshore oceanographic conditions, they vary mainly in response to riverine inputs including primarily those brought by the Western Maine Coastal Current and the Merrimack River outflow to the north, and to a lesser extent the smaller amounts delivered via Boston Harbor. There is a seasonal cycle in vertical structure that includes transitions between well-mixed conditions, present from fall through early spring due to higher winds and atmospheric cooling, and strong density stratification during the late spring and summer due mainly to increased surface temperatures resulting from atmospheric heating.

The biology of the system is plankton-based and exhibits clear seasonal cycles that are tied closely to those hydrodynamic features, but with more pronounced spatial and inter-annual variability. Phytoplankton abundance typically peaks most strongly during bloom-favorable conditions in the late winter and early spring, as temperatures rise, light increases, and nutrients remain plentiful near the surface due to the active vertical mixing. Following the transition from spring to summer, near-surface

nutrient concentrations become depleted as density stratification impedes the vertical mixing that replenishes them. Zooplankton abundance and biomass generally peak in late summer, following the spring increase in phytoplankton prey levels. Primary productivity is commonly sustained at modest levels through summer and typically there is a second increase in phytoplankton during fall, when vertical mixing increases again and delivers nutrients to the surface while temperature and light conditions are still favorable before winter. Dissolved oxygen concentrations are influenced by a combination of biological and physical processes; the net result is a seasonal peak in late spring, due to phytoplankton production increasing winter levels already high due to strong reaeration, then steady decreases to a late summer minimum due to respiration and reduced reaeration. The summer oxygen minimum is lower at depth, where stratification limits reaeration.

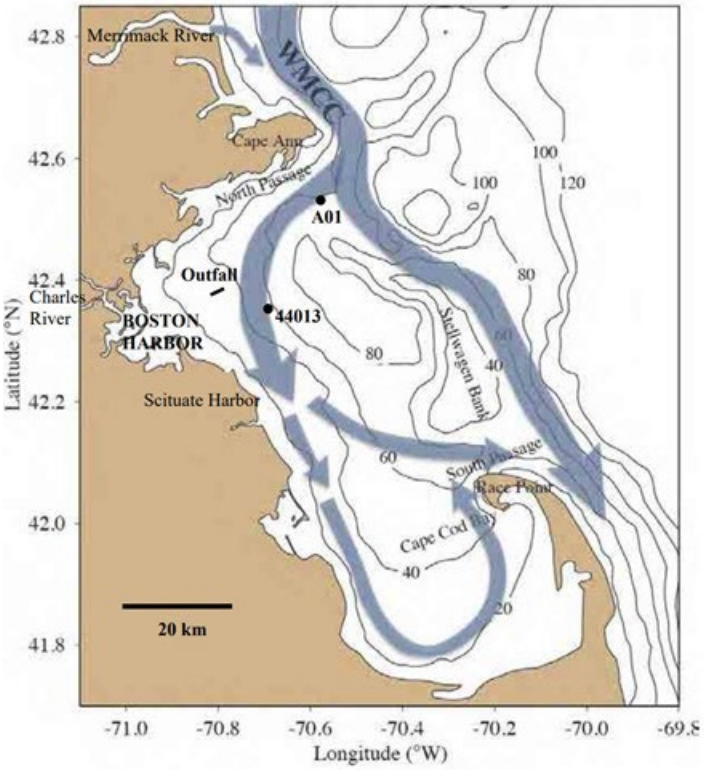


*Figure 1-1 Geography, bathymetry, schematic long-term mean circulation. WMCC = Western Maine Coastal Current. A01 = Oceanographic mooring (Northeastern Regional Association of Coastal and Ocean Observing Systems). 44013 = Weather buoy (National Data Buoy Center). Contours = water depth in meters. Figure from Zhao et al. (2017), adapted from Xue et al. (2014).*

## 1.2 Summary of observed 2019 conditions

To provide context for descriptions of model simulations of 2019 throughout this report, a brief summary is given here of observed 2019 conditions based on monitoring results (Libby et al., 2020). Higher than typical spring river flow caused an unusually strong spring freshet which led to much fresher surface water than in a typical year. Stratification was stronger than typical from May into September, initially due to the fresher water, then later in summer due to unusually warm surface temperatures. Inflow of current to the bays from offshore was stronger than typical, with several pulses of southwestward surface current observed at A01 in spring and early summer, possibly due to the strong stratification weakening resistance against shallow flow. Nutrient conditions were mostly typical of other years, and somewhat higher in summer at depth, possibly due to the strong stratification.

Chlorophyll levels were moderate overall but relatively higher during February, April, and late May in Massachusetts Bay, during February to April in Cape Cod Bay, during late May and August in Boston Harbor, and during September across all these areas when a large dinoflagellate bloom occurred. No strong bay-wide winter-spring diatom or *Phaeocystis* bloom was observed on the routine monthly vessel surveys, but satellite imagery and nutrient depletion suggested a diatom bloom occurred prior to the April survey. Dinoflagellates were more abundant that typical, largely due to the late summer bloom, which was dominated by *Karenia mikimotoi*. Oxygen concentrations in Massachusetts Bay increased due to a mixing event in July, and for the remainder of the year were similar to the typical seasonal cycle, including the late summer minima. Oxygen levels in a shallow southern portion of Cape Cod Bay, after a similar July increase, decreased to hypoxic levels not seen before in the monitoring program. The combination of organic matter from the *K. mikimotoi* bloom, strong stratification with delayed fall mixing, and the small volume of water beneath the pycnocline due to its position close to the relatively shallow seafloor is thought to have contributed to the hypoxia (Scully et al., 2022).

# 2 Methods

A complete model description is documented in MWRA's technical report 2021-02 and its appendices (Deltares, 2021). The model is set up in the Delft3D Flexible Mesh Suite, developed by Deltares. Technical details on the model set-up, its grid and forcing is presented in Appendix A of Deltares (2021). A description of the software package and underlying hydrodynamic and water quality equations are available in Section A1 of Deltares (2021), and in Deltares (2019a, b). The model has been calibrated for the years 2012-2016, as described in Appendix B of Deltares (2021). The results of the model validation are given in the main report body of Deltares (2021).

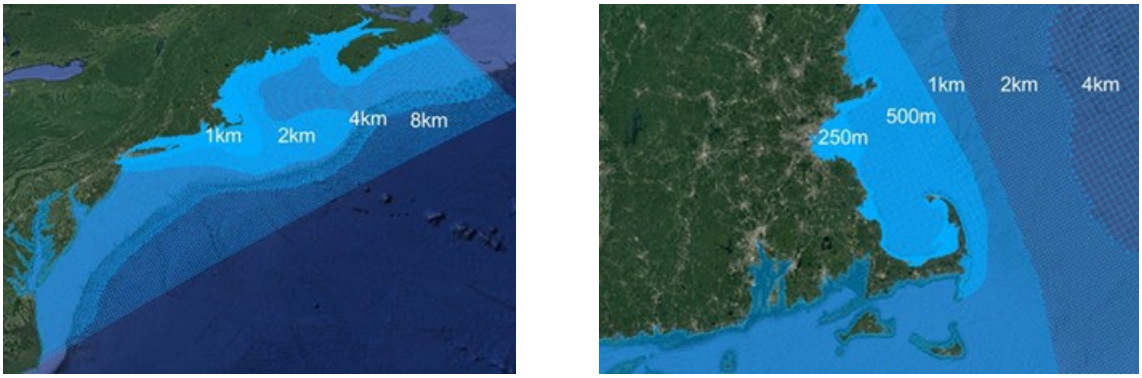


*Figure 2-1 Model grid of the entire model domain (left) and zoomed-in for Massachusetts Bay (right)*

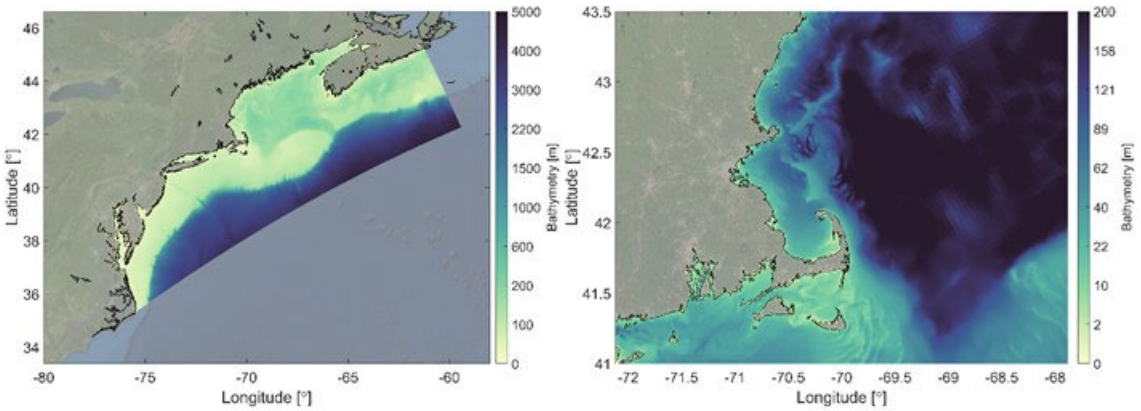


*Figure 2-2 Model bathymetry of the entire model domain (left) and zoomed-in for Massachusetts Bay (right)*

The model domain is large in order to best handle influences of offshore boundaries, as explained in Deltares (2021); it covers the entire Gulf of Maine region as well as the coastal region to the south, down to and including Chesapeake Bay (Figure 2-1 and Figure 2-2). Model performance in comparison to field measurements has been demonstrated most carefully in the area of Massachusetts Bay nearest the outfall, using MWRA observations (Deltares, 2021). The horizontal resolution is roughly 8 km at the open ocean and is gradually refined toward the coast, with a maximum resolution of 250 m in Boston Harbor and along the surrounding coastline, including at the outfall location.

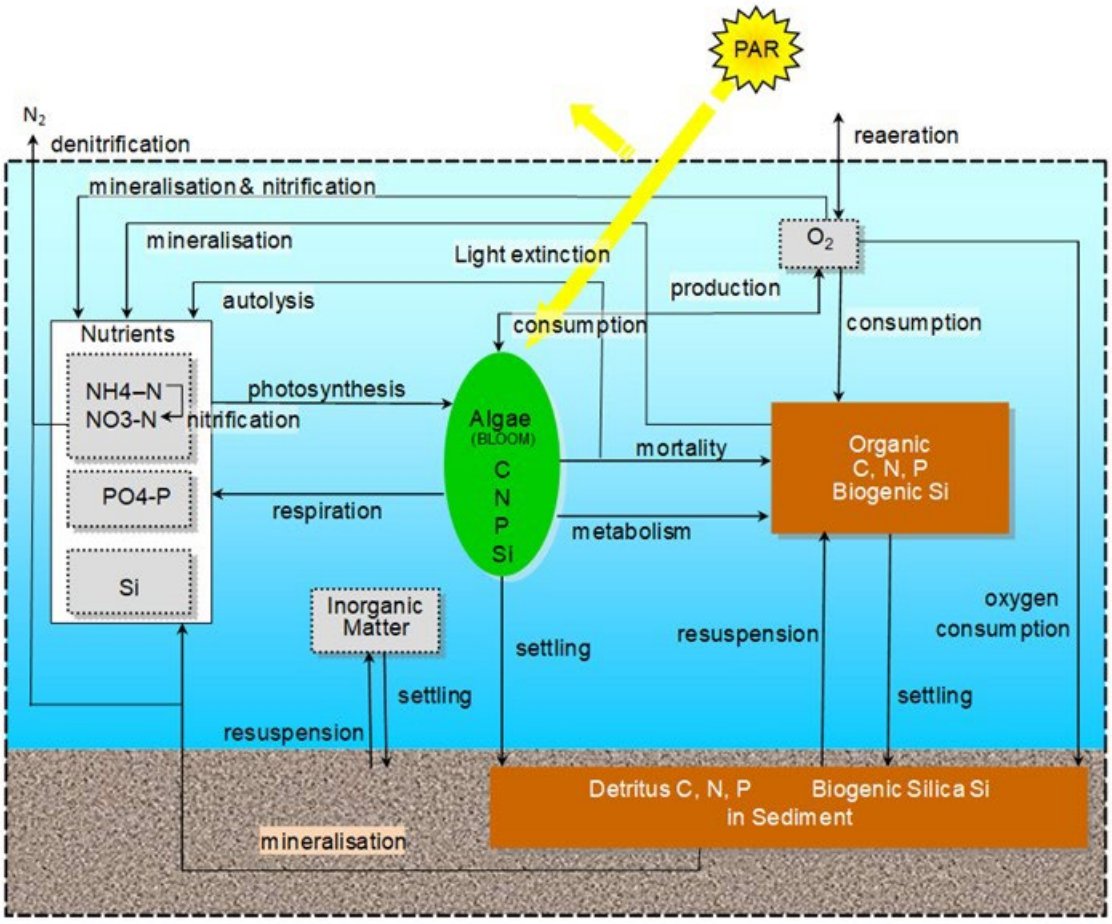


*Figure 2-3 Schematic overview of all state variables and processes. Reproduced from Deltares (2021). Note that Inorganic Matter, Algae and Detritus affect light extinction in the water column.*

Figure 2-3 provides an overview of the simulated state variables and processes for the water quality component. Four functional groups of pelagic phytoplankton are simulated (“Algae” in the figure): diatoms, dinoflagellates, other flagellates, and *Phaeocystis*.

The monitoring stations used to assess model performance and the transects along which water quality variables are examined are mapped in Figure 2-4. Model-observation comparison time-series are plotted for a representative selection of eight stations: N01 in the Northern Mass Bay, F22 with a greater oceanic influence, F23 near the outlet of Boston Harbor, N18 close to the MWRA outfall, N07 southeast of the outfall, F13 and F06 toward the south shore, and F02 in Cape Cod Bay.

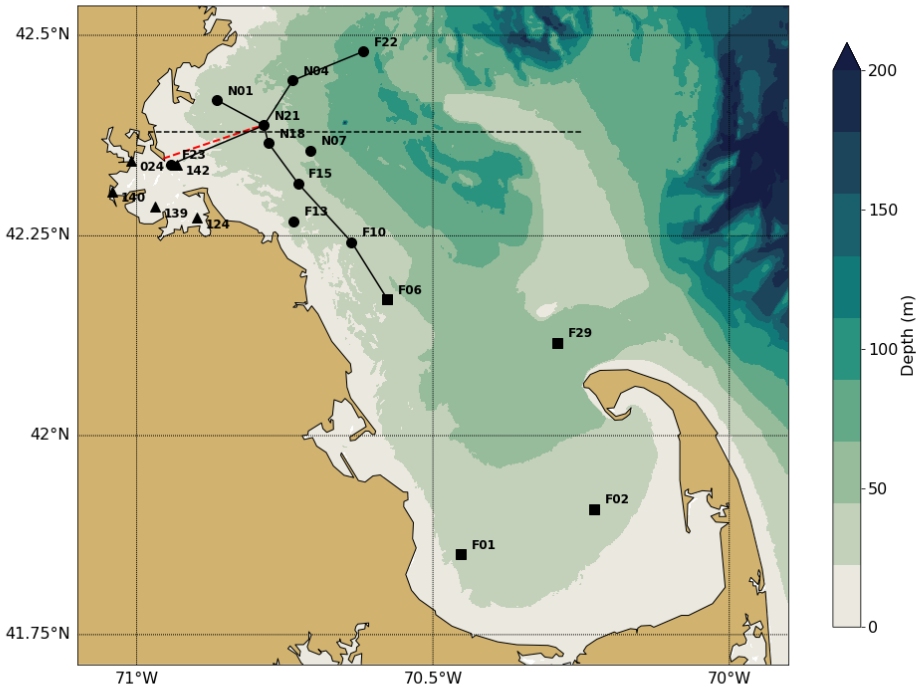


*Figure 2-4 Location of MWRA monitoring locations (circles=Northern stations, squares=Southern stations, triangles=Harbor stations). The red dashed line indicates the tunnel to the outfall diffusers. The black lines are the West-East and North-South transects used for model-observation comparisons. The horizontal black dashed line represents the transect through the outfall on which model results are presented in later figures.*

## 2.1 Updated methods

In the 2019 BEM run, instead of the multiyear reanalysis product from the Copernicus Marine Environment Monitoring Service (CMEMS), the forecast product (*Global Ocean 1/12° Physics Analysis and Forecast*[1]) was used for the forcing of the hydrodynamic open boundary condition (water level, salinity, temperature). This change was required due to the limited temporal coverage of the previously used reanalysis product. Underlying methods and models of the CMEMS products have not changed, and this change does not affect comparability of the 2019 simulation with simulations of prior years. Simulations of 2019 start using the last field of the simulation for 2018 (Deltares, 2022b), which was forced using the CMEMS multiyear reanalysis products.

[1] https://resources.marine.copernicus.eu/product-detail/GLOBAL_ANALYSIS_FORECAST_PHY_001_024

# 3 Forcing

## 3.1 Wind, heat flux, solar radiation, and rivers

### 3.1.1 Wind

In Figure 3-1, the main characteristics of the monthly-mean wind forcing for the simulated year 2019 are compared to the means of the previous 20 years (1998-2018) for the A01 mooring location off Cape Ann (Figure 1-1). Ranges of the standard deviation and of the minimum and maximum values are also shown.

The seasonal pattern of the vector-averaged velocities (top frame) largely followed the long-term mean. Differences were visible in the months February and October, where the eastward component was weaker than usual, and the wind direction was more toward the south. Winds in April were directed more to the north and in November the southward component was stronger than in previous years.

Wind speeds (second frame) mostly followed the long-term mean. Weak average wind speeds were observed in December and specifically in February, when it fell below the long-term minimum of 8.2 m/s, reaching 6.5 m/s. Wind speeds in October and November were relatively high. Monthly-mean wind stress magnitudes (third frame) show a similar pattern.

North-south wind stresses (bottom frame) are an indicator for upwelling. These were large in magnitude in October and November and small in February, compared to the long-term mean.

### 3.1.2 Heat flux

A comparison between time series of the calculated net air-sea heat flux (including solar radiation) for 2019 and for the previous years is given in Figure 3-2. A moving average with a window of 3 days is applied to visualize the instantaneous values. The time series of the net flux includes the ranges of the standard deviation from the mean and of the minimum and maximum values. The cumulative flux (middle frame) is presented without any filtering.

The seasonal pattern in 2019 (top frame) showed an overall negative heat flux in winter (loss of heat from the surface, cooling of the ocean) and an overall positive heat flux in summer (heating of the ocean). This closely followed the average pattern in the previous years. At the end of the year from November onward, it was slightly below average.

As a result, the cumulative flux (middle frame) was similar to the long-term mean and the cumulative anomaly (bottom frame) stayed close to zero throughout the year.

### 3.1.3 Solar radiation

The solar radiation from the meteorological forcing product is given in Figure 3-3. The solar radiation was similar to the long-term mean until June. From June to September it was slightly above average, after which it was slightly below average. At the end of the year the cumulative flux was at about 0.05 GJ $m^{-2}$ above the long-term mean. So, on an annual-mean basis, 2019 had slightly more incident surface solar radiation than a typical year.

The net surface heat flux in 2019 was close to the long-term average despite the slightly higher than typical incident radiation in 2019. Every year there is a net influx of solar radiation of about 5.5 GJ $m^{-2}$. Since the net air-surface heat flux is about 0.5 GJ $m^{-2}$, around 5 GJ $m^{-2}$ is lost through other air-sea heat fluxes every year. These fluxes consist of evaporative and convective turbulent fluxes or long-wave radiation.

### 3.1.4 Rivers

In Figure 3-4 the volume transport for Merrimack River is presented. The figures include the daily-averaged discharges (top frame) for the simulated year 2019 and for the previous twenty years (1998-2018). Ranges of the standard deviation and of the minimum and maximum values are also given.

In 2019, three major discharge events occurred in the Merrimack River in late January, late April and mid-December. Throughout the rest of the year, the discharge was often slightly above average. This was clearly visible in the total discharged volume (middle frame). The cumulative anomaly of the discharged volume (bottom frame) remained positive throughout the year and was about 1.6 $km^3$ above the long-term mean at the end of the year.

The combined volume transport for the rivers discharging directly to Massachusetts Bay and Cape Cod Bay is presented in Figure 3-5. These rivers are Saugus, Mystic, Charles, Neponset, North and Jones. The combined discharge stayed close to the long-term mean. Three major discharge events were visible with timing similar to the Merrimack River events. The cumulative anomaly of the discharged volume (bottom frame) remained positive throughout the year and was about 1.8 $km^3$ above the long-term mean at the end of the year.

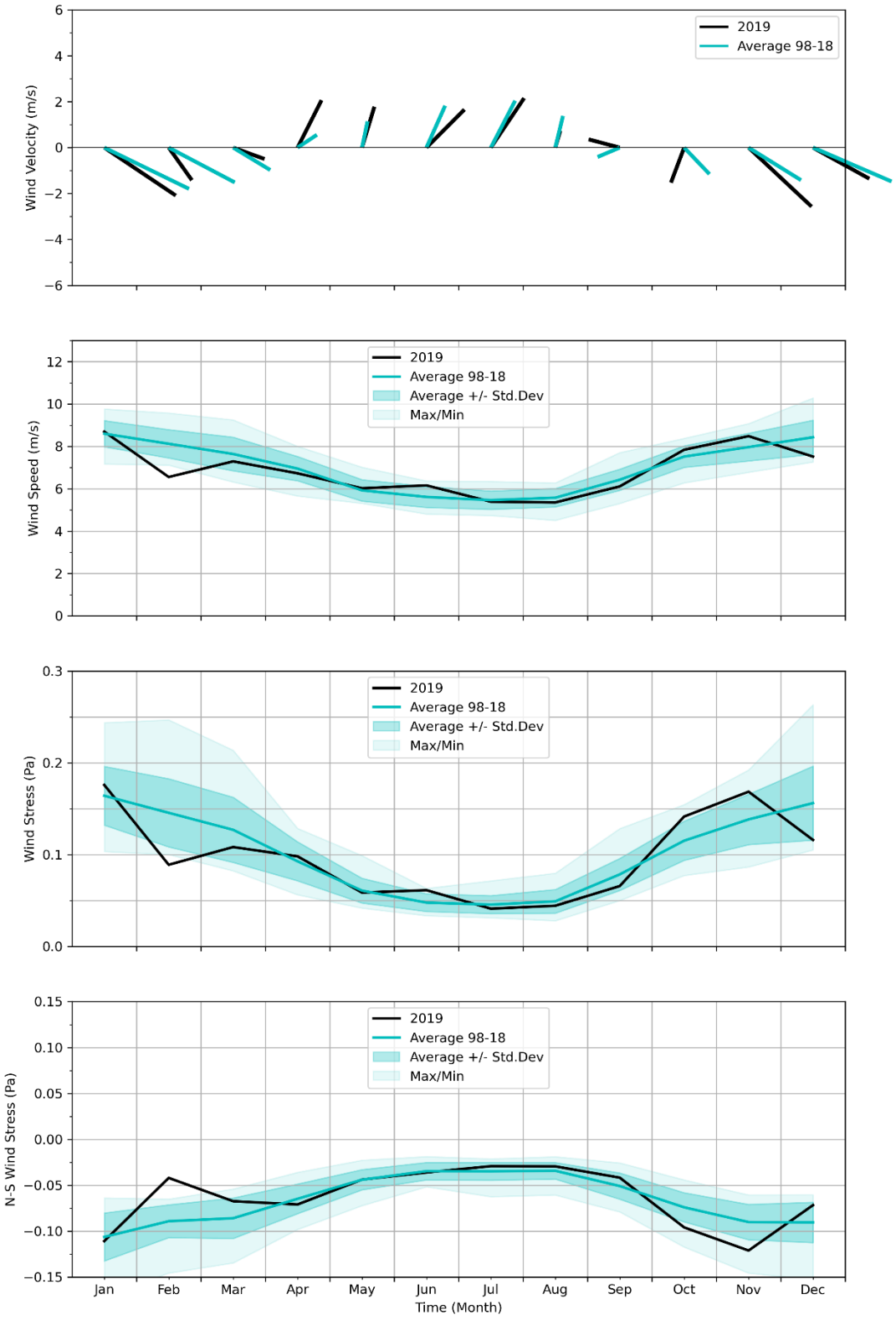


*Figure 3-1 Surface wind forcing, monthly averages, compared to prior 20-year period.*

*Top frame: Vector-averaged wind velocities. Second frame: Wind speed. Third frame: Wind stress magnitude. Bottom frame: North-south component of wind stress, an indicator for wind-driven upwelling.*

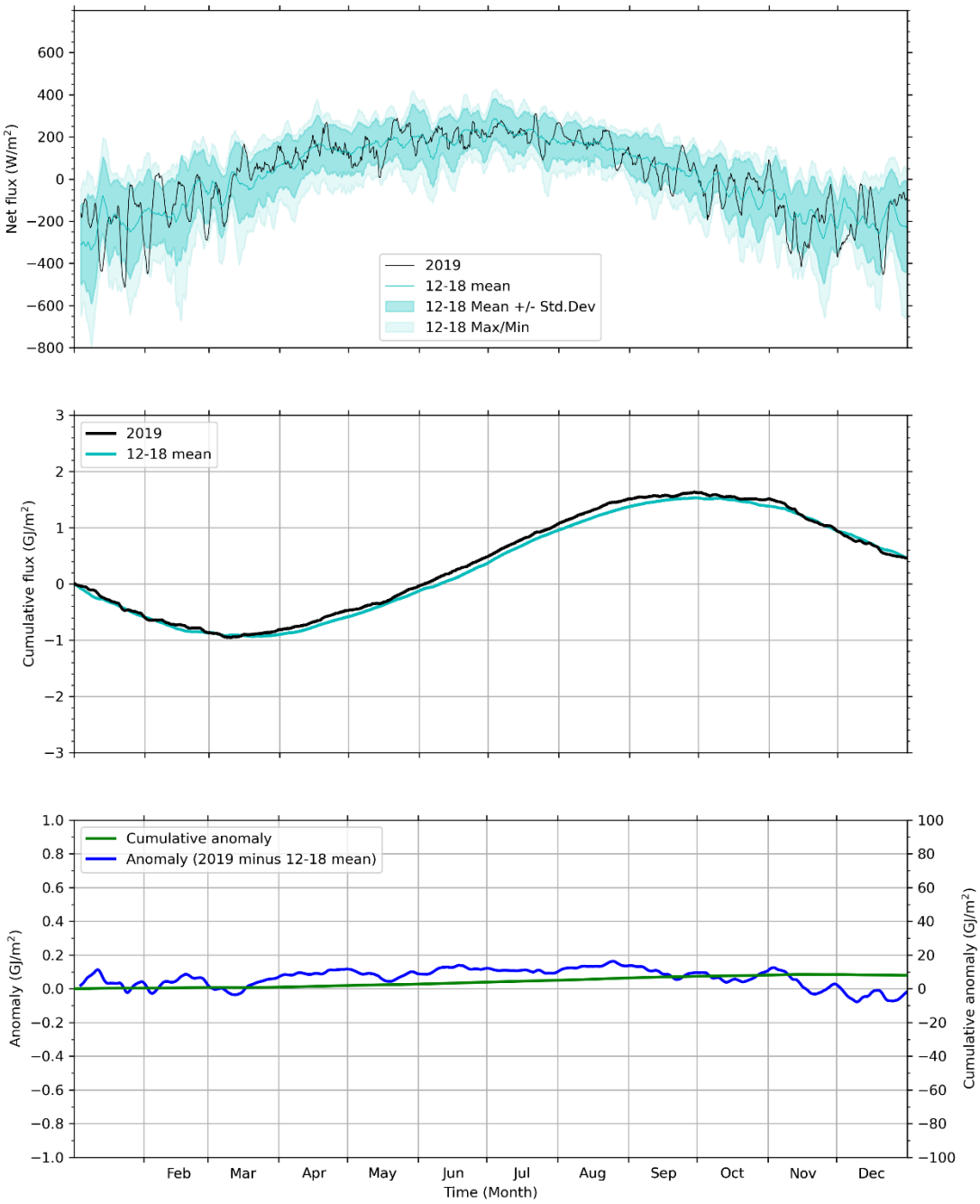


*Figure 3-2 Surface heat flux, compared to prior 7-year period.*

*Top frame: Net heat flux into ocean. Middle frame: Cumulative net heat flux starting from January 1. Bottom frame: Anomaly (blue, left axis) and cumulative anomaly (cumulative sum of daily mean anomaly; green, right axis) of 2019 net cumulative heat flux relative to 2012-2018 average. The 2012-2018 reference period has been used because direct simulation output is available; it is shorter than the 20 years used for the long-term mean.*

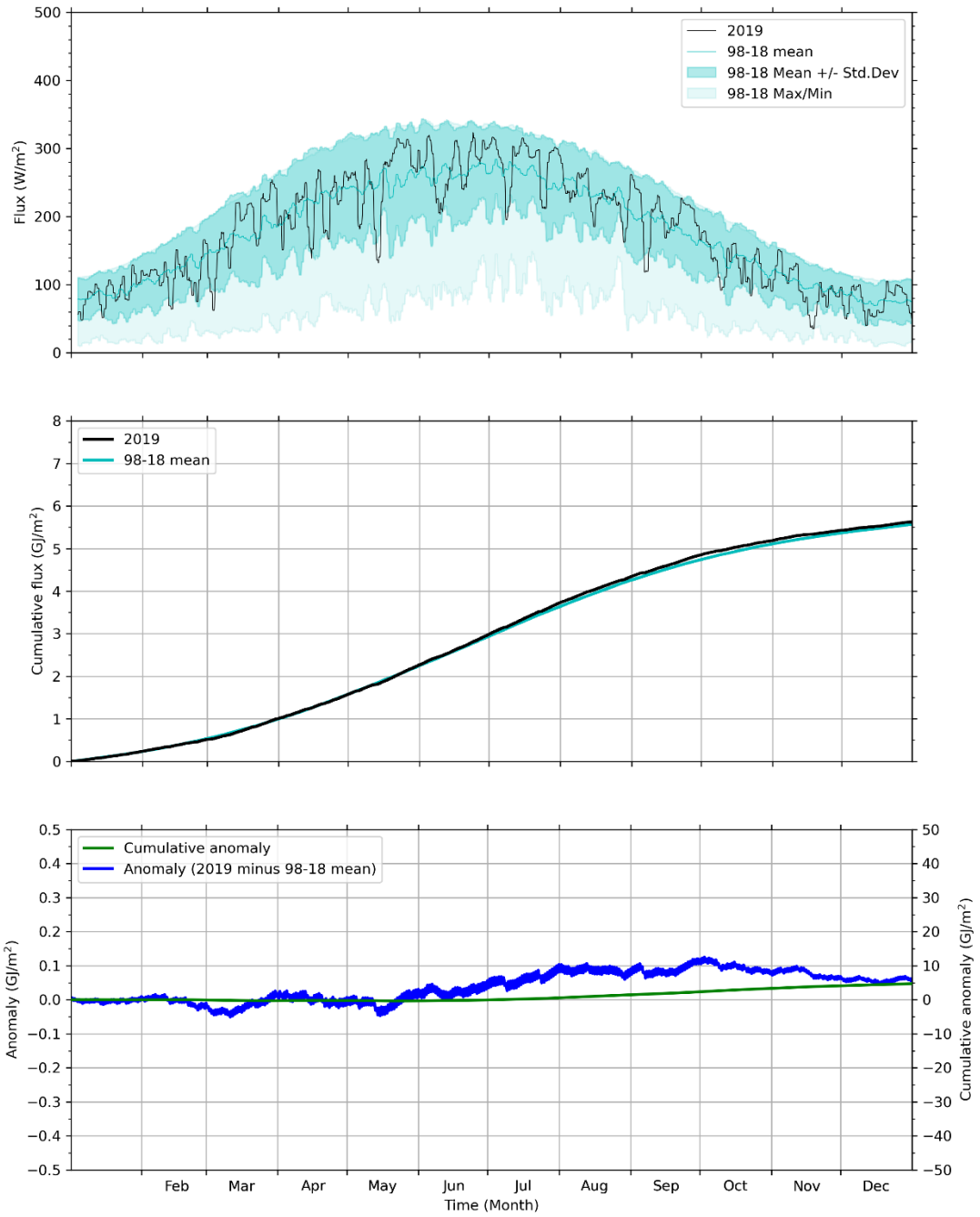


*Figure 3-3 Solar radiation, compared to prior 20-year period.*

*Top frame: Solar radiation into ocean. Middle frame: Cumulative solar radiation starting from January 1. Bottom frame: Anomaly and cumulative anomaly (cumulative sum of daily mean anomaly) of 2019 cumulative solar radiation relative to 1998-2018 average.*

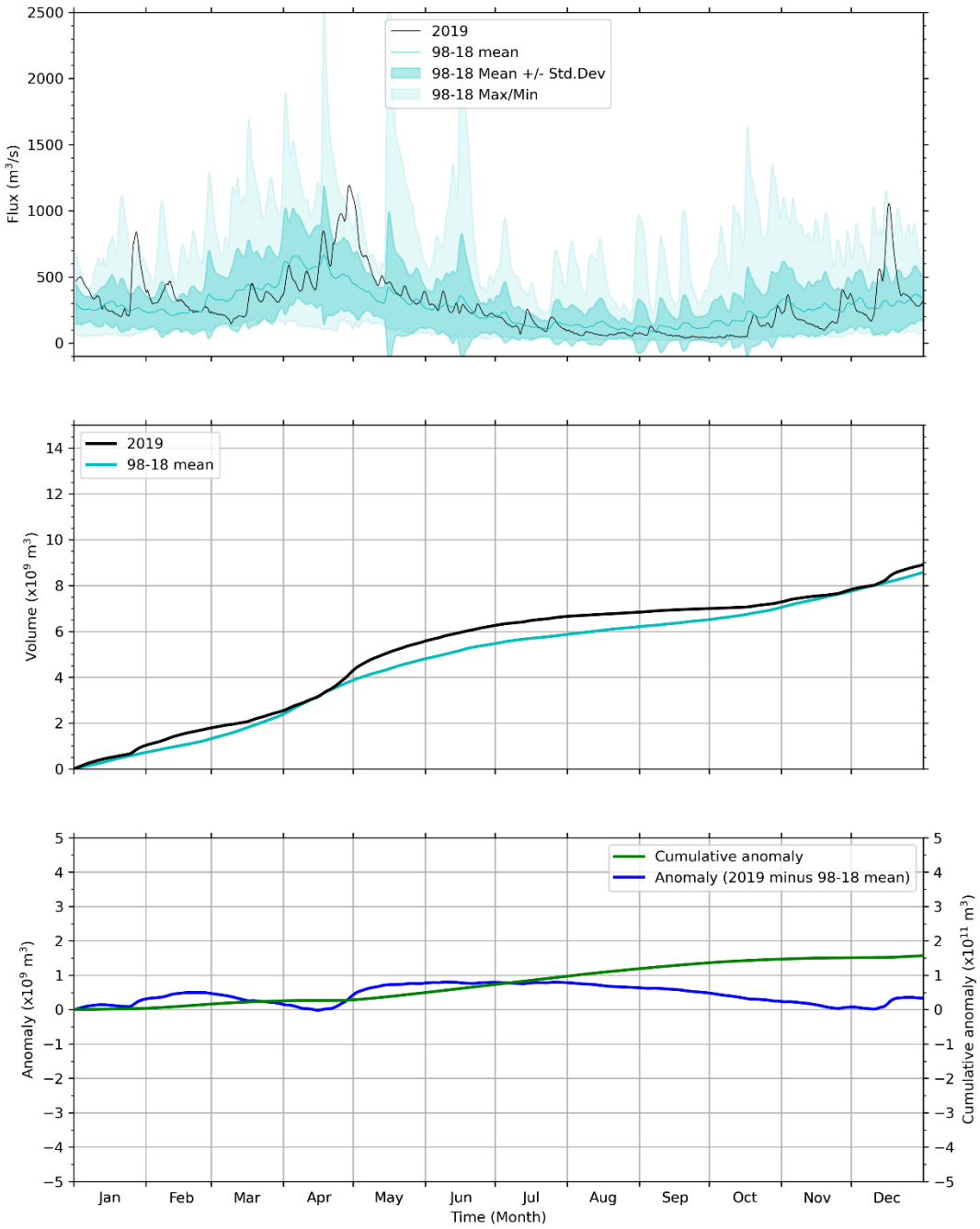


*Figure 3-4 Merrimack River daily/cumulative flux and anomaly relative to previous 20 years.*

*Top frame: Merrimack River volume flux. Middle frame: Cumulative flux relative to January 1. Bottom frame: Anomaly and cumulative anomaly (cumulative sum of daily mean anomaly) of flux in 2019 relative to 1998-2018 average.*

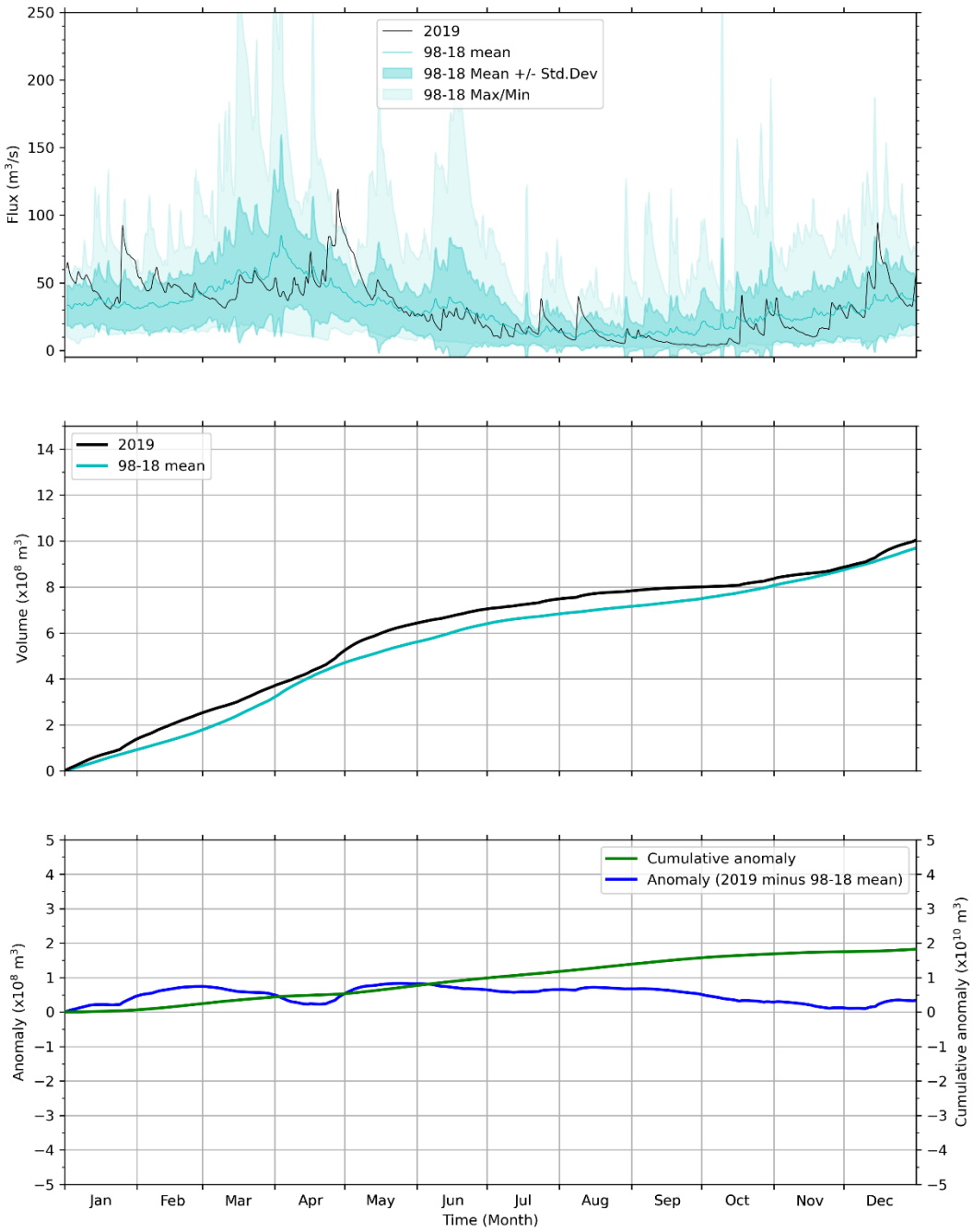


*Figure 3-5 Summed discharge of all modeled rivers (Saugus, Mystic, Charles, Neponset, North, and Jones) flowing directly in to Massachusetts and Cape Cod Bays.*

*Presented as in Figure 3-4.*

## 3.2 Loading of organic carbon, nitrogen, and phosphorous

Loads directly entering Massachusetts and Cape Cod Bays from rivers, the Deer Island treatment plant, and the atmosphere are shown in Figure 3-6. Loads entering the system through its offshore boundary are marked “oceanic input”, for example originating from rivers to the north including the Merrimack.

Model results show that oceanic input was the dominant source of organic carbon (OC), nitrogen and phosphorus (both in organic and inorganic forms), accounting for 99%, 92% and 96% of their total inputs, respectively (Figure 3-6). The simulated oceanic input of total nitrogen (TN) was comparable to the estimates based on the simulation of 1992 conditions from Hunt et al. (1999), reported by Zhao et al. (2017). The latter indicated that 93% of the TN entering the Mass Bay originated from the Gulf of Maine.

Rivers were the second largest source of OC, accounting for 79% of the non-oceanic input. MWRA loads constitute the main non-oceanic source of TN and total phosphorus (TP). These occur mainly in the inorganic form. Atmospheric deposition accounted for approximately 10% of the non-oceanic TN inputs. Finally, rivers are the smallest source of TN and TP to Massachusetts and Cape Cod Bays, representing 6% and 4% of their non-oceanic inputs, respectively. Proportions of river inputs in total OC, TN and TP loads are similar to 2017 and slightly lower than for 2018 that had periods of higher-than-average river discharges (Deltares, 2022b).

The 2019 OC loads from the MWRA effluent were slightly higher than in the preceding years 2014-2017 and similar to 2018. The 2019 TN effluent loads are slightly higher than for the other years of the 2014-2018 period, with a higher organic fraction. The 2019 TP effluent loads were slightly lower than for previous years, with an organic fraction close to the average of preceding years.

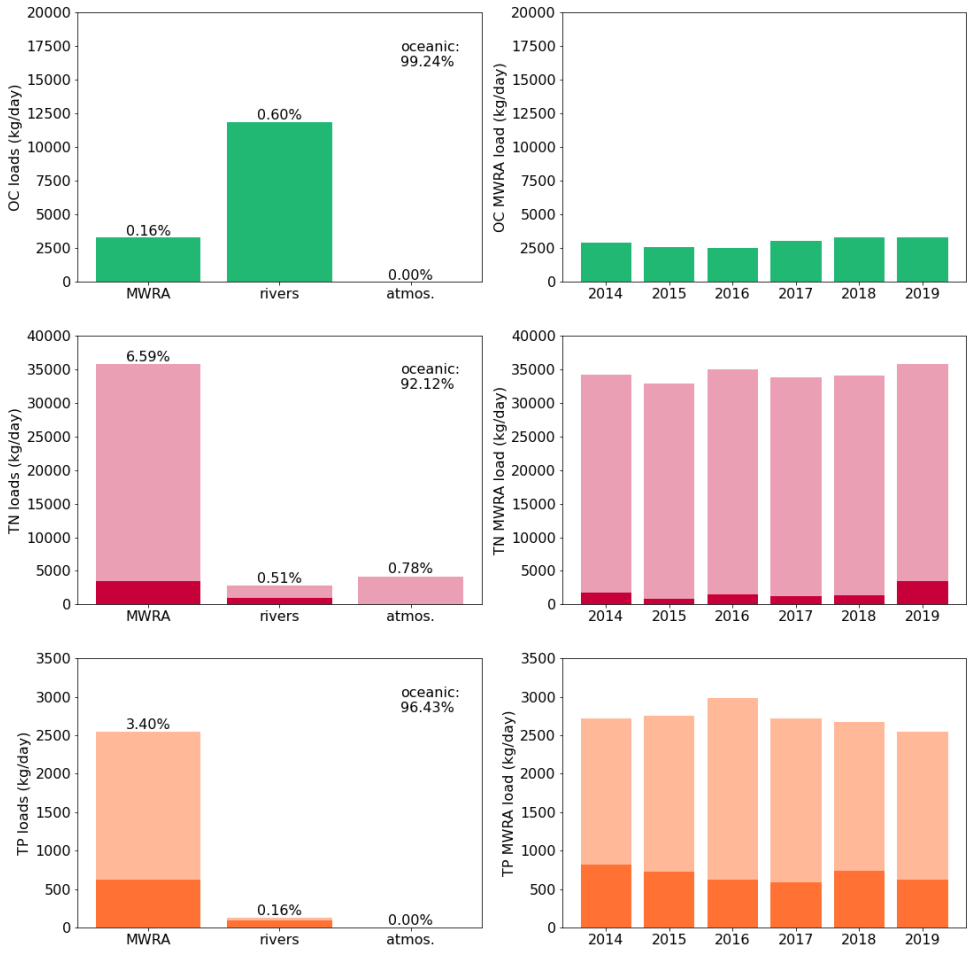


*Figure 3-6: Organic Carbon (OC), Total Nitrogen (TN) and Total Phosphorus (TP) loads to Massachusetts and Cape Cod Bays in 2019. In the TN and TP plots, the darker sections of the bars represent the organic fractions. Left: loads from non-oceanic sources; percent of total is shown at top of each bar, and percent oceanic input (offshore boundary) shown at upper right. (Percentages correspond to summed organic and inorganic fractions.) Right: Deer Island Treatment Plant loads since 2014. OC=organic carbon; TN=total nitrogen; TP=total phosphorus.*

# 4 Hydrodynamic Model

In this section the performance of the hydrodynamic model is discussed, and model results are compared to measurements.

## 4.1 Verification of model performance

The model skill was assessed for surface and bottom temperature and salinity by means of a statistical analysis. Three quantitative skill measures (correlation, normalized standard deviation Std*, and normalized unbiased root mean square error uRMSE*) were determined, based on simulation results and vessel-based observations by MWRA surveys. The result is presented in four pairs of Taylor diagrams in Figure 4-1. The left column shows the 2012-2016 validation period (Deltares, 2021) and the right column shows the 2019 simulation. See also the box below for further details and an explanation of the statistics in the diagrams.

Temperatures had correlation of over 0.98 and 0.90, Std* of 0.90-1.10 and 0.85-1.20, and uRMSE* of under 0.20 and 0.50, at the surface and bottom respectively. The performance at both the surface and the bottom was similar to the validation result, with the exception of poorer skill at the Boston Harbor station F23.

The skill of simulated salinity varied more per observation station in 2019 than in the validation period. There were values for correlation of 0.70 or greater and 0.75 or greater, for Std* of 0.65-0.90 and 0.50-1.55, and for uRMSE* of up to 0.70 and 0.85, at the surface and bottom respectively. The performance at the surface improved compared to the validation result, again except for station F23. At the bottom, the performance improved slightly, but the spread of the stations was still large.

Overall, the figures presented here serve to verify that the performance of the hydrodynamic model in the simulations of 2019 did not deviate substantially from its performance during the 5-year validation period. For completeness, Taylor diagrams broken out for individual years 2012-2016, are presented in Appendix A of the Annual BEM Report on 2017 (Deltares, 2022a).

**How to read a Taylor diagram**

A Taylor diagram consists of a combination of three quantitative skill measures:

- Correlation Coefficient, represented in the plot by the azimuthal angle or blue lines.
- Normalized Standard Deviation (Std*), the Standard Deviation of the model results, normalized (*) by the standard deviation of the corresponding measurements. This ratio represents the relative amplitude of the modeled and observed variations, with a value of less than one indicating less modeled variability. It is represented in the plot by the radial distance from the origin (0,0).
- Unbiased Root-Mean-Square Error or standard deviation of the error, normalized with the standard deviation of the corresponding measurements (uRMSE*). It is represented in the plot by the grey contours, whose values are proportional to the radial distance from the target (black star).

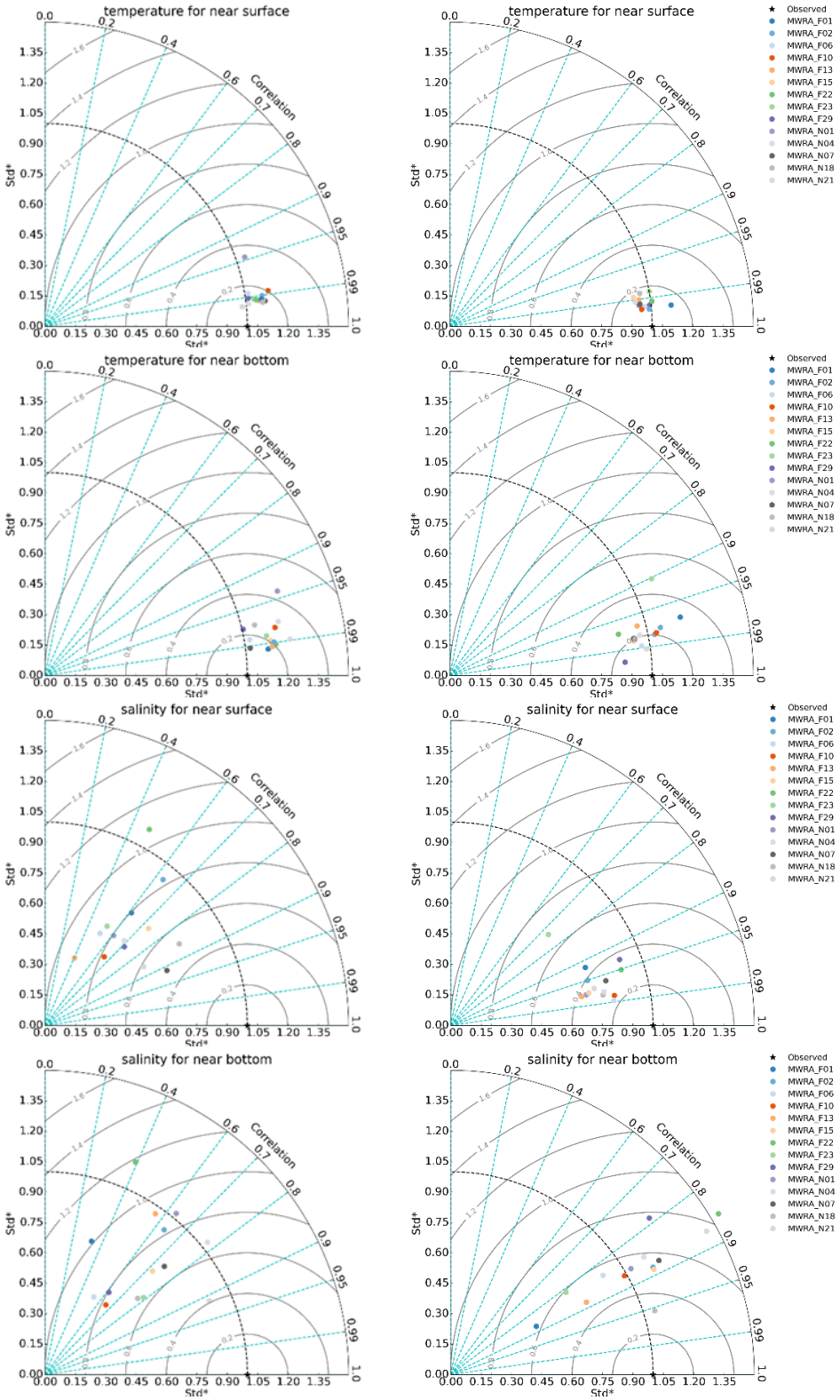


*Figure 4-1 Taylor diagrams of model quality for MWRA vessel-based survey observations.*

*Temperature (upper frames), salinity (lower frames); 2012-2016 validation period (left column) and 2019 simulation (right column).*

## 4.2 Model-observation comparisons

The simulation for 2019 was compared to observations to assess the level of agreement between them for temperature and salinity, both in time and space.

### 4.2.1 Time series of temperature and salinity

For eight observation stations in Massachusetts Bay and Cape Cod Bay, simulation time series of the surface (less than 5 m deep) and bottom (within 5 m of seafloor) temperature and salinity are presented in Figure 4-2 and Figure 4-4. Additionally, a comparison at three levels within the water column, between the surface and seafloor, is given in Figure 4-3 and Figure 4-5 (described below).

In these figures, vessel-based observations by MWRA surveys are included as individual symbols. The locations of the observation stations are given on a bathymetric map in the upper left frame. They include four stations generally surrounding the outfall (N01, N07, N18, and F13), one to the south (F06), one farther offshore (F22), one at the mouth of Boston Harbor (F23), and one in central Cape Cod Bay (F02).

In Figure 4-3 and Figure 4-5, showing results from within the water column, the depths vary from station to station and survey to survey but are nominally at 25%, 50%, and 75% of the water depth. The model output between surveys is not shown on these figures because the depths used, set by the observations, differ from survey to survey.

Overall, the seasonal cycle and most events were well captured by the model. Simulated stratification was similar to observations. At most stations, the onset of stratification occurred in the second half of April with the strongest salinity stratification in early May and the strongest temperature stratification between early July and mid-August. The water column started to mix in September and suddenly became mixed in early October due to a strong storm event (see Figure 4-12). This event caused a sudden increase in bottom temperature from about 8°C to 13°C in most of the stations. Other events with a smaller effect were simulated for September. Model-observation differences for temperature in these plots are at most 1°C at the surface and seafloor, and slightly larger within the water column. For salinity a bias of about 0.5 PSU was present throughout the water column, as discussed in Deltares (2021), with differences of up to 1.5 PSU at stations N01 and F13. In general, the model-observation differences were larger in the upper part of the water column and during the summer, when stratification occurred.

### 4.2.2 Spatial representation of temperature and salinity

To assess the simulation spatially, maps have been plotted for surface and seafloor conditions, with the mean of the modeled results averaged over a period of 5 days centered on the observation dates. The five presented periods span the seasonal cycle of stratification. This is given in Figure 4-6 and Figure 4-7 for temperature and in Figure 4-8 and Figure 4-9 for salinity. For the model-observation comparison, the available observations are plotted over the simulation fields as colored symbols. Note that the presented simulation fields are the average over 5 days, whereas the observations are instantaneous values, usually measured in the morning. This might introduce a bias.

These figures show good agreement between the simulation and observations. The spatial variation at both the surface and bottom was comparable, with near-shore temperatures warmer in summer and colder in winter. At both depths, salinities were generally fresher near the coast. The freshwater plume in June was well captured by the model with maximum differences of 0.5 PSU at both the surface and seafloor. Model-observation differences for temperature were largest in August with underestimation of up to 2°C at the surface. In other months, they were at most 1°C.

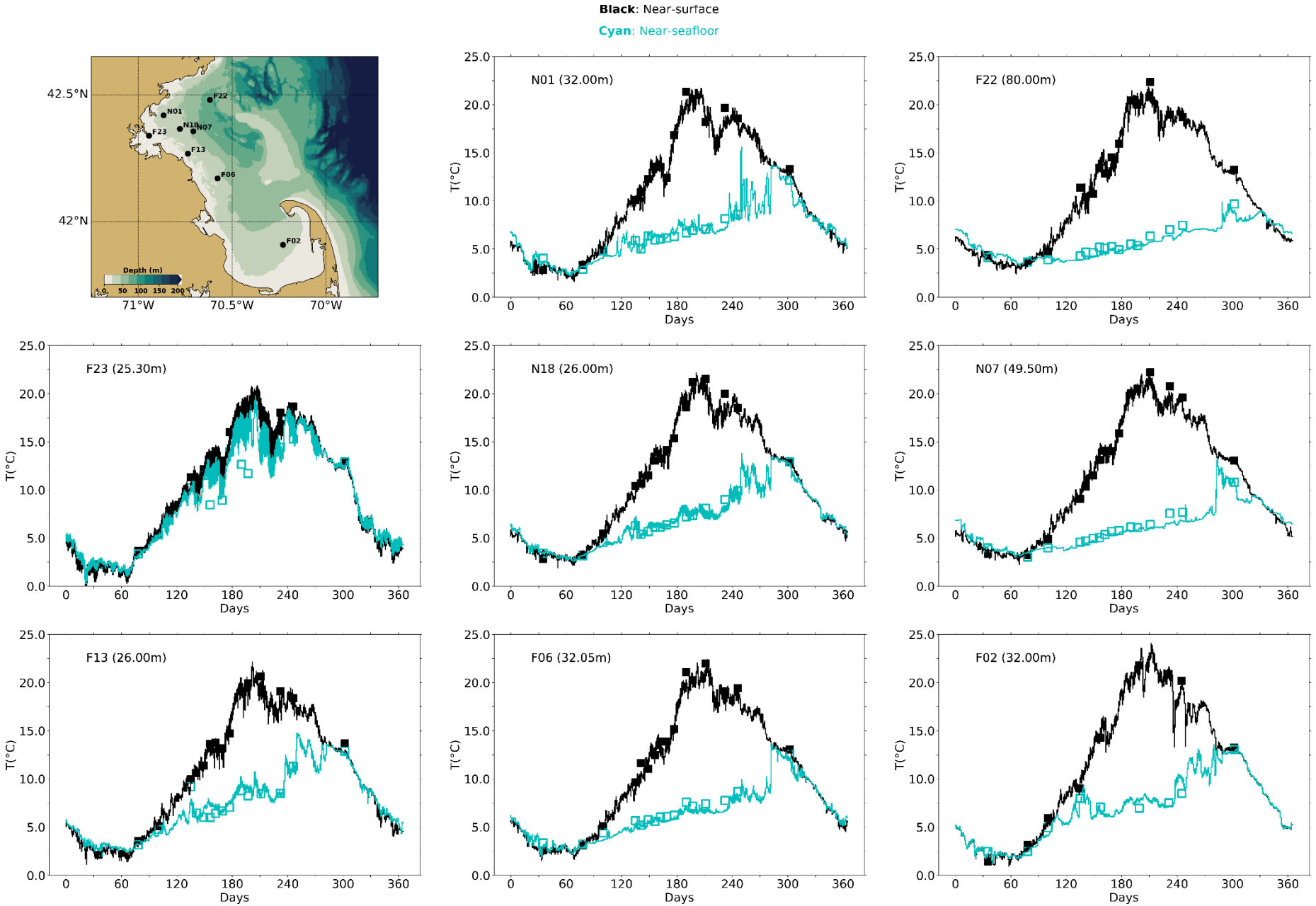


*Figure 4-2 Temperature time series, model-observation comparison near surface (black) and seafloor (cyan).*

*Model results: lines. MWRA vessel-based survey observations: symbols.*

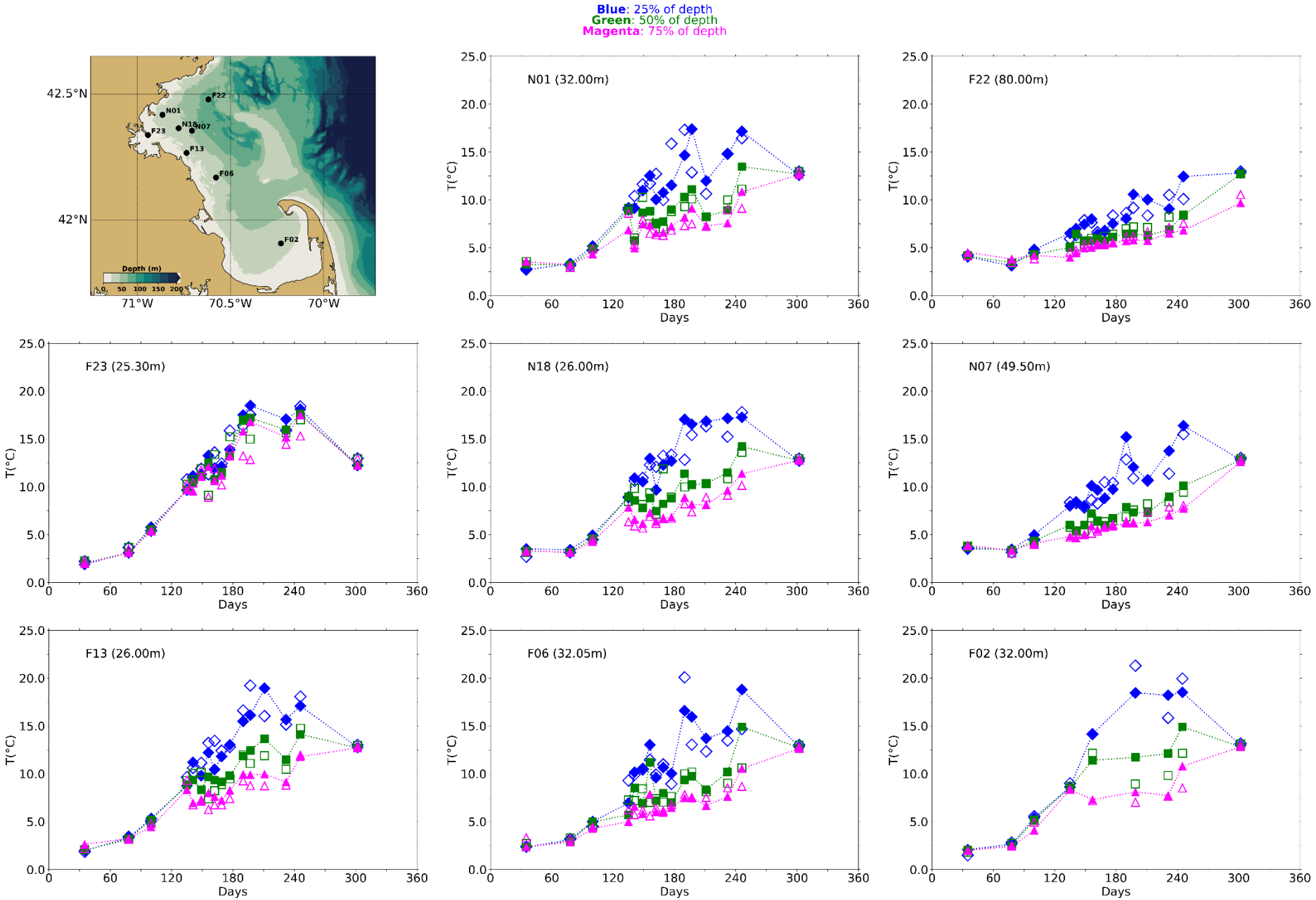


*Figure 4-3 Temperature time series, model-observation comparison within water column (between surface and seafloor).*

*Model results: lines with filled symbols. MWRA vessel-based survey observations: open symbols.*

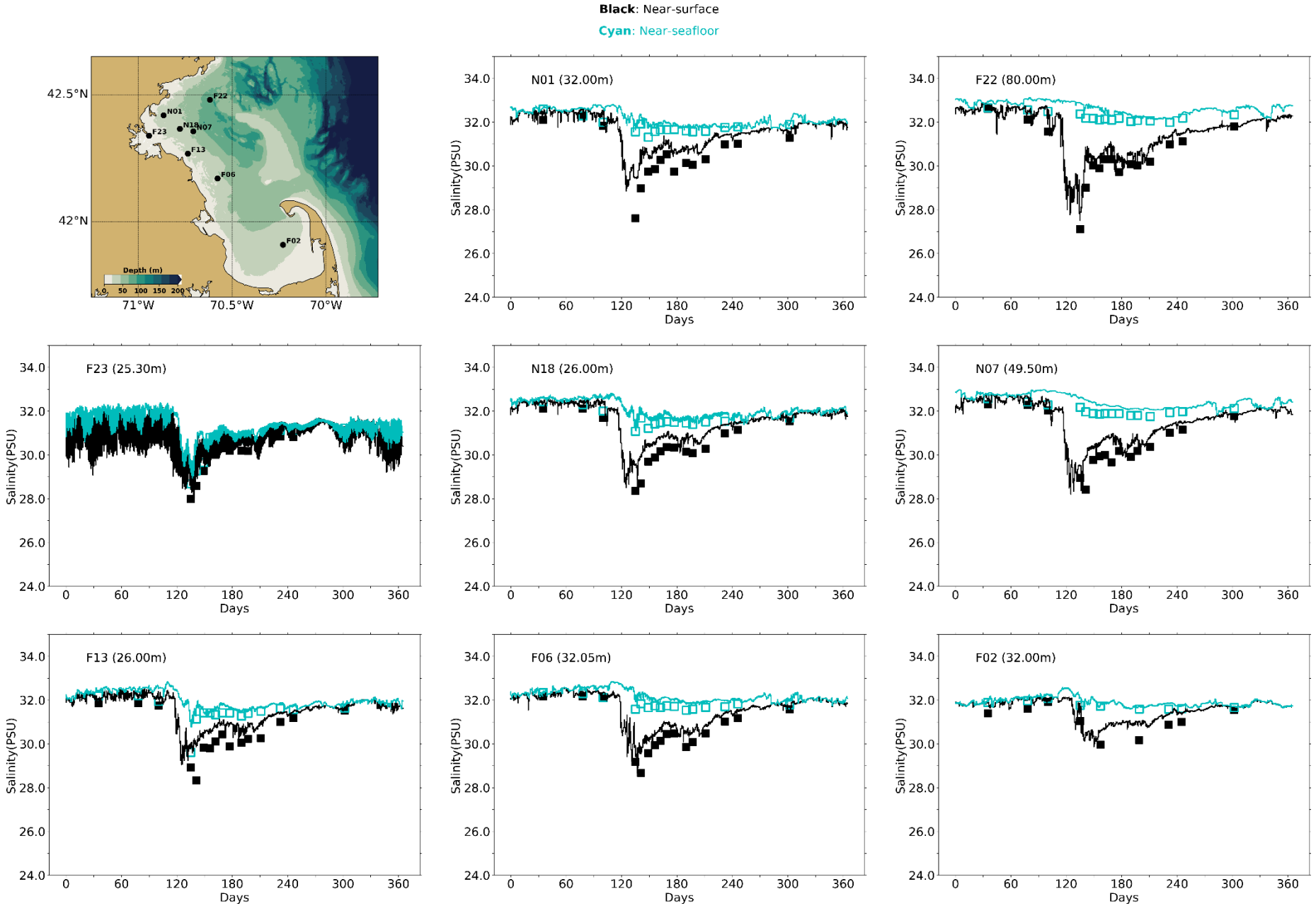


*Figure 4-4 Salinity time series, model-observation comparison near surface (black) and seafloor (cyan).*

*Model results: lines. MWRA vessel-based survey observations: symbols.*

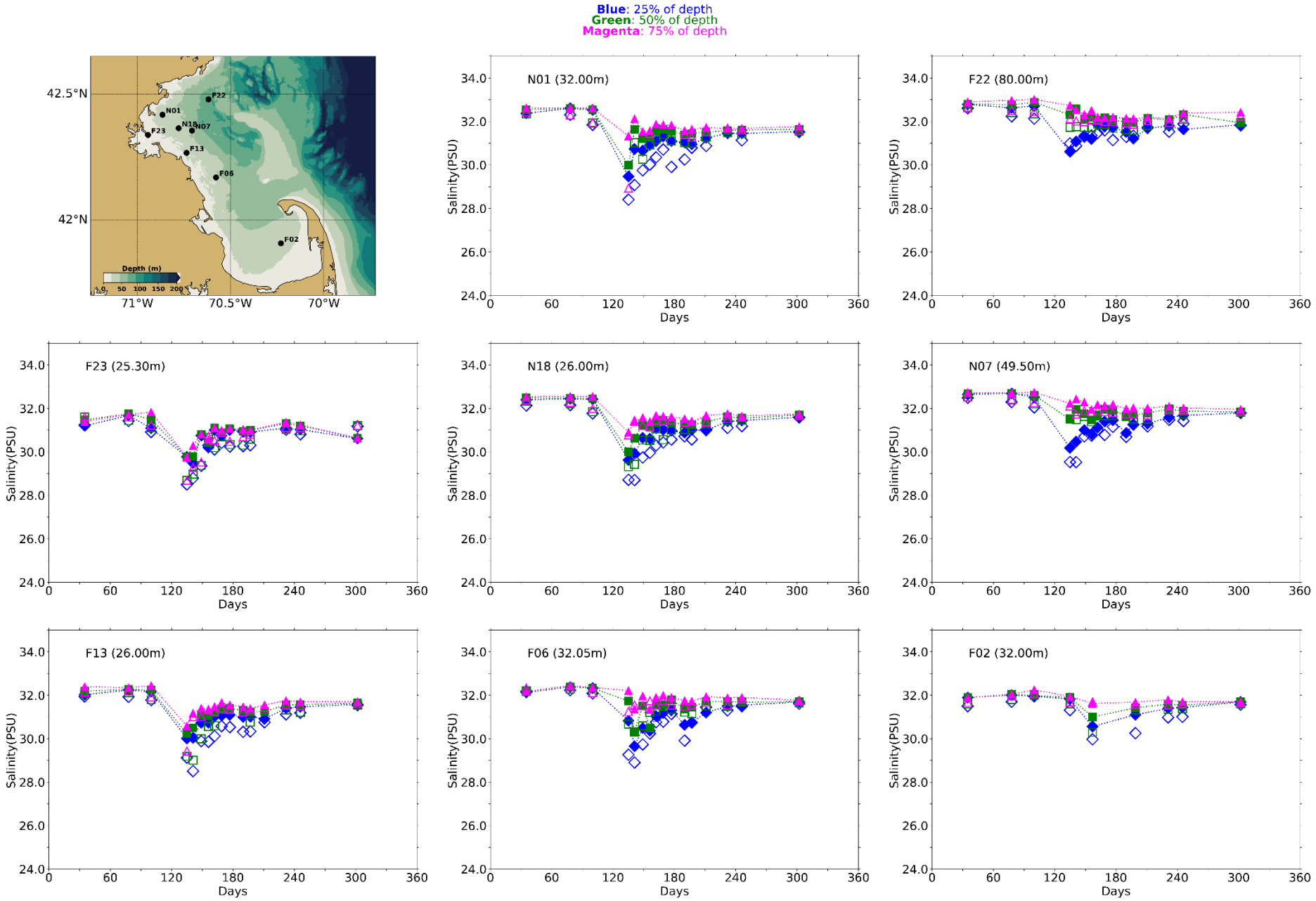


*Figure 4-5 Salinity time series, model-observation comparison in water column (between surface and seafloor).*

*Model results: lines with filled symbols. MWRA vessel-based survey observations: open symbols.*

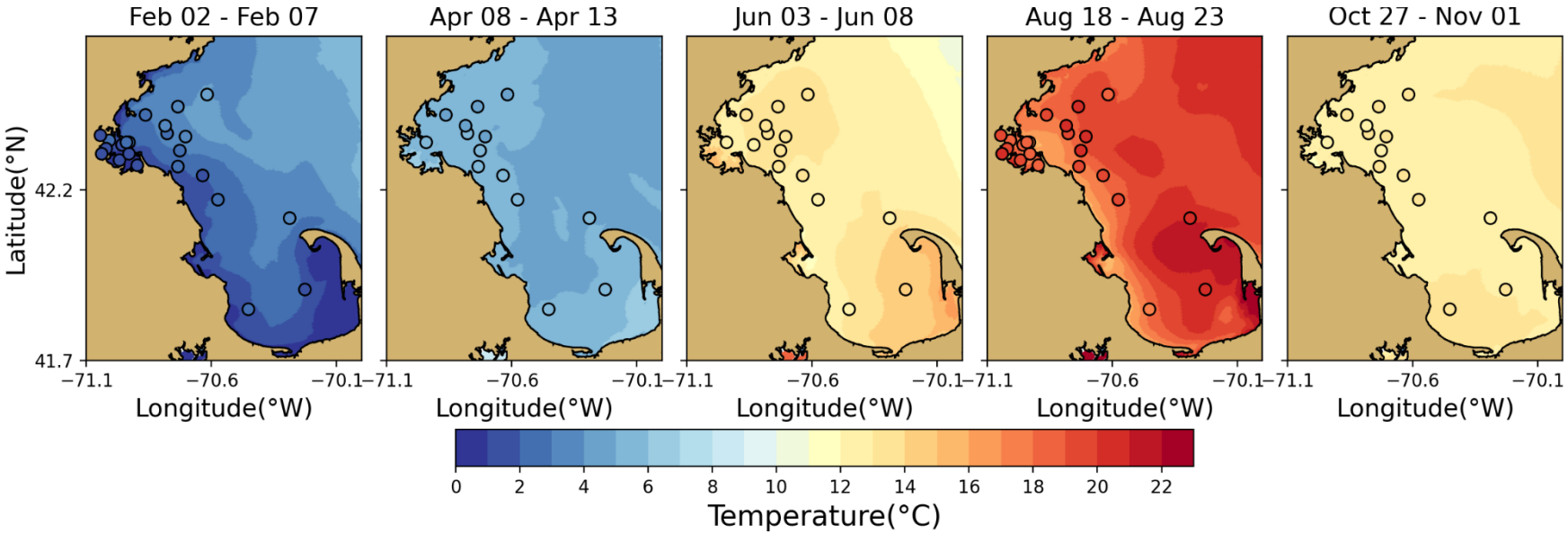


*Figure 4-6 Temperature spatial structure, at/near sea surface, model-observation comparison.*

*Model results: background. MWRA vessel-based survey observations: symbols. Model results are averaged over the 5-day period centered on the measurement date.*

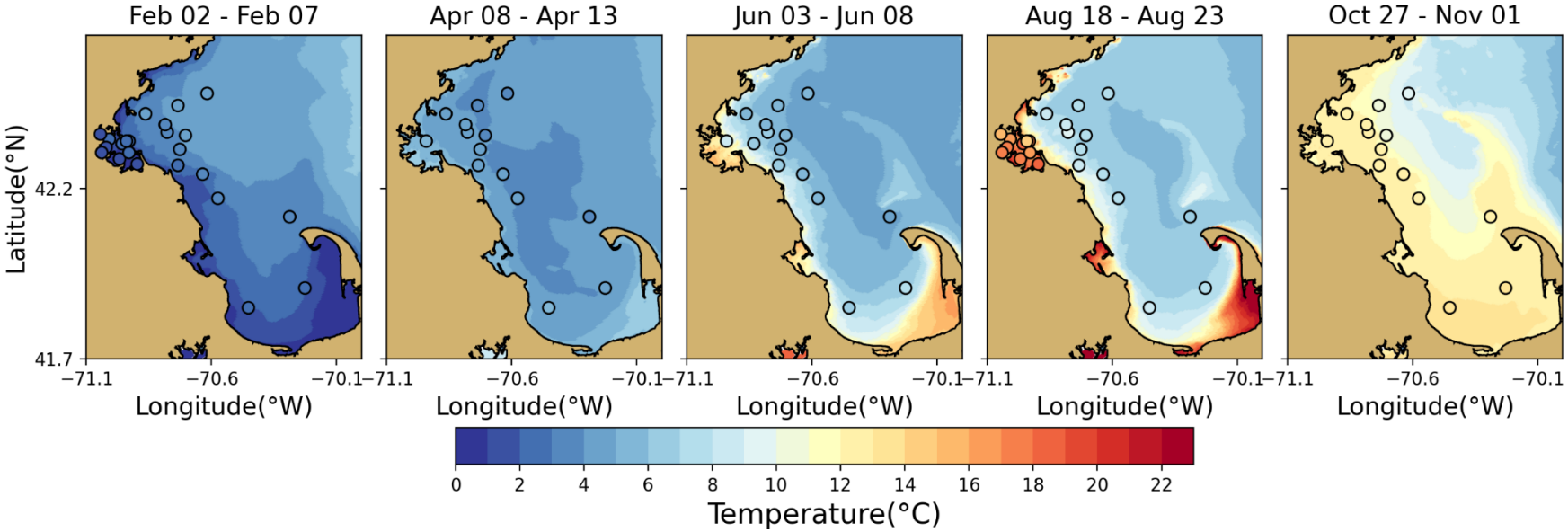


*Figure 4-7 Temperature spatial structure, at/near seafloor, model-observation comparison.*

*Model results: background. MWRA vessel-based survey observations: symbols. Model results are averaged over the 5-day period centered on the measurement date.*

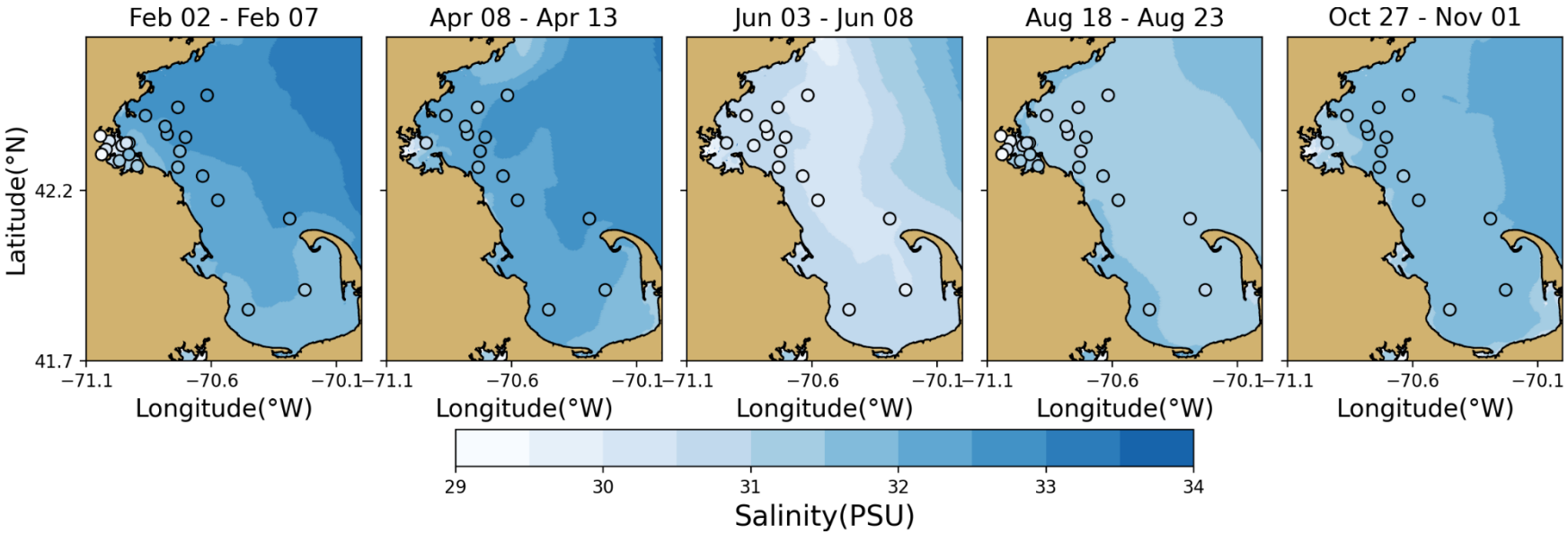


*Figure 4-8 Salinity spatial structure, at/near sea surface, model-observation comparison.*

*Model results: background. MWRA vessel-based survey observations: symbols. Model results are averaged over the 5-day period centered on the measurement date.*

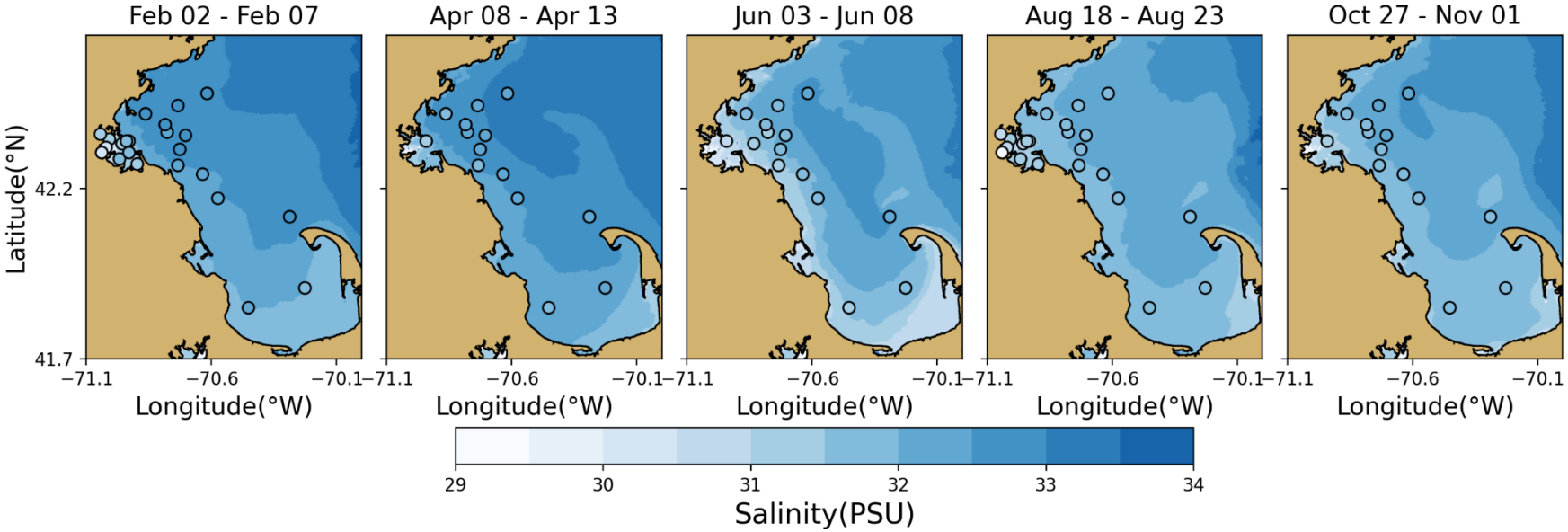


*Figure 4-9 Salinity spatial structure, at/near seafloor, model-observation comparison.*

*Model results: background. MWRA vessel-based survey observations: symbols. Model results are averaged over the 5-day period centered on the measurement date.*

### 4.2.3 Continuous measurements of temperature and salinity

Continuous hourly measurements were available from Mooring A01 at multiple depths. This station is located south of Cape Ann, northeast from MWRA station F22. To provide a more complete assessment of the model-observation comparison in time, time series for this station are presented in Figure 4-10. For three depths (1m, 20m and 50m) the simulated and observed temperature and salinity are given. This is also done for the vertical temperature and salinity difference between 1m and 20 m as well as 1m and 50 m, as a measure of stratification. In the measurements some outliers were present, visible as spikes in the salinity and bottom temperature.

The time series compare well, showing that the model captured the strength and timing of the seasonal cycle of temperature and salinity, as well as the stratification of these quantities. Furthermore, many observed event-based changes in stratification on timescales of days to weeks occurred in the model. The simulated temperature was slightly better represented than the salinity. The bias of 0.25-0.5 PSU more saline water in the simulation, throughout the water column as explained in Deltares (2021), is clear in the second frame of the figure; no such bias occurs for the salinity stratification (fourth frame). The model-observation difference of the bottom temperature gradually increased during summer to an underestimation of about 2°C. After the sudden mixing event in early October this underestimation did not persist. Overall, the model captures features of observed stratification well, as is important for the water quality simulation because stratification is a main influence on vertical transport.

### 4.2.4 Continuous measurements of non-tidal currents

For Mooring A01, observed currents were available as well, although surface currents in the first five months of 2019 were missing. In Figure 4-11 and Figure 4-12 a model-observation comparison is presented for the first and second halves of the year, respectively. In the top frame, time series of wind from the meteorological product used to force the model is given for context. In the frames below, simulated and observed time series of non-tidal currents at four depths (2m, 10m, 22m and 50m) are given alternately. To remove the tidal variability, time series have been filtered using a low-pass filter with a 33h filter half amplitude (Alessi, 1985). The resulting signal consists mainly of weather-related and seasonal changes. For plotting this has been subsampled to a 6h resolution.

The time series of the filtered wind shows wind in all directions. Winds were generally changing on timescales of several days. In general, the wind speeds were lower during the calmer summer months. Winds included a dominantly eastward component year-round, with a mostly southward component in winter and a dominant northward component in summer.

The simulated and observed non-tidal currents showed a similar pattern with a prevailing direction to the south and west. The simulated currents showed less variability in direction than observed, but the order of magnitude of their amplitudes was similar. For the first five months, no observations of surface currents were available. However, effects of storm events were visible at 10m depths, where the model and observations were similar. The model-observation difference throughout the year was small. This model-observation comparison at a specific location is a challenging test of the hydrodynamic simulation performance. The agreement between the two was sufficient to conclude that the representation of processes in the hydrodynamic model was adequate to support water quality modelling.

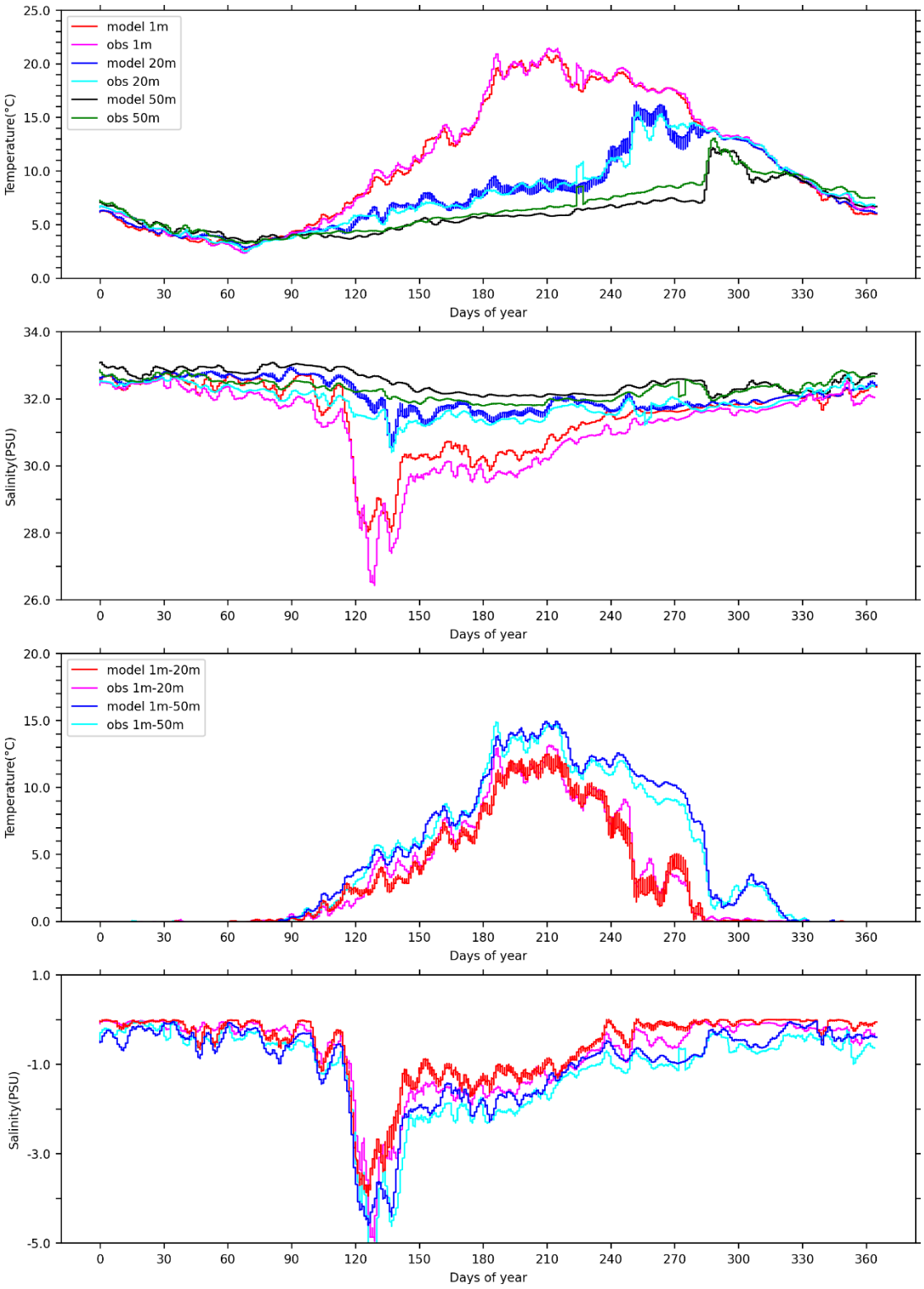


*Figure 4-10 Time series Mooring A01 temperature/salinity model-observation comparison (3-day means), three depths and two stratification levels.*

*Temperature (upper frames), salinity (lower frames).*

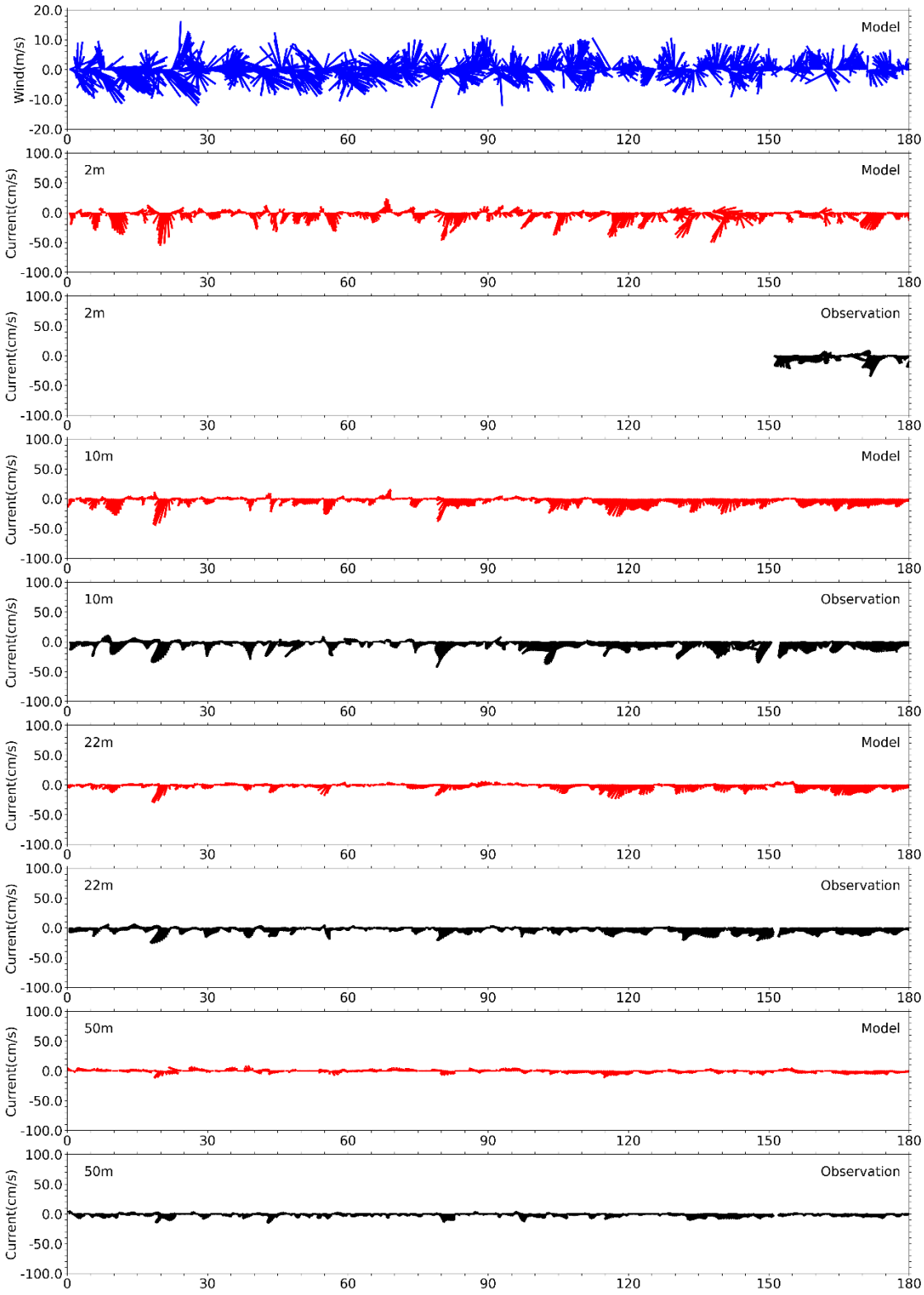


*Figure 4-11 Currents time series model-observation comparison, Jan – Jun.*

*Sticks point in the direction of flow, away from zero line; north/eastward flow up/rightward.*

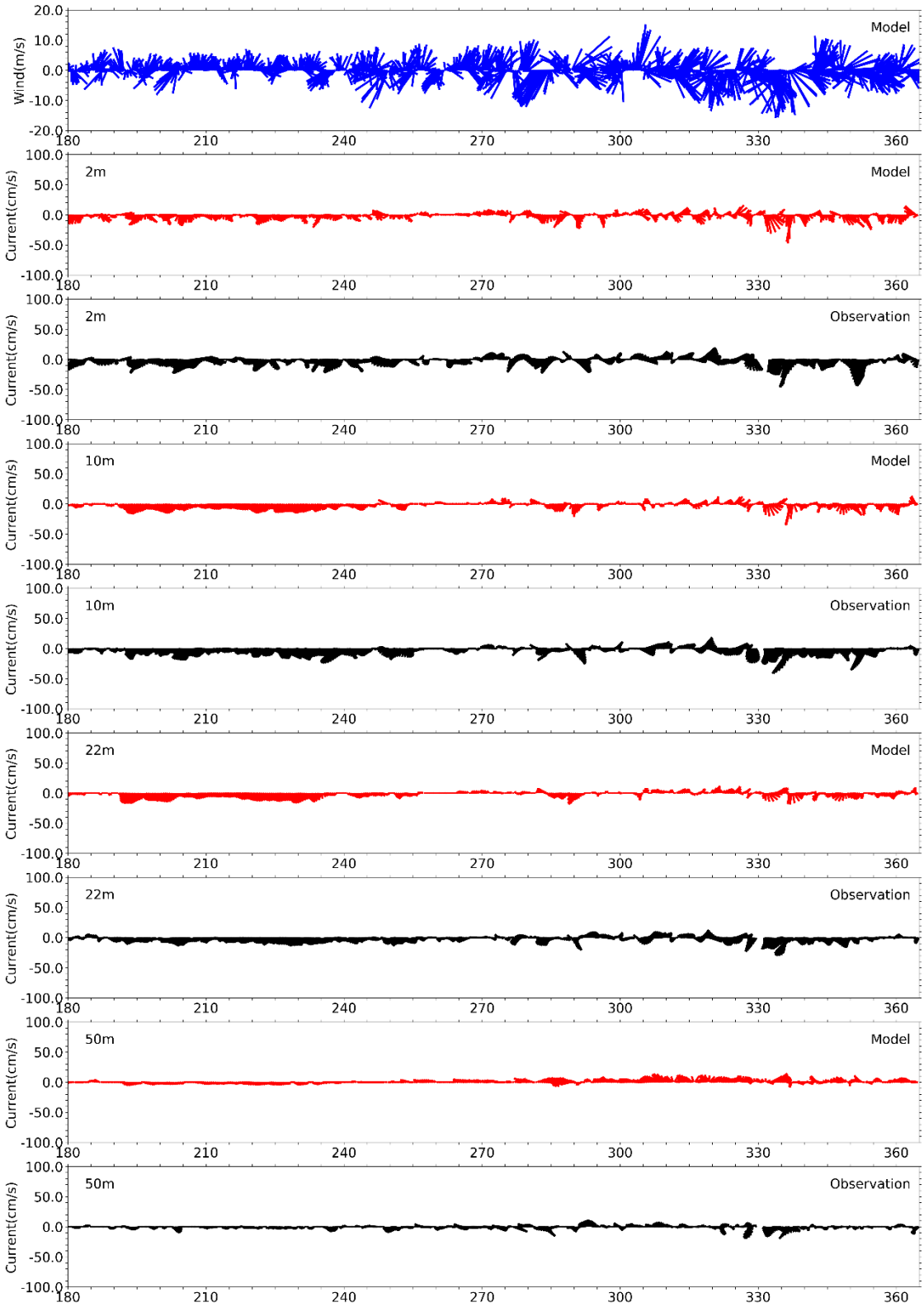


*Figure 4-12 Currents time series model-observation comparison, Jul – Dec.*

*Sticks point in the direction of flow, away from zero line; north/eastward flow up/rightward.*

## 4.3 Model monthly-mean circulation

Figure 4-13 and Figure 4-14 present the simulated monthly-mean currents at the surface and at a depth of 15 m. Flow was largely consistent with the general circulation pattern recognized to hold (Figure 1-1).

This schematic pattern was most apparent in the residual surface currents between January and August and in December. In September and October residual currents off Cape Ann were weak and in November residual currents at Cape Ann were directed to the east. Surface currents were largest off Cape Ann and Cape Cod with the largest magnitudes from May and June, reaching up to 0.30-0.35 m $s^{-1}$. Residual currents within Massachusetts Bay were strongest in May with magnitudes up to 0.20 m $s^{-1}$ near North Passage and South Passage. The north-eastward currents in North Passage in November did not exceed 0.15 m $s^{-1}$.

In general, the circulation pattern at 15 m depth (Figure 4-14) was somewhat similar to the general circulation pattern of Figure 1-1, including a flow directed into northern Massachusetts Bay from offshore, and changed little from month to month. Current magnitudes were lower than at the surface, with maxima in May of up to 0.30 m $s^{-1}$ at Cape Cod. Within Massachusetts Bay, residual currents were smaller than at the surface, reaching up to 0.20 m $s^{-1}$ at North Passage. In Cape Cod Bay, residual current magnitudes at this level were weaker, due to its limited depth and sheltered geometry.

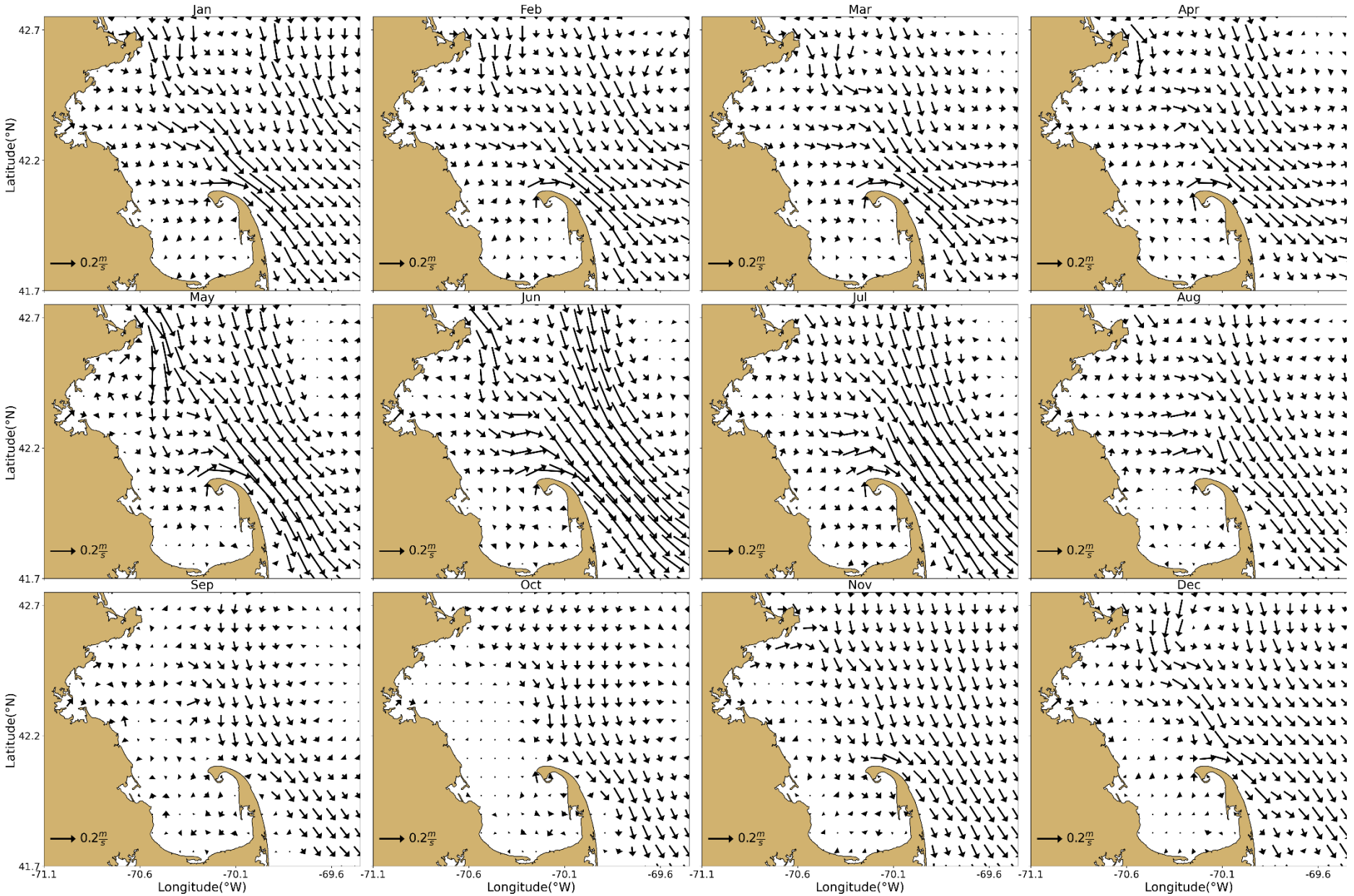


*Figure 4-13 Model currents, monthly-mean spatial structure, at sea surface.*

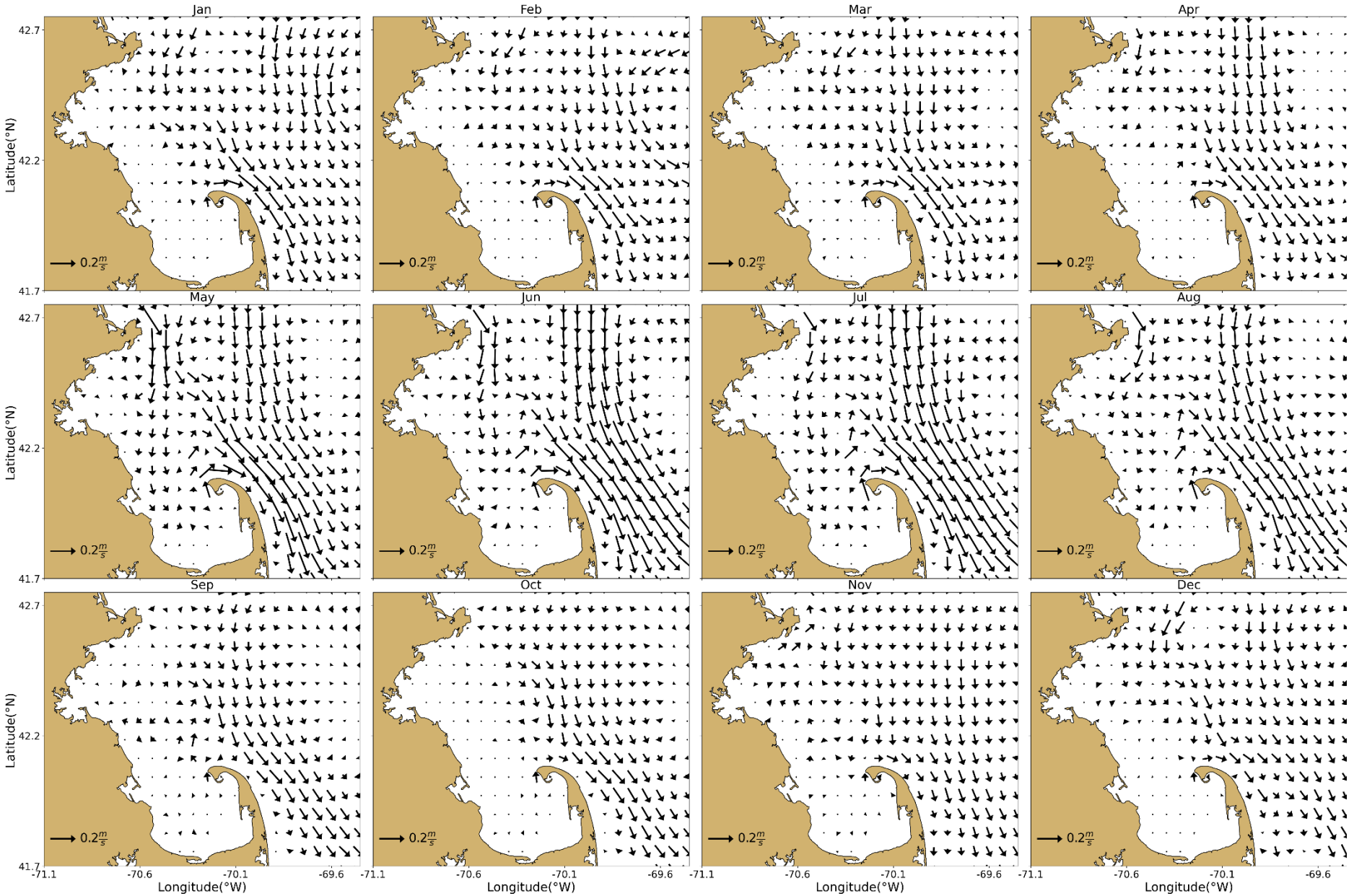


*Figure 4-14 Model currents, monthly-mean spatial structure, 15 m deep.*

# 5 Water Quality Model

In this section the performance of the water quality model is discussed, and its results are compared to measurements.

## 5.1 Verification of model performance

To demonstrate that the model performance during 2019 was comparable to the performance for the calibration and validation period 2012-2016, skill metrics were calculated and plotted on Taylor diagrams as in Section 4. Station N21 directly on top of the outfall was excluded, as a comparison to field data is of limited value for this station, as discussed by Deltares (2021). Information on how to interpret Taylor diagrams can be found in section 4.1 (box “How to read a Taylor diagram”).

Taylor diagrams are plotted for the light extinction coefficient and dissolved inorganic nitrogen (DIN) in Figure 5-1, and for chlorophyll a and dissolved oxygen (DO) in Figure 5-2. These parameters were selected because they are key drivers of ecosystem functioning. Statistics for the period 2012-2016 are plotted on the left side and statistics for 2019 on the right side. For reference, the 2017 simulation report (Deltares, 2022a) provides, in its Appendix A, similar diagrams for the individual years 20212-2016. The plots show statistics for three clusters of monitoring stations: Northern Bay stations (F22, N01, N04, N07, F10, N18, F15, F13 and F23), Southern Bay and Cape Cod stations (F06, F29, F01 and F02) and harbor stations (024, 140, 142, 139 and 124) (see Figure 2-4 for station locations).

Extinction skill metrics (Figure 5-1) for 2019 show slightly higher correlations and lower unbiased RMSE errors than for 2012-2016, while 2019 correlations are relatively weak. While variability at some Northern stations was overestimated for the period 2012-2016, and in annual runs for 2017 (Deltares, 2022a) and 2018 (Deltares, 2022b), in 2019, extinction variability is mostly underestimated at many observation stations (except for stations F13 and F01).

Skill metrics for DIN (Figure 5-1) for 2019 show better correlations than 2012-2016 for near-surface concentrations at most Northern and Southern stations. However, at Southern stations the model overestimates variability near the surface more than previous years, probably due to low observed winter concentrations, for example at station F02. Bottom concentrations at Northern stations show weak correlations compared to those in 2012-2016, leading to higher unbiased RMSE errors. Skill metrics at the harbor stations are similar to those for 2012-2016.

Skill metrics for chlorophyll a (Figure 5-2) include smaller dimensionless unbiased RMSE errors than in 2012-2016, mostly because of a smaller simulated variability than observed. This is similar to the 2017 and 2018 results and was diagnosed as a result of the low sampling frequency in combination with the highly transient character of algae blooms (Deltares, 2022a). Moreover, the underestimation of chlorophyll a variability in 2019 is most likely due to the fact that the model does not reproduce a phytoplankton bloom observed in September, as noted below.

DO skill metrics (Figure 5-2) for 2019 show slightly lower correlations and higher unbiased RMSE errors at the Northern stations, near the surface and seafloor, compared to the period 2012-2016.

Overall, the figures presented here serve to verify that the performance of the water quality model in the simulations of 2019 does not deviate substantially from the validation period 2012-2016.

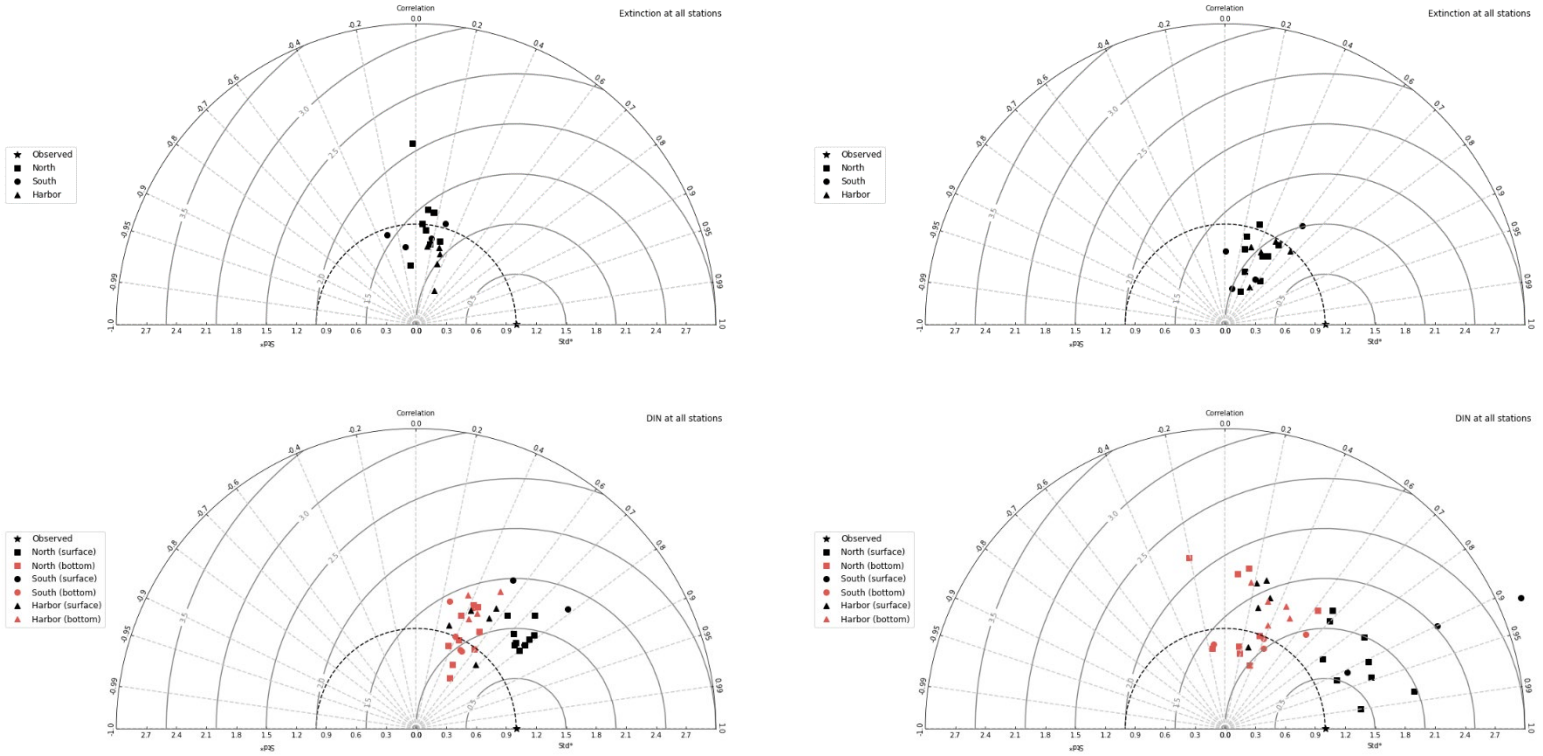


*Figure 5-1: Taylor diagrams for MWRA vessel-based survey observations. Top panels show the parameter Extinction and bottom panels Dissolved Inorganic Nitrogen. Left panels show results for the simulation period 2012-2016 and right panels for the year 2019.*

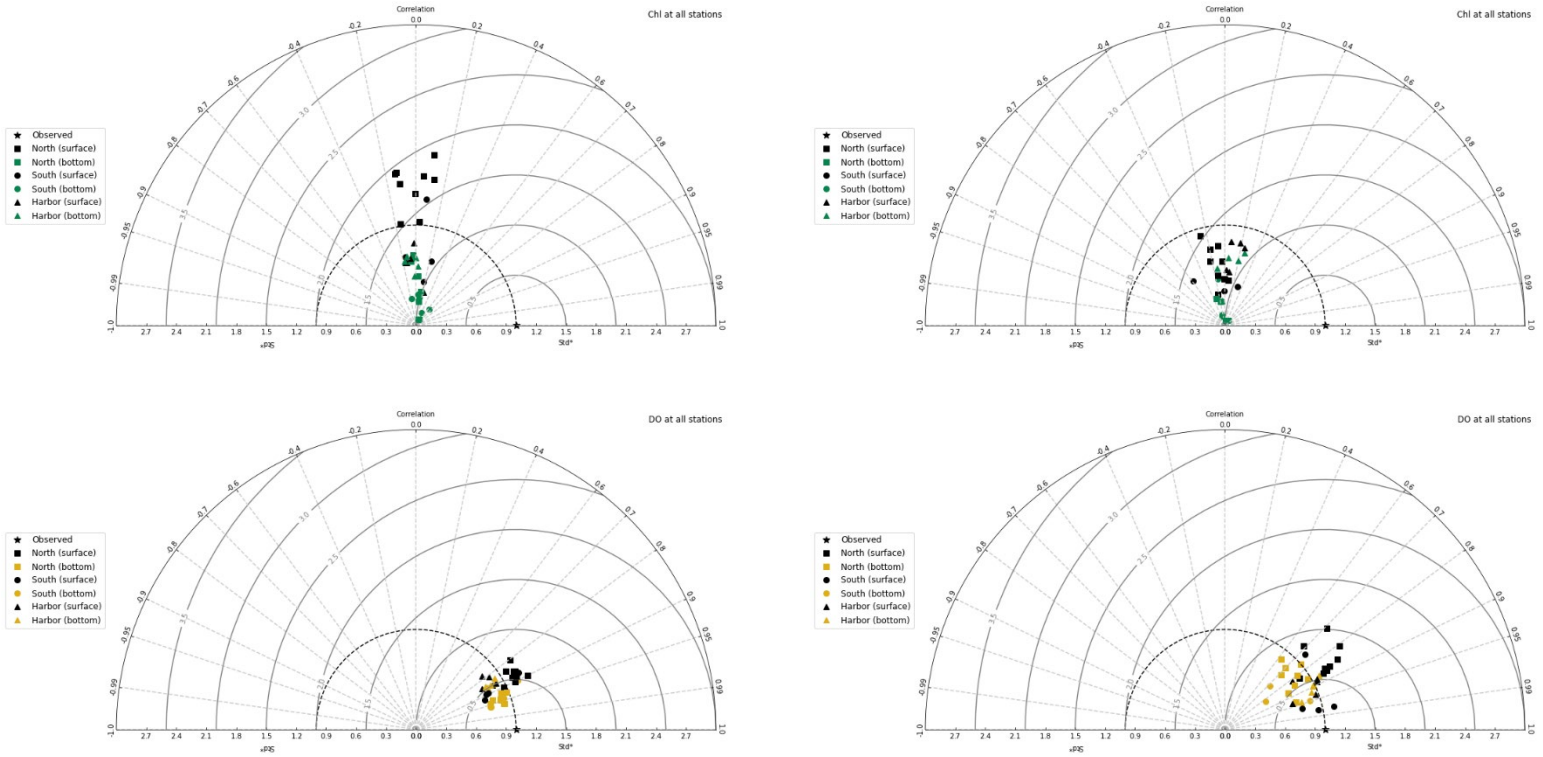


*Figure 5-2: Taylor diagrams for MWRA vessel-based survey observations. Top panels show the parameter Chlorophyll-a and bottom panels Dissolved Oxygen. Left panels show results for the simulation period 2014-2018 and right panels for the year 2019.*

## 5.2 Model-observation comparisons

In this section model-observation comparisons in the same format as for the hydrodynamic model (Section 4) are provided. For time series plots, a 3-day moving average is applied to the model outputs to smooth high-frequency variability.

To assess the simulation spatially, vertical transects have been plotted along North-South (N-S) and West-East (W-E) transects (Figure 2-4). Model results in these figures are 5-day averages centered around the field sampling date indicated in each plot.

### 5.2.1 Light extinction

Measured extinction for the year 2019 (Figure 5-3) ranged from 0.1 to 0.6 at all stations, except at F23, near the harbor, where it ranged between 0.2 and 0.9. These values are slightly higher than for previous years. Spatial differences were however similar to previous years for which higher and more variable extinction was observed at harbor stations (e.g. Zhao et al., 2017). The model reproduced the extinction fairly well, but slightly underestimated highest values at most stations. The model predicted lower extinction in winter than during the rest of the year, in association with lower particulate organic carbon (POC) levels.

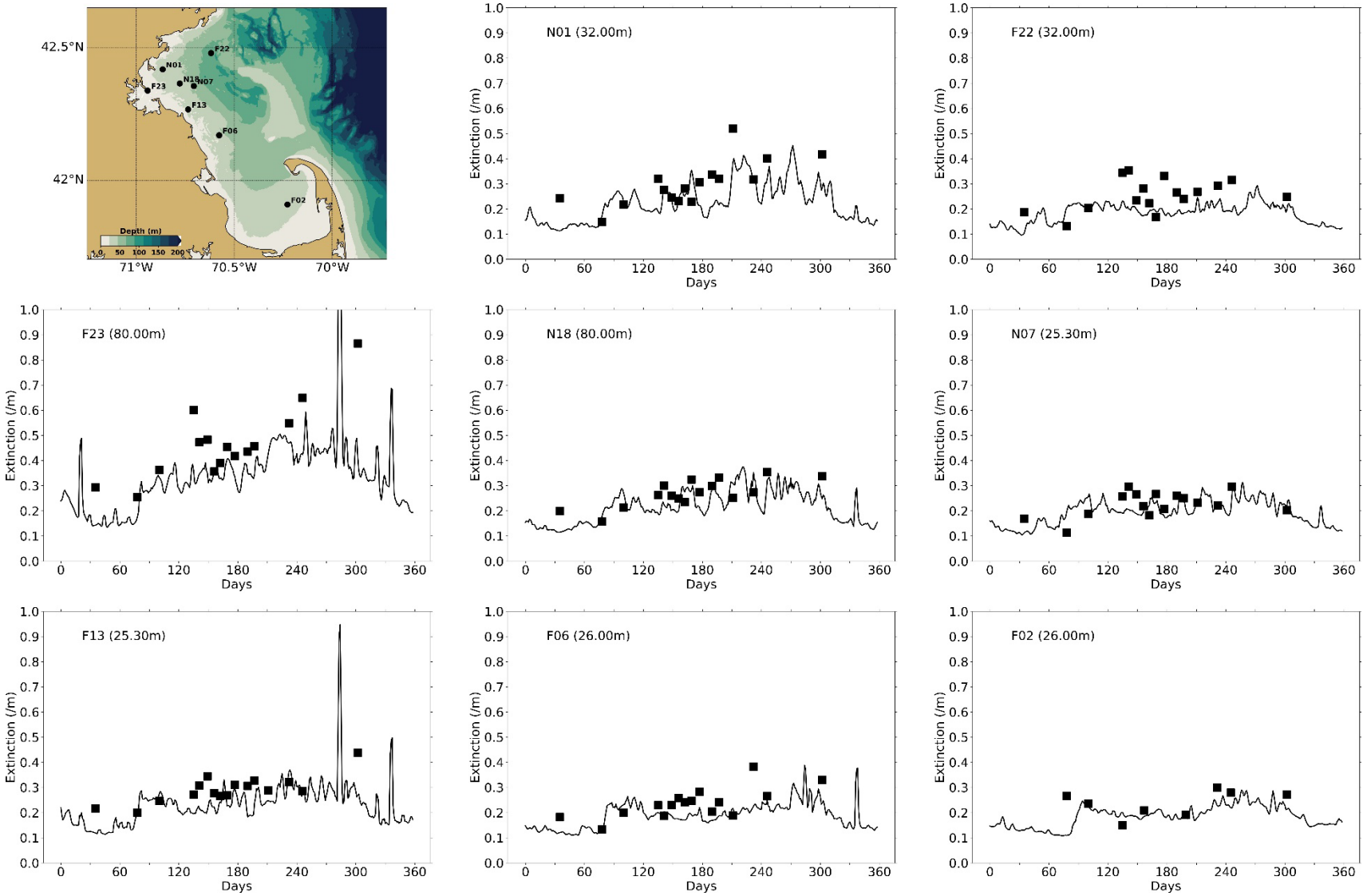


*Figure 5-3: Extinction time series, model-observation comparison for 2019. Model: lines. MWRA vessel-based survey observations: symbols.*

### 5.2.2 Dissolved inorganic nitrogen

Seasonal variations of surface and bottom DIN concentrations in 2019 were overall similar to those observed and simulated for previous years (Figure 5-4). Surface and bottom were comparable in winter, when the water column was well mixed. Surface DIN concentrations declined in March and April and were depleted throughout the rest of spring and summer, before increasing again in fall. Bottom concentrations declined to a much lesser degree in spring and summer. The model generally reproduced these observed seasonal variations and vertical differences. At stations N01, F23, F13 and F06, bottom concentrations were, however, overestimated during summer (July-September). This is likely related to the fact that the model did not reproduce a large observed bloom of phytoplankton (dinoflagellates) which occurred in that period. Winter DIN concentrations in Cape Cod Bay (F02) were also underestimated, which could also be related to the underestimation of phytoplankton biomass in the model (nearly-zero in the model, while about 6 µg $L^{-1}$ of chlorophyll a were measured). Observed variations at intermediate depths in the water column were also generally reproduced by the model (Figure 5-5).

According to the model results, the signature of the outfall in terms of DIN concentrations was visible all year round, leading to increased concentrations up to a distance of about 10 km or more (Figure 5-6). The increased DIN remained in the lower layers of the water column during the period of stratification (May-September). During the other months, the effluent led to an increase in DIN concentrations throughout the water column over the outfall (station N21). This was similar to simulations of previous years. In the model during stratified periods, the highest concentrations at N21 (directly over the outfall) were always simulated at the bottom of the water column, while highest measured concentrations were sometimes higher up in the water column (e.g. May 16th, June 6th, August 21st).

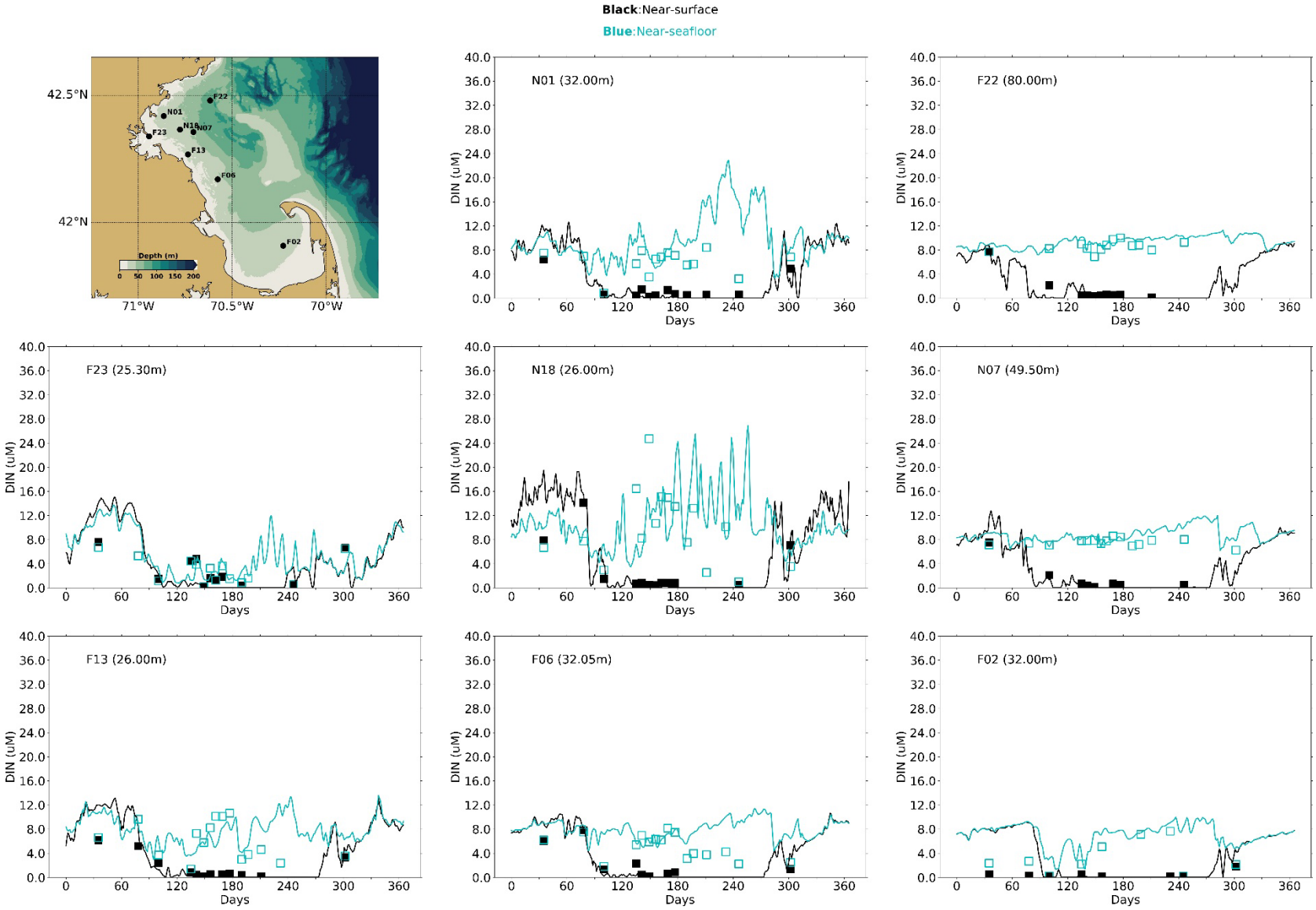


*Figure 5-4: Dissolved Inorganic Nitrogen time series, model-observation comparison near surface (black) and seafloor (cyan). Model results: lines. MWRA vessel-based survey observations: symbols.*

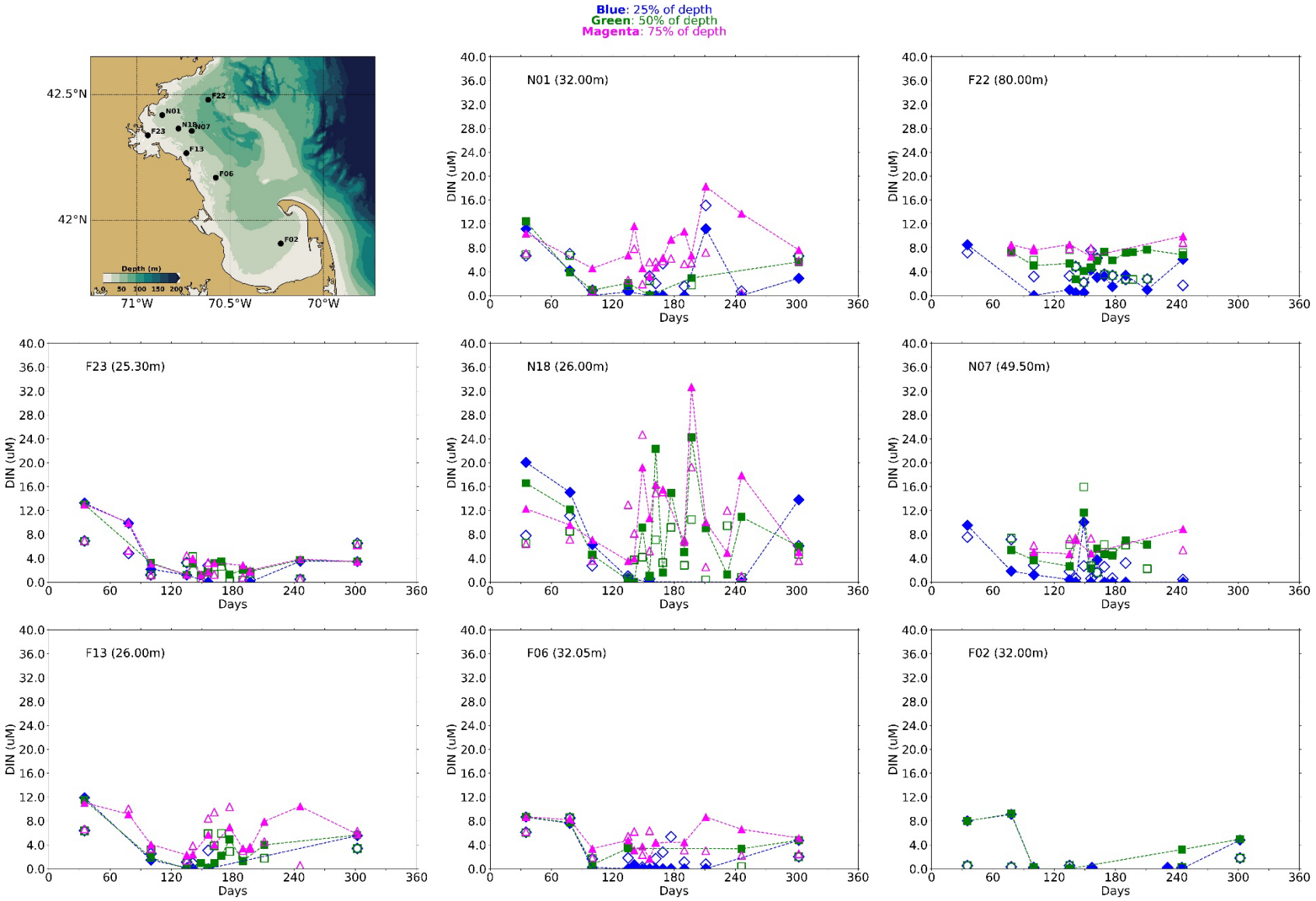


*Figure 5-5: Dissolved Inorganic Nitrogen time series, model-observation comparison within water column (between surface and seafloor). Model results: lines and full symbols. MWRA vessel-based survey observations: open symbols.*

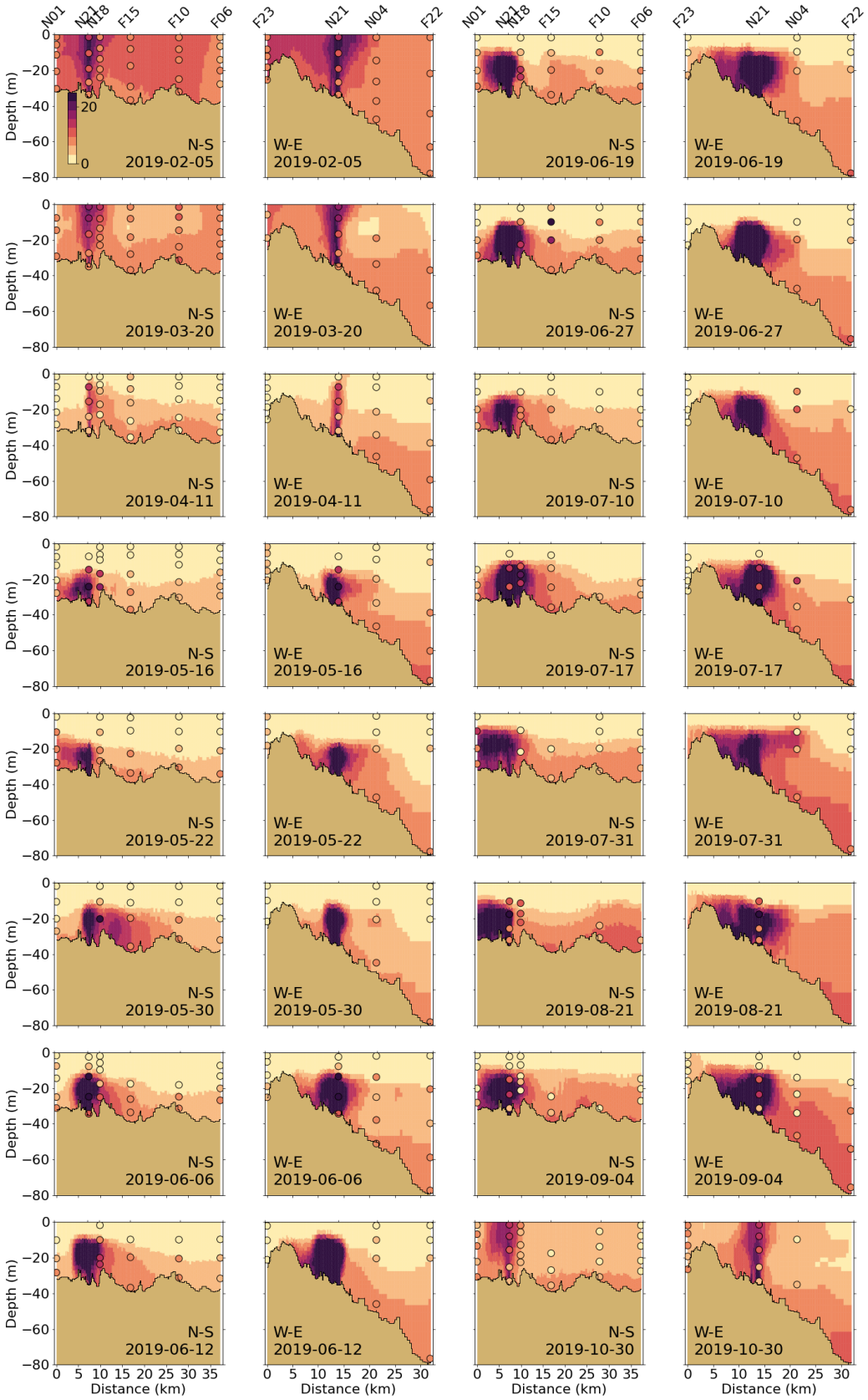


*Figure 5-6: Dissolved Inorganic Nitrogen (μM) for 2019 along North-South (N-S) and West-East (W-E) transects (Figure 2-4). MWRA measurements are plotted with round symbols. Model results are 5-day averages around sampling date.*

### 5.2.3 Chlorophyll a

Seasonal variations of chlorophyll a observations in 2019 showed increased values mostly in spring and fall (Figure 5-7), although the sampling frequency of the MWRA observations makes it difficult to see a clear seasonal pattern. Highest concentrations were observed in fall at all plotted stations. While for previous years, the largest chlorophyll a concentrations for the second half of the year usually occurred at the end of October or beginning of November, highest chlorophyll a values in 2019 were reported at the start of September. This is probably due to the fact that the peak in surface water temperature occurred earlier than in the previous years (in 2019 in July, compared to September in 2018). This end-of-summer-bloom is dominated by dinoflagellates, while fall blooms are usually diatom-dominated. The model does simulate a peak of dinoflagellate biomass in the end of summer (Figure 5-20), but most likely underestimates it. Moreover, in the BEM, the chlorophyll-to-carbon ratio for dinoflagellates is lower than that of diatoms, and the ratio for nutrient-limited ecotypes (here, the system was nitrogen-limited at the end of summer) lower than for light-limited ones. The observed chlorophyll a peak was therefore not captured by the model, which simulated higher concentrations during the fall bloom.

As in 2018, bottom chlorophyll a concentrations were very small at the deeper F22 station; and were closer to (or even higher than) surface concentrations at some other stations (F23, N18 and F02). As in the simulations for previous years, near surface simulated concentrations were in the same range as observations, except for September, but the detailed temporal variability was not always reproduced. This was to some extent related to the relatively low field sampling frequency and the high temporal variability. As in the simulations for previous years, simulated bottom chlorophyll a was underestimated at many stations. Chlorophyll a concentrations in summer and in the beginning of fall were underestimated at the observation stations at intermediate depths as well (Figure 5-7 and Figure 5-8).

Simulated chlorophyll a concentrations decreased eastward from the coast between May and September (Figure 5-9). Early spring increases occurred throughout the water column as it was relatively well mixed. During the months in which stratification occurred, simulated bottom chlorophyll a remained low and highest values occurred in the subsurface. The observations generally showed that chlorophyll a concentrations were highest in April and September. In these periods, high concentrations were observed up to about 30 m deep or more. The spring peak started too early in the model, with higher concentrations in March than were observed, and the high observed September concentrations were not captured by the model.

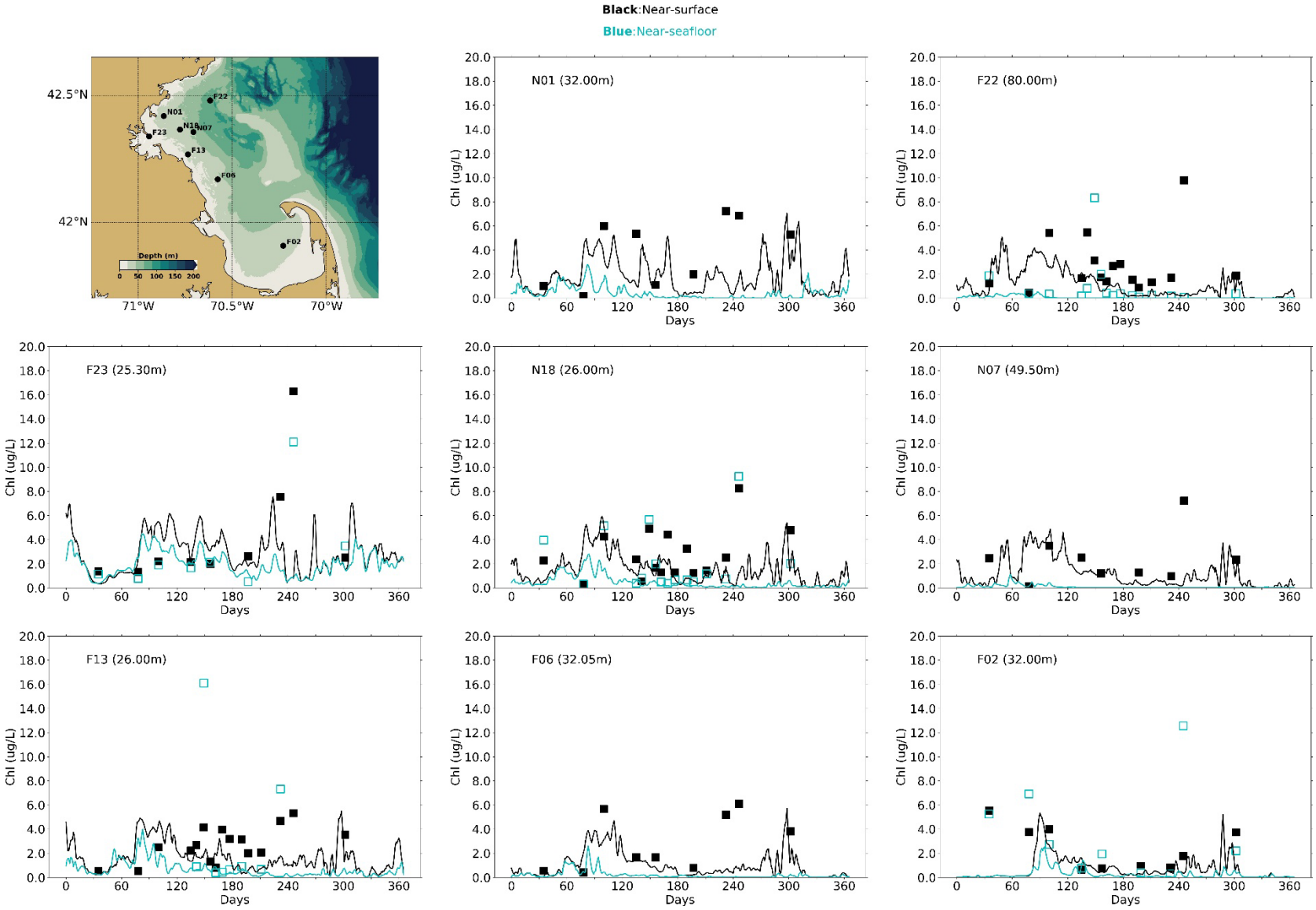


*Figure 5-7: Chlorophyll a time series, model-observation comparison near surface and seafloor. Model results: lines. MWRA vessel-based survey observations: symbols.*

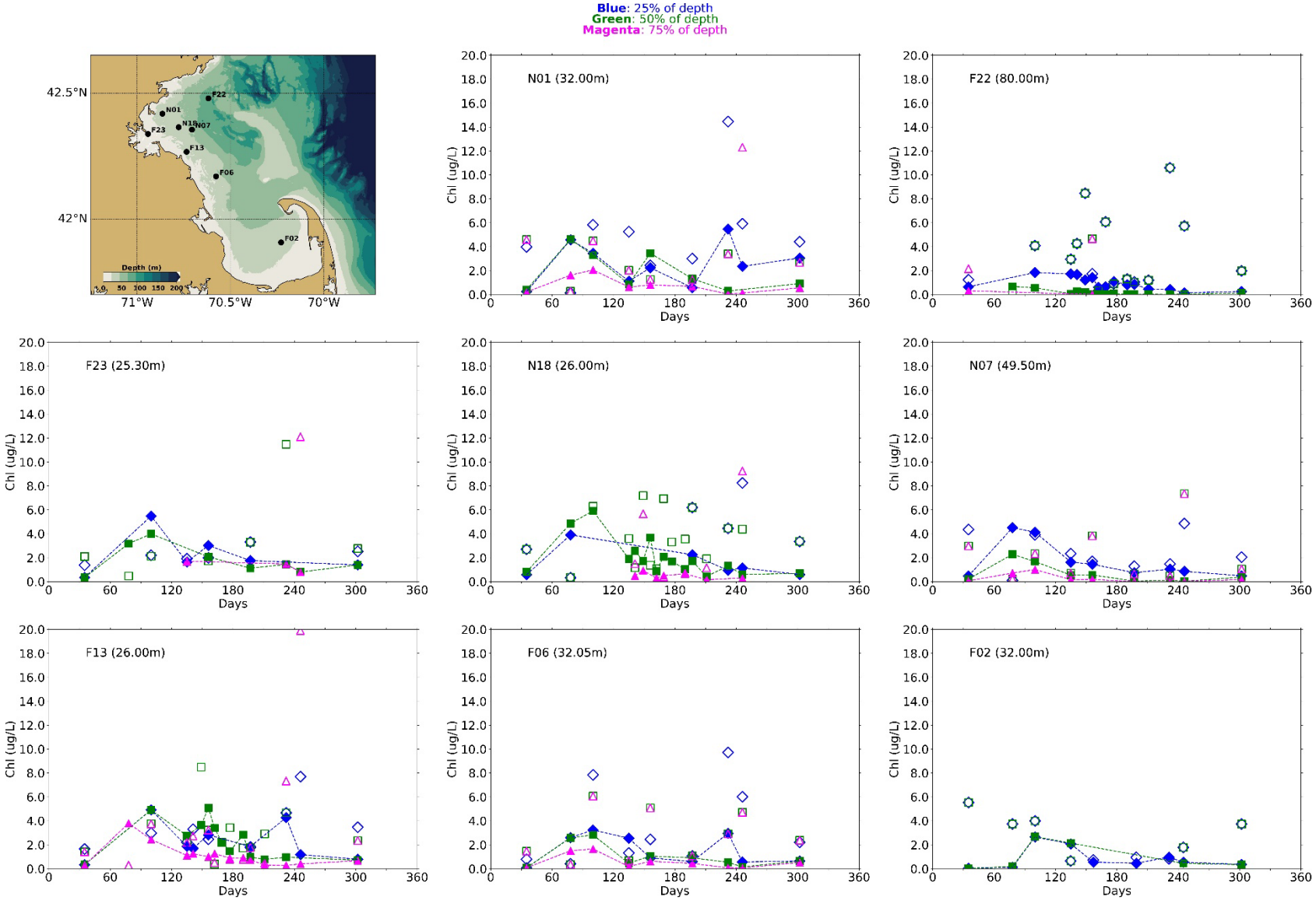


*Figure 5-8: Chlorophyll a time series, model-observation comparison within water column (between surface and seafloor). Model results: lines and full symbols. MWRA vessel-based survey observations: empty symbols.*

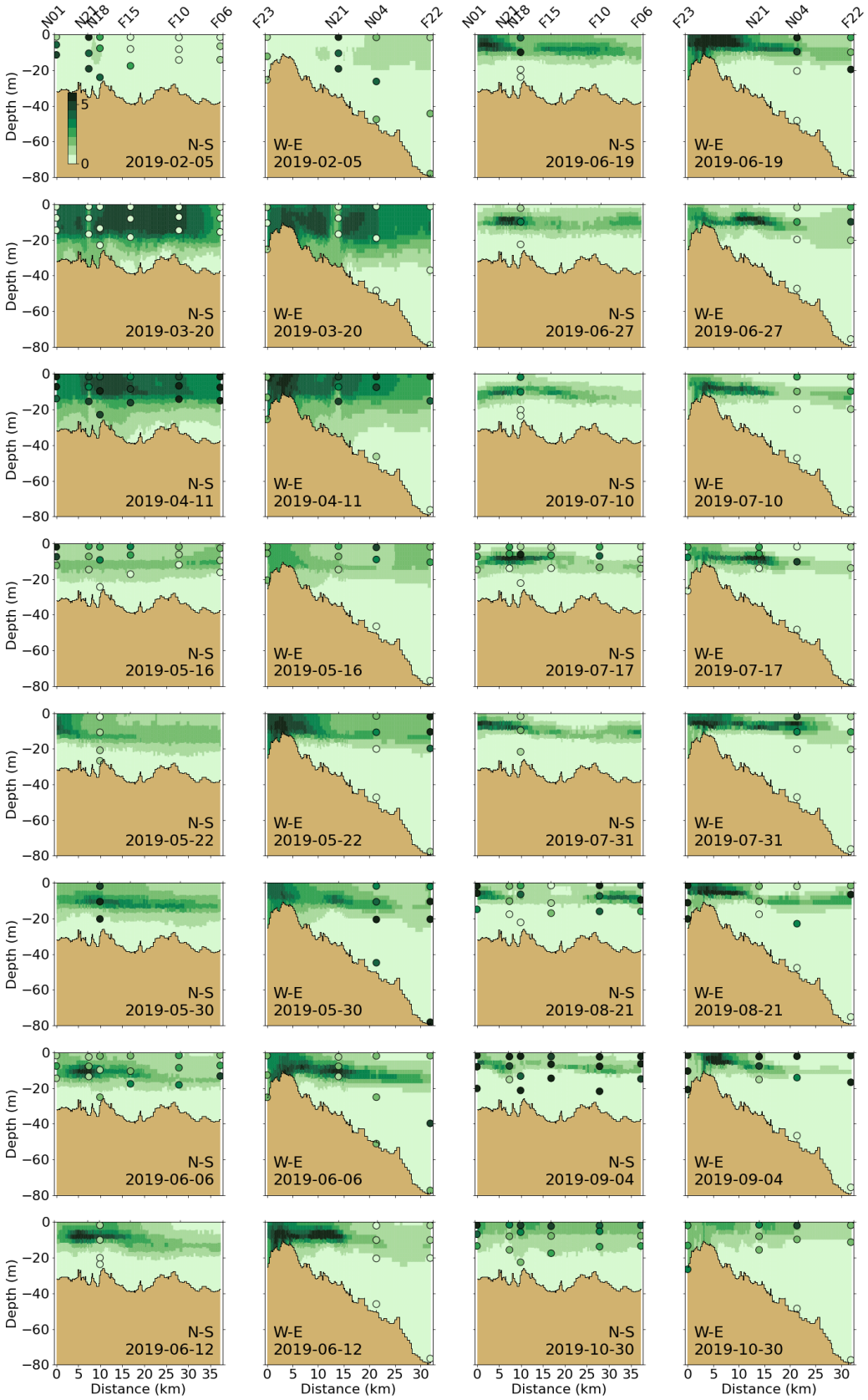


*Figure 5-9: Chlorophyll a (µg/L) for 2019 along North-South (N-S) and West-East (W-E) transects (Figure 2-4). MWRA measurements are plotted with round symbols. Model results are 5-day averages around the sampling date.*

### 5.2.4 Particulate organic carbon

POC concentrations at the observation stations were extremely variable and it was difficult to identify a clear seasonal pattern (Figure 5-10). Concentrations were, however, slightly lower in winter than the rest of the year. Among the plotted stations, POC concentrations were highest at F23, closer to the harbor, likely due to POC inputs from rivers. Concentrations were significantly lower near the bottom than at the surface.

The model generally captured POC concentration ranges, variability and vertical gradients at the plotted locations (Figure 5-10 and Figure 5-11). As in the 2018 simulation, POC concentrations were generally overestimated at F23, closer to the harbor. Peaks in POC concentrations measured at stations F22 and F06 in September were not captured by the model. This is probably related to the observed phytoplankton bloom during that period, which the model did not capture.

According to the model results, POC concentrations decreased from the coast eastward (Figure 5-12). The signature of the outfall was not visible along either the North-South or the West-East transects. This was consistent with the fact that the MWRA outfall only represented a small part of the total non-oceanic OC inputs to the study area (Figure 3-6). Highest simulated concentrations occurred in July and August, in the entire water column near the harbor and in the subsurface further from the harbor area. Highest concentrations were measured in August. In general, the observed concentration ranges, as well as horizontal and vertical gradients, were captured well by the model.

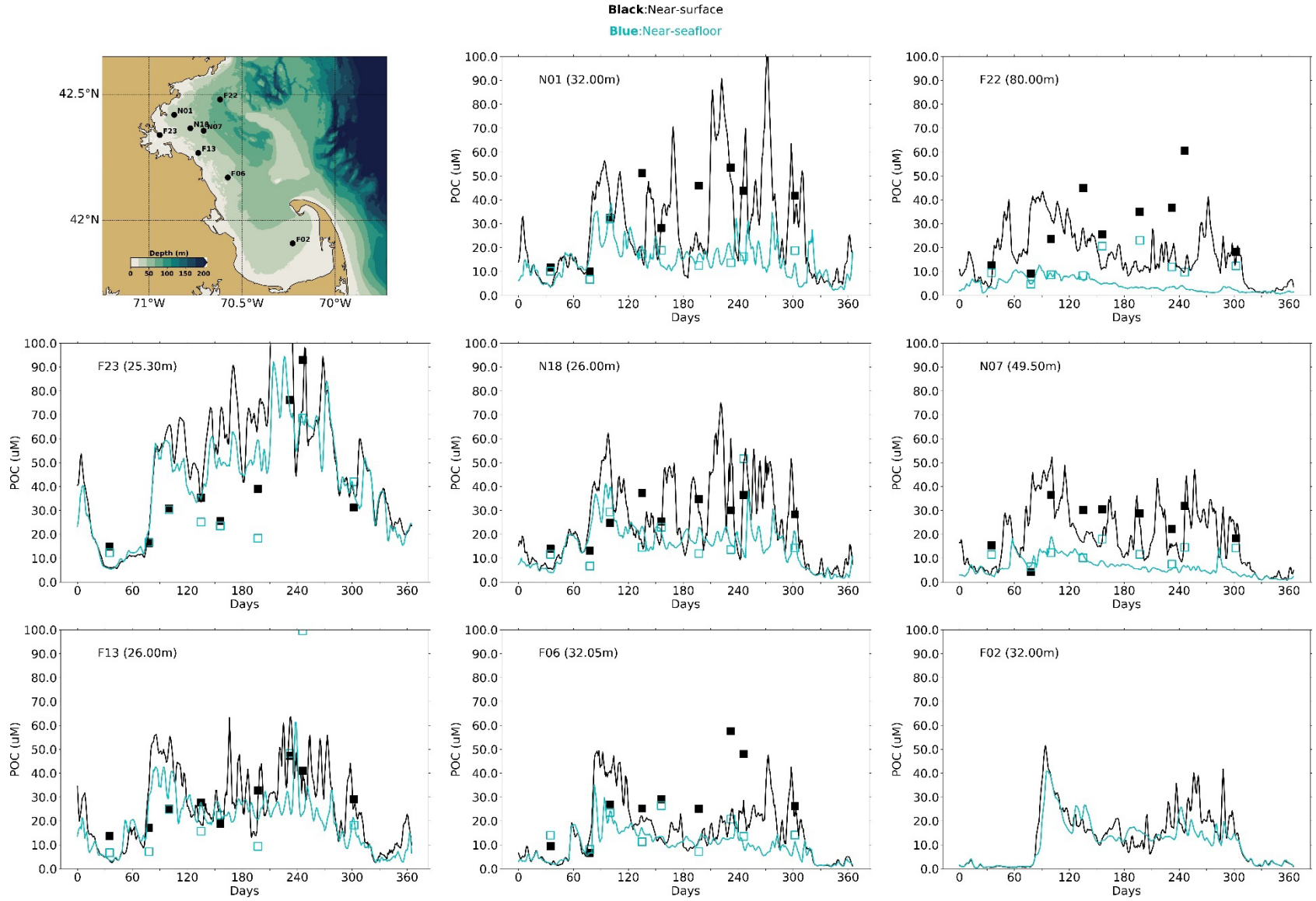


*Figure 5-10: Particulate Organic Carbon time series, model-observation comparison near surface and seafloor. Model results: lines. MWRA vessel-based survey observations: symbols.*

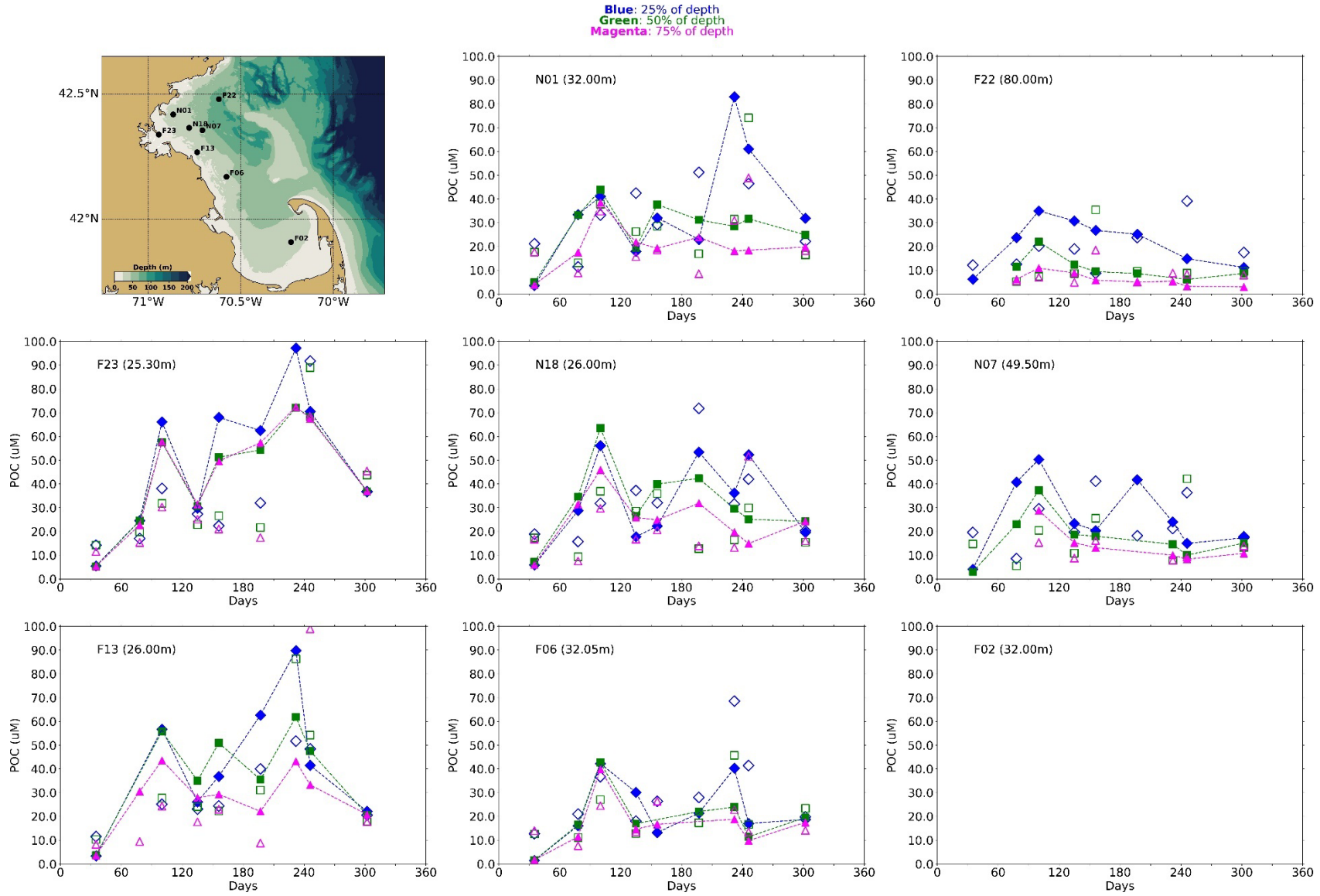


*Figure 5-11: Particulate Organic Carbon time series, model-observation comparison within water column (between surface and seafloor). Model results: lines and full symbols. MWRA vessel-based survey observations: empty symbols.*

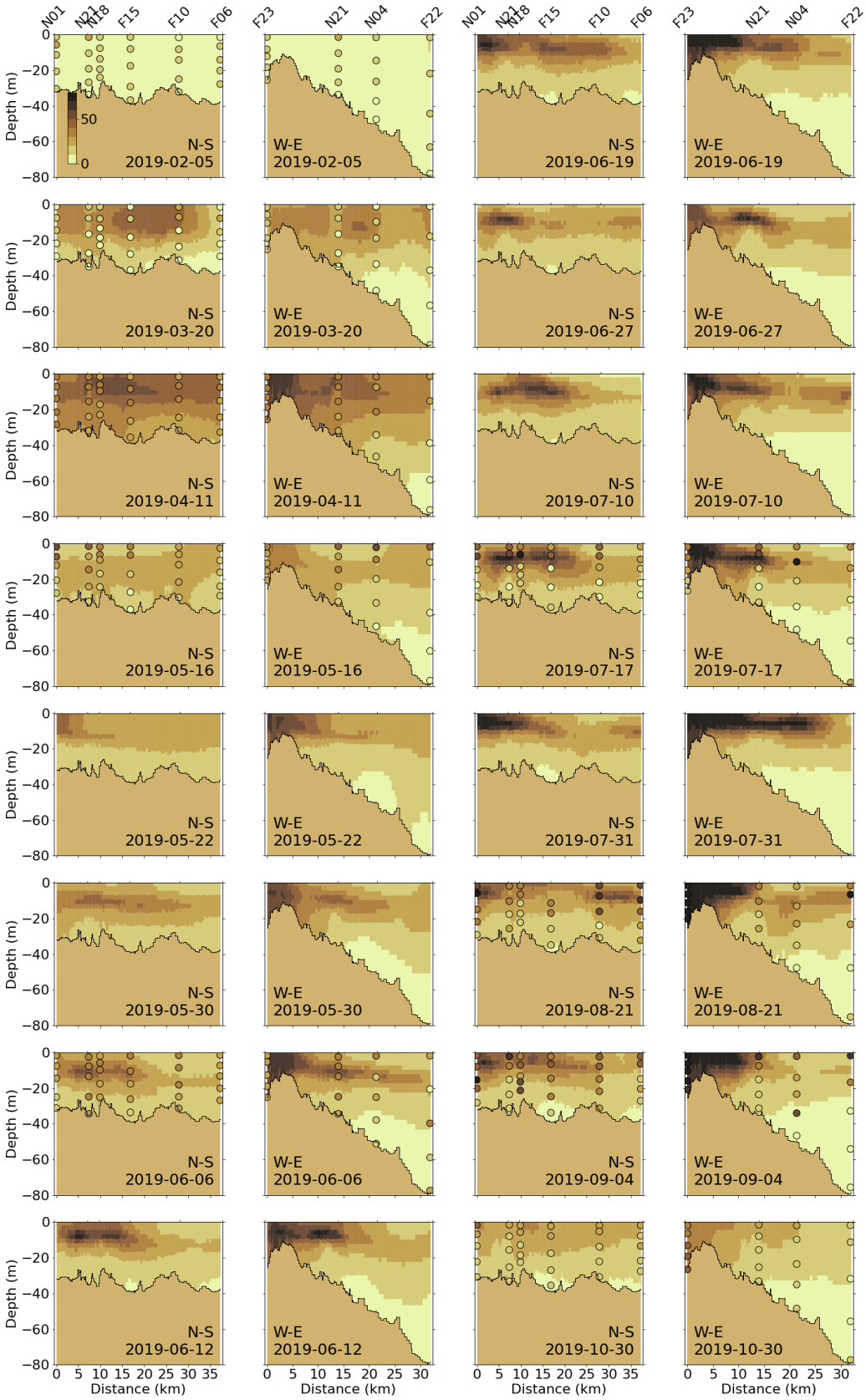


*Figure 5-12: Particulate Organic Carbon (μM) for 2019 along North-South (N-S) and West-East (W-E) transects (Figure 2-4). MWRA measurements are plotted with round symbols. Model results are 5-day averages around the sampling date.*

### 5.2.5 Dissolved oxygen

The observed 2019 seasonal patterns in measured DO concentrations were similar to previous years and well reproduced by the model, with maximum concentrations observed at the end of winter or beginning of spring and decreasing until fall before rising again (Figure 5-13). While winter concentrations at the surface and the bottom were comparable, bottom concentrations dropped lower in fall. Differences between top and bottom concentrations reached about 2-3 mg $L^{-1}$ at the end of October at several stations (N01, N07). The model reproduced these seasonal patterns well. As for previous years, the model reproduced minimum observed values at some stations, but not all. In May-June, differences between observed surface and seabed DO concentrations were larger than for previous years, with seabed concentrations 1-2 mg $L^{-1}$ lower than at the surface at all stations except for F23. The model does not capture this. In that period, the model slightly underestimated surface DO concentrations, while overestimating those at the bottom, simulating higher concentrations near the seabed than at the surface. The model-observation comparison at intermediate water depths showed similar behavior. For 2019, the model usually underestimated vertical gradients at intermediate depths (Figure 5-14).

At the A01 mooring station, the model reproduced the general seasonal pattern in the observed DO well, although it simulated a DO peak at the end of spring that did not appear in the measurements, and as in past years, slightly overestimated the end-of-fall minimum (Figure 5-15).

The North-South and West-East cross-section plots show that DO generally had weak vertical gradients (Figure 5-16). Concentrations were higher at the end of winter and beginning of spring and decreased until fall. Higher concentrations were observed and simulated in the subsurface in periods with higher primary production, for example June. In periods with visible vertical gradients in DO concentrations, the model captured the depth of highest DO concentrations well; amplitudes of DO concentrations in the growing season did not always coincide, due to mismatches between the timing of observed and simulated blooms.

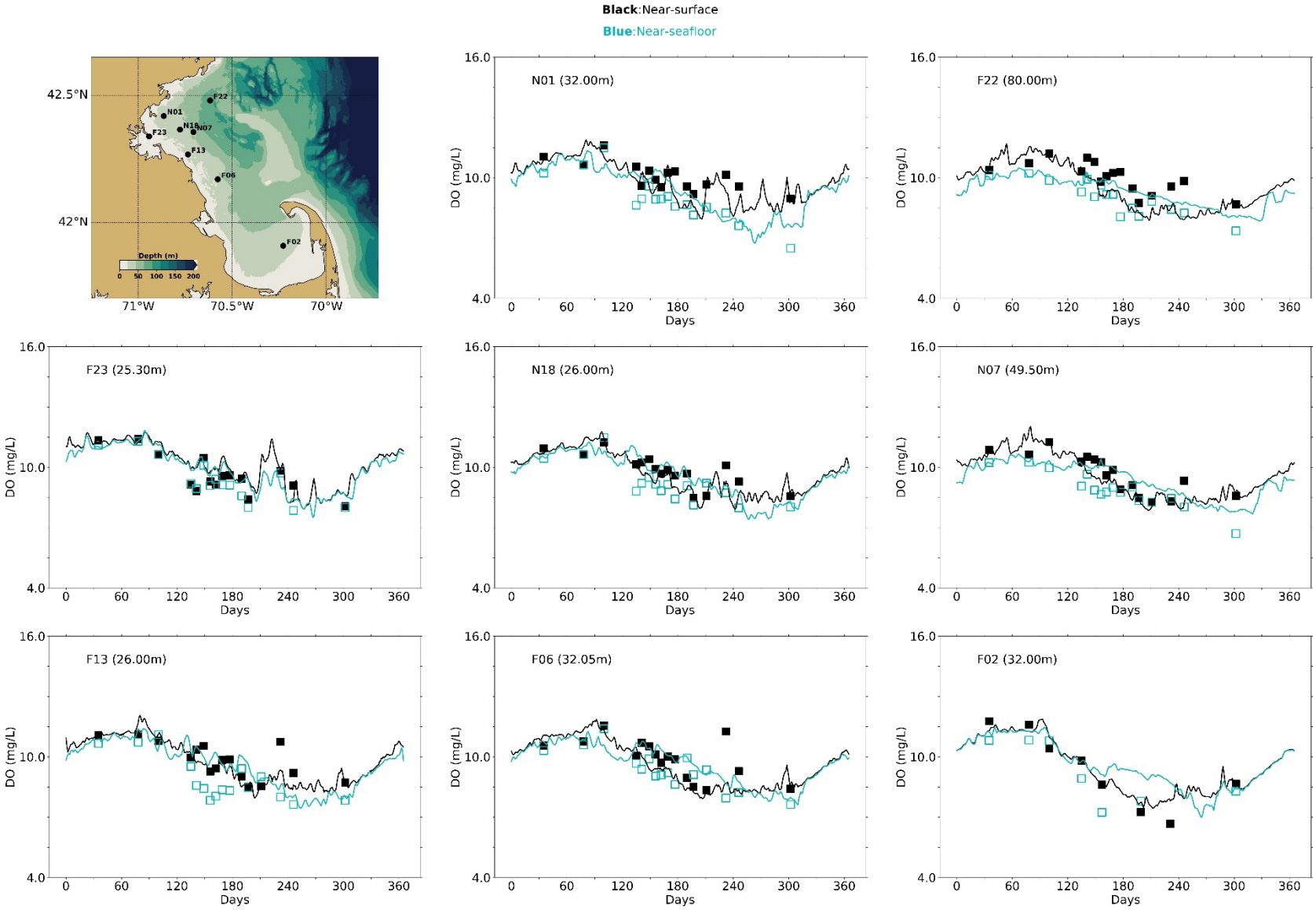


*Figure 5-13: Dissolved Oxygen time series, model-observation comparison near surface and seafloor. Model results: lines. MWRA vessel-based survey observations: symbols.*

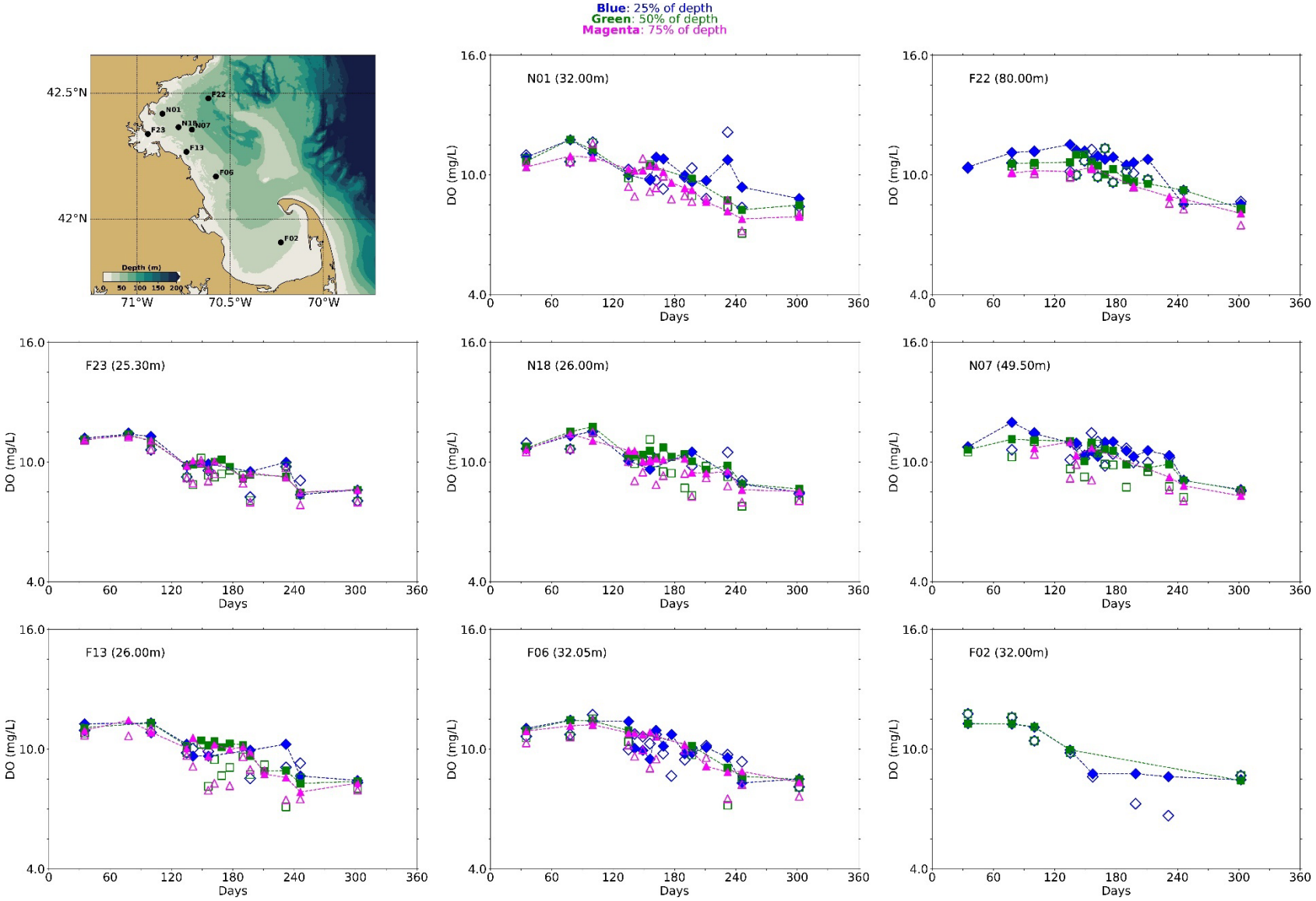


*Figure 5-14: Dissolved Oxygen time series, model-observation comparison in water column. Model results: lines and full symbols. MWRA vessel-based survey observations: open symbols.*

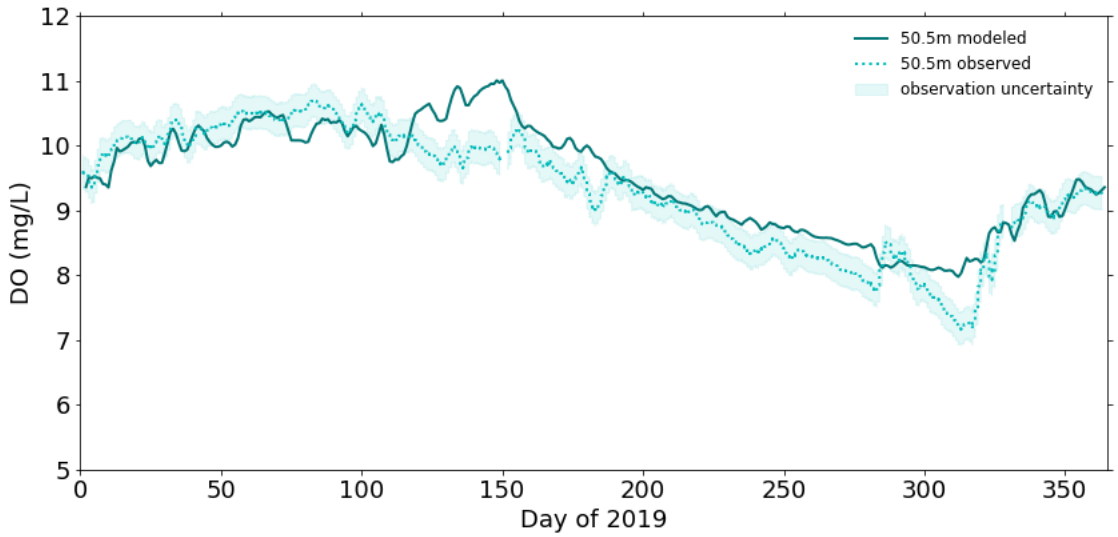


*Figure 5-15: Dissolved Oxygen time series 50.5m deep at A01 mooring site, model-observation comparison for 2019.*

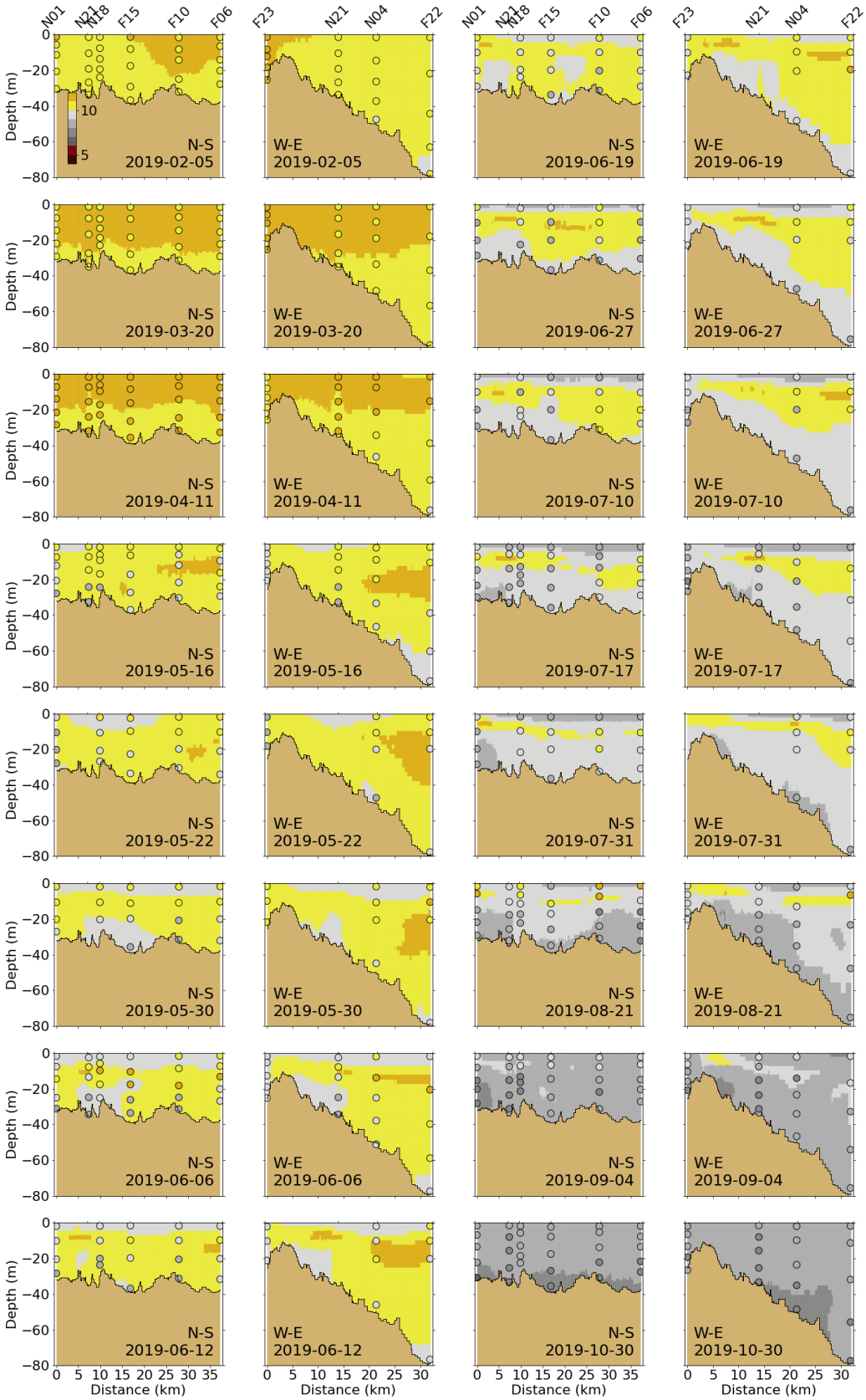


*Figure 5-16: Dissolved Oxygen (mg/L) for 2019 along North-South (N-S) and West-East (W-E) transects (Figure 2-4). MWRA measurements are plotted with round symbols. Model results are 5-day averages around the sampling date.*

### 5.2.6 Primary production

Simulated primary production was compared to historical measurements at three monitoring locations (Figure 5-17). Box whiskers represent the 9th, 25th, 50th, 75th and 91st percentiles of primary production observations over the period 1995-2010 (Keay et al., 2012). Simulated primary production for 2019 was in the range of historical measurements for the entire year at F23, N04, N18. It was also quite typical in comparison to the model validation years 2012 to 2016 (Deltares, 2021), with no exceptional peaks nor prolonged periods of exceptionally low production. As for the years 2012-2016, in 2019, simulated production at F23 was very low.

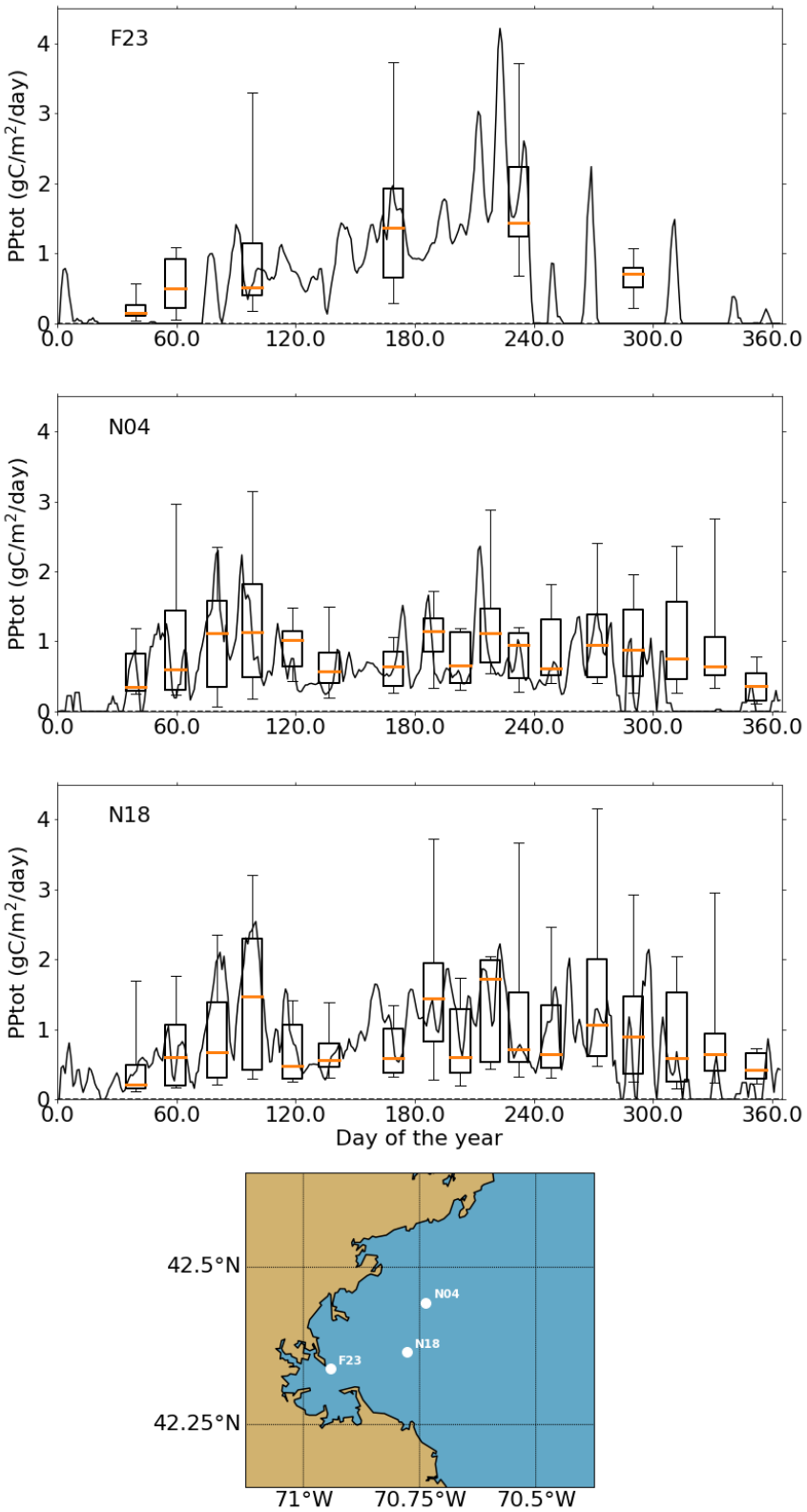


*Figure 5-17: Simulated (lines; 2019) and observed (box-whiskers; 1995-2010) primary production.*

### 5.2.7 Sediment fluxes

Sediment $NH_4$ fluxes (Figure 5-18) and sediment oxygen demand (Figure 5-19) outputs from the model were compared to measurements from the 2001-2010 period from Tucker et al. (2010) at stations located in Boston Harbor and Massachusetts Bay, using plots in the same format as Figure 5-17.

Simulated sediment fluxes were low in winter and peaked in the summer and early fall due to higher temperatures favorable to biogeochemical activity, which mineralizes organic matter in the sediment. Sediment fluxes were higher in the harbor area than in Massachusetts Bay, which was captured by the model. Results for the year 2019 were similar to those from the individual years 2012 to 2016. These were mostly in the range of historical measurements, except for $NH_4$ sediment fluxes at the Mass Bay stations (MB01, MB03 and MB05). This discrepancy is related to the simplified representation of sediment biogeochemical processes (see Deltares, 2021).

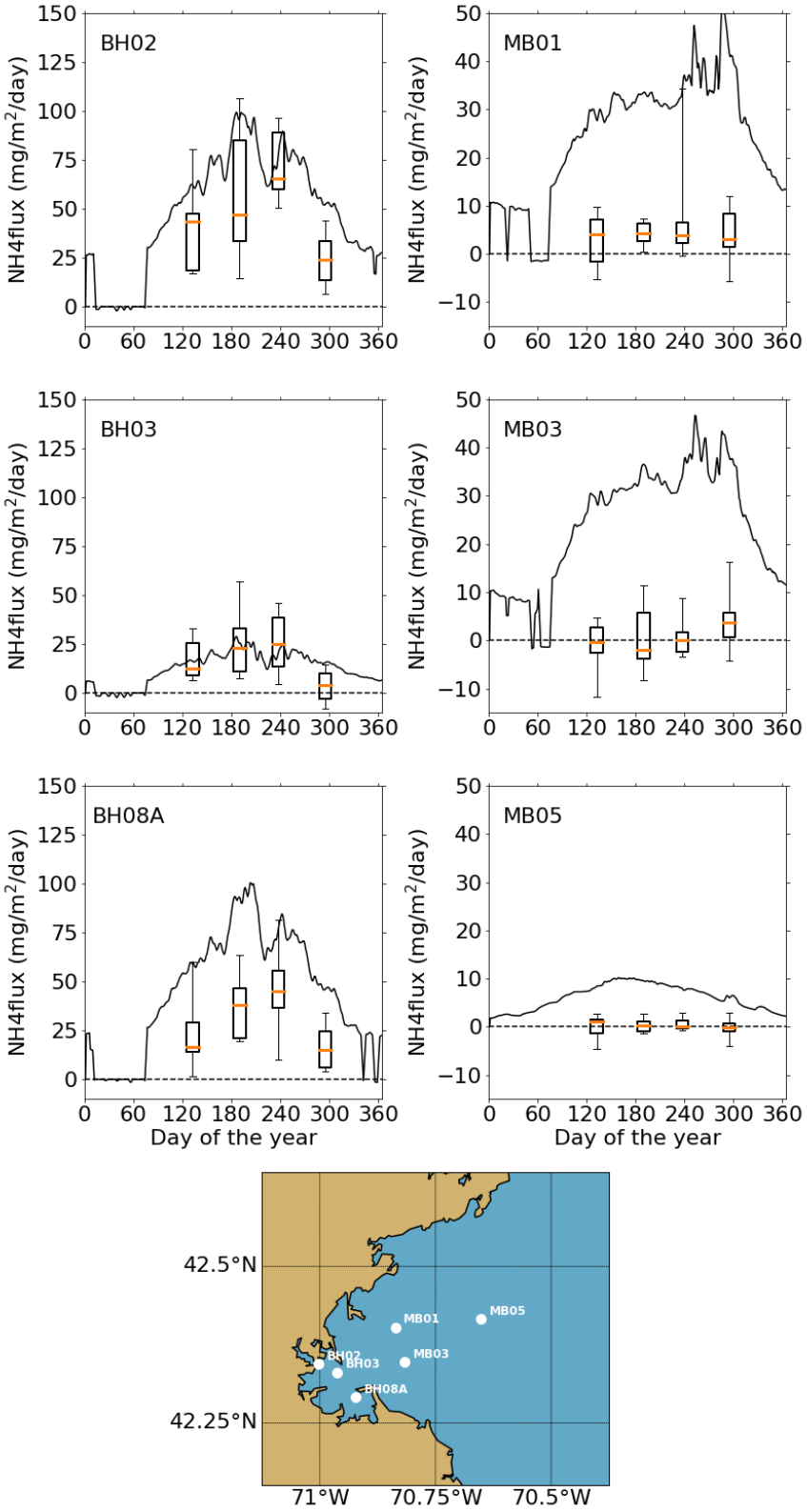


*Figure 5-18: Simulated (line; 2019) and observed (box-whiskers; 2001-2010) sediment flux of ammonium. Note change of scale between the Boston Harbor stations (left) and Mass Bay stations (right).*

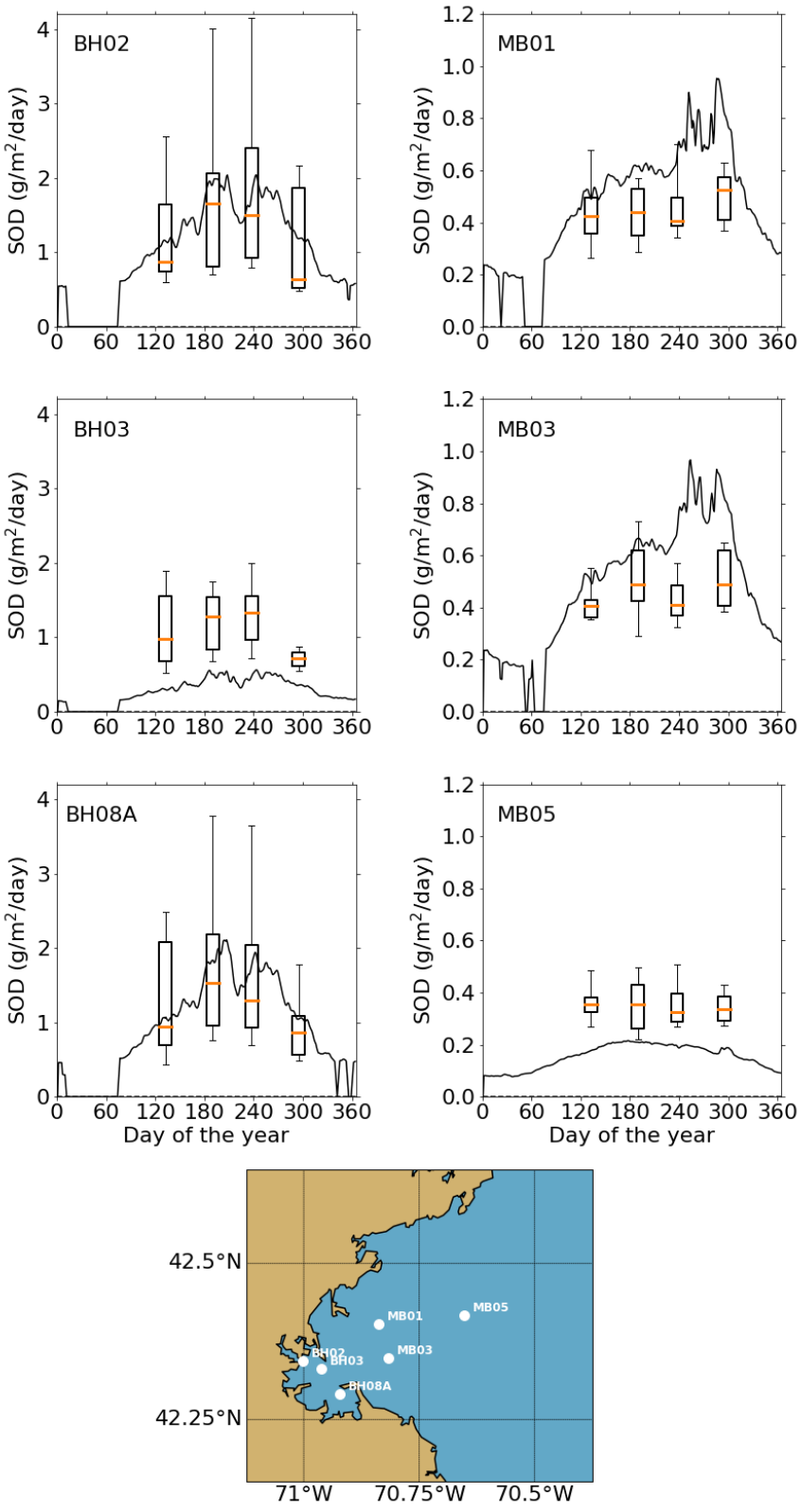


*Figure 5-19: Simulated (line; 2019) and observed (box-whiskers; 2001-2010) sediment oxygen demand. Note change of scale between the Boston Harbor stations (left) and Mass Bay stations (right).*

## 5.3 Phytoplankton community composition

Model phytoplankton community/species composition was not validated against field observations during model setup and calibration/validation. However, it is of interest to verify that its main characteristics in the model are not inconsistent with general patterns known to characterize the bays, based on monitoring observations.

The phytoplankton sub-module (BLOOM) simulated the dynamics of 4 functional groups and their adaptation to changing environmental conditions (i.e. light and nutrient limitation). BLOOM simulates the rapid shifts in phytoplankton communities due to these changes, using linear programming to optimize whole-community net primary production (Los, 2009). Simulated phytoplankton groups include: diatoms, dinoflagellates, other marine flagellates, and *Phaeocystis*. Their parameterization was initially based on that used in the North Sea eutrophication model (Blauw et al., 2009) and tuned during the BEM calibration process to better represent chlorophyll a as well as observed PON:POC ratios at MWRA monitoring locations (see Appendix B of Deltares, 2021).

Figure 5-20 shows the share of the different simulated phytoplankton groups in the total phytoplankton biomass near the water surface. Although total phytoplankton biomass temporal dynamics differed from station to station for the year 2019, phytoplankton composition showed similar temporal patterns. Marine diatoms dominated in the winter period and were succeeded in spring by marine flagellates. Dinoflagellates clearly dominated from June to the end of October. These species successions are similar to those simulated for previous years.

The proportion of *Phaeocystis* in total phytoplankton biomass in the model remained low at all stations throughout the year 2019.

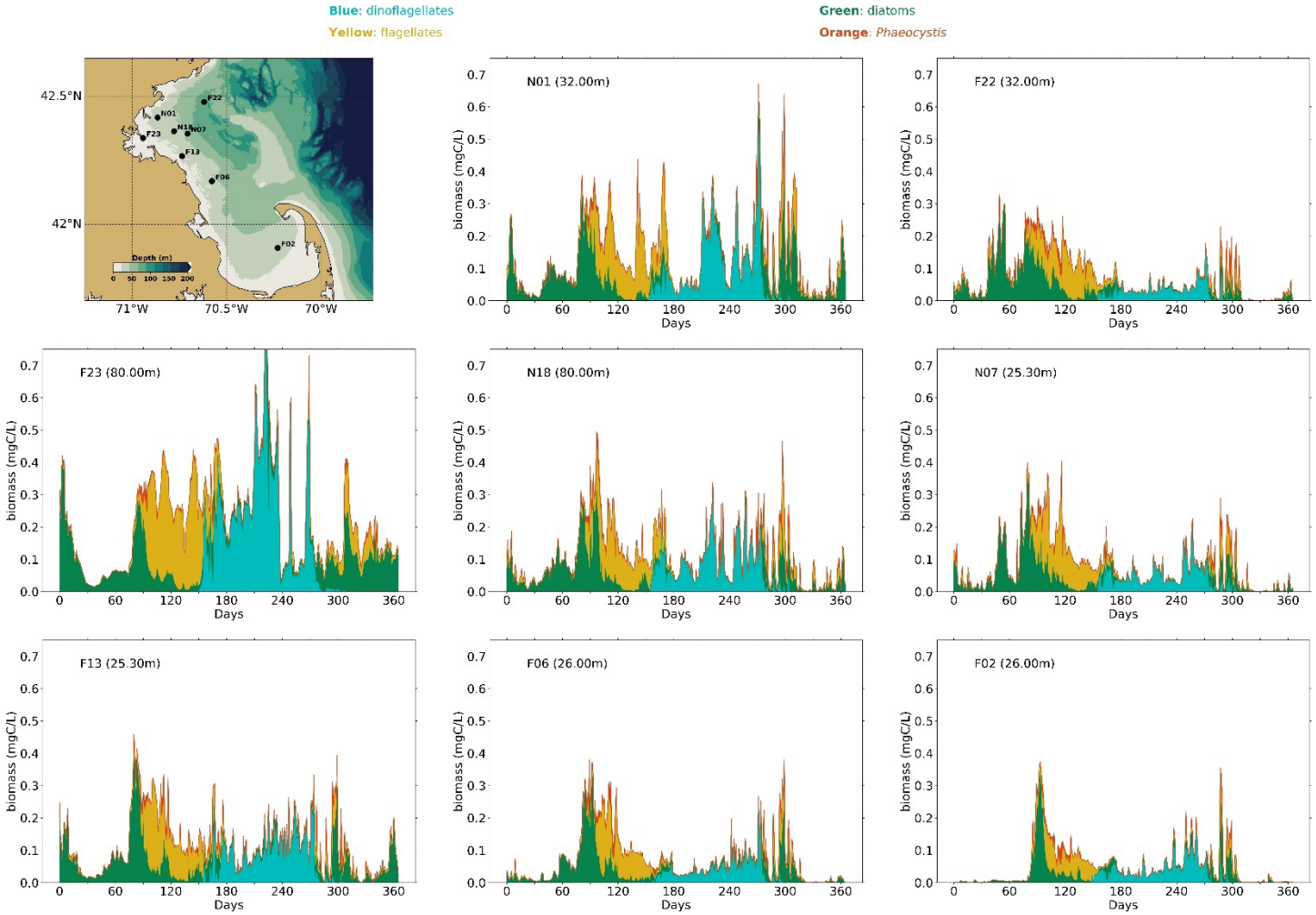


*Figure 5-20: Simulated phytoplankton biomass time-series. Biomasses of the 4 simulated species groups (dinoflagellates, other flagellates, diatoms and* Phaeocystis*) are stacked.*

## 5.4 Conditions on West-East transect through outfall

The signature of the outfall in terms of DIN concentrations was visible all year round, with increased concentrations up to a distance of about 10 km (Figure 5-21). The increased DIN was trapped in the lower layers of the water column in the period of stratification (April-September). During the other months, the effluent led to an increase in surface DIN concentrations as well. These temporal patterns were similar to those observed in previous years, even though the stratification in October was weaker than in previous years.

All year round, chlorophyll a concentrations were usually higher nearshore (Figure 5-22). This was most likely due to the nutrient inputs from rivers to the harbor area, promoting algal growth. Further offshore, highest chlorophyll a concentrations were simulated in spring and, during the summer months, maximum chlorophyll a concentrations occurred at a depth of ~15 m. As for DIN, these patterns were similar to those simulated for previous years. Any effect of the outfall on chlorophyll a concentrations was difficult to detect.

The vertical cross-sections of DO concentrations for 2019 showed similar temporal and spatial patterns as for previous years (Figure 5-23), with the highest concentrations occurring near the surface between February and May. Simulated surface concentrations were slightly higher than for previous years for the period May-August. The highest concentrations occurred slightly under the surface between April and August, which corresponded to the depths at which chlorophyll a was the highest. As for chlorophyll a, no effect of the outfall on DO concentrations was visible in the plotted cross sections.

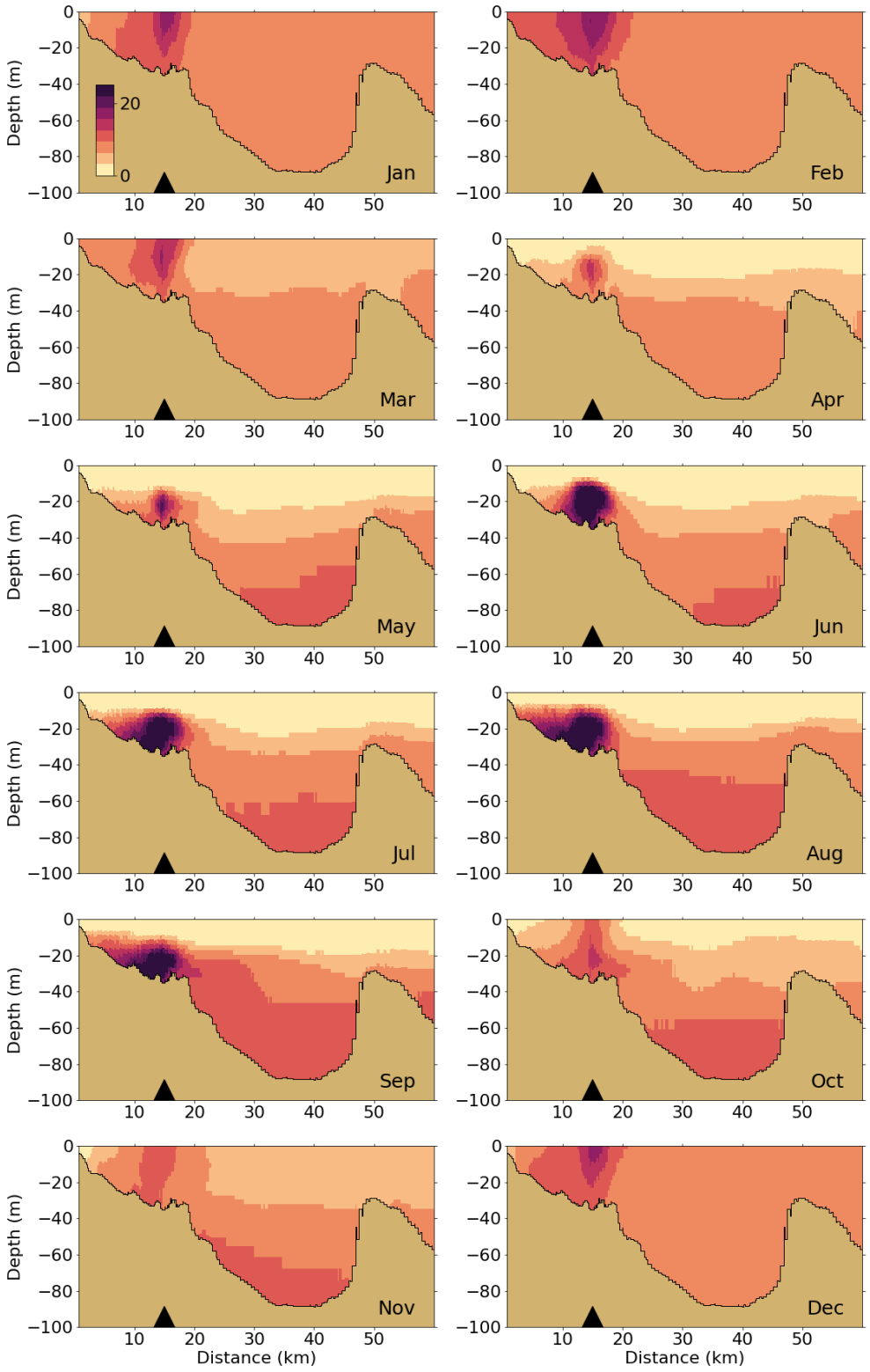


*Figure 5-21: Dissolved Inorganic Nitrogen (μM) for 2019 along west-east transect (Figure 2-4). Horizontal axis is distance eastward from coast; black triangle indicates the location of the outfall on the seafloor.*

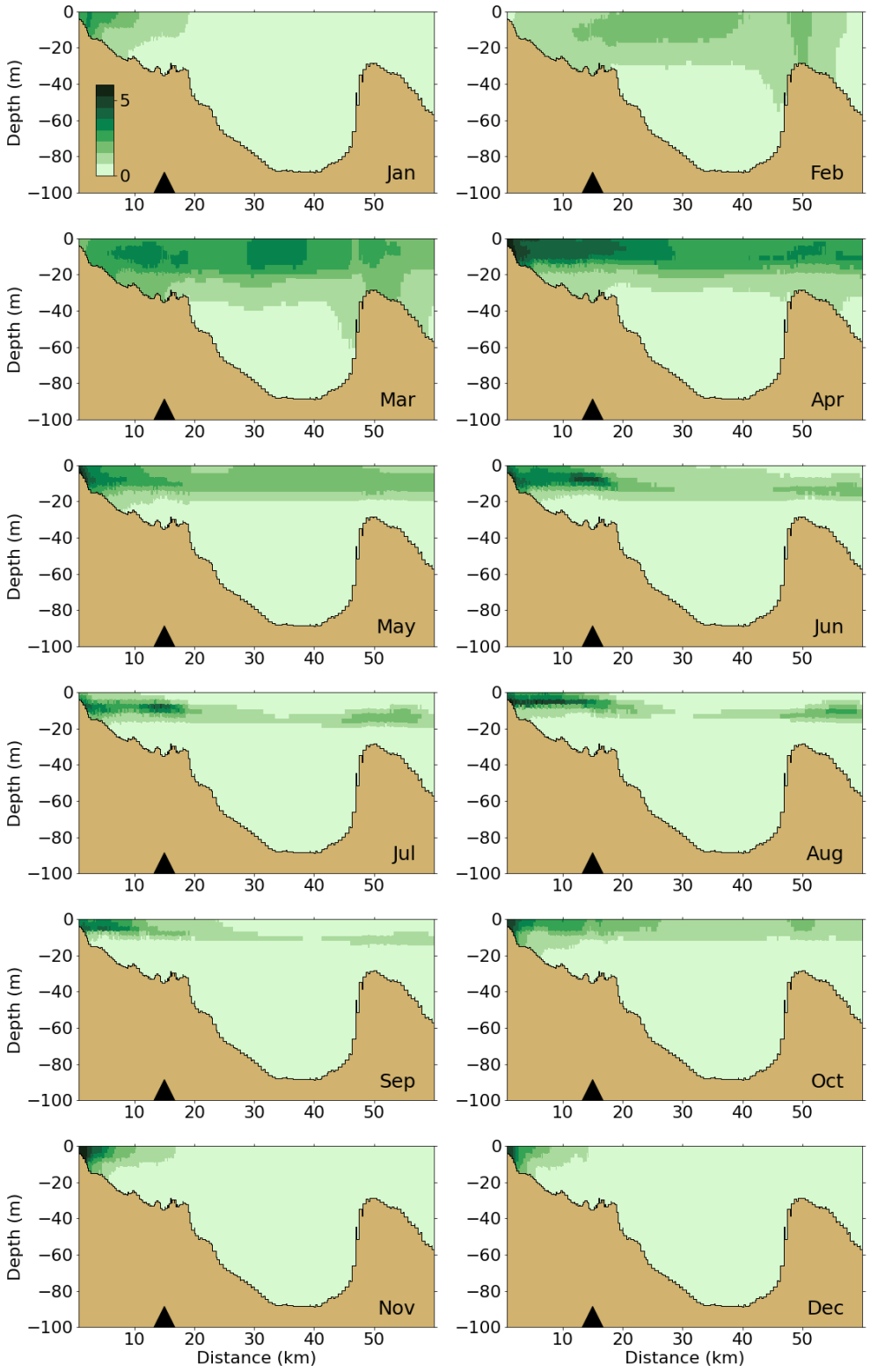


*Figure 5-22: Chlorophyll a (µg/L) for 2019 along west-east transect (Figure 2-4). Horizontal axis is distance eastward from coast; black triangle indicates the location of the outfall on the seafloor.*

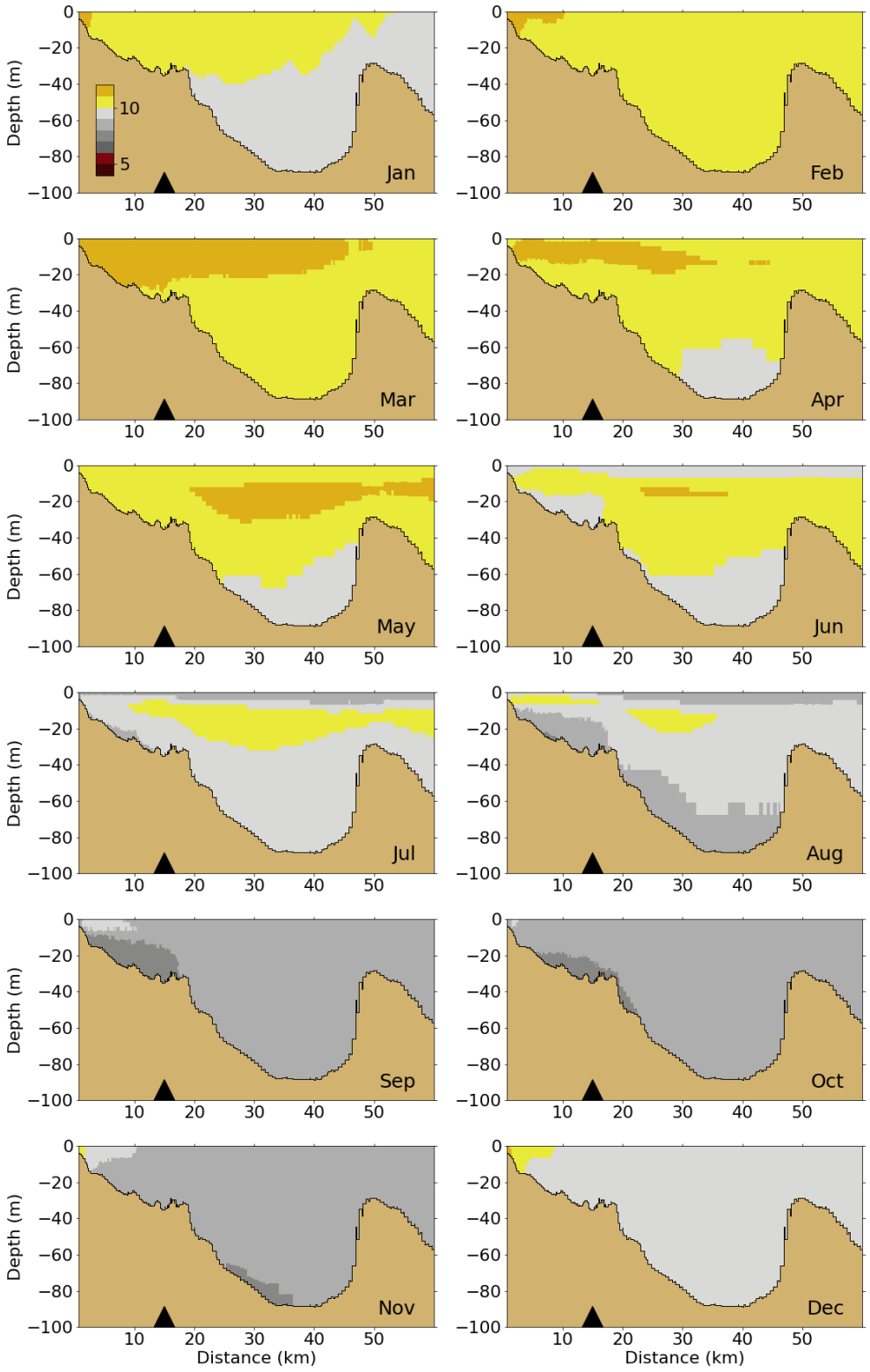


*Figure 5-23: Dissolved Oxygen for 2019 along west-east transect (Figure 2-4). Horizontal axis is distance eastward from coast; black triangle indicates the location of the outfall on the seafloor.*

# 6 Synthesis/Application

The synthesis/application topic in this report is a study of how the eutrophication-related aspects of the system would differ in a hypothetical scenario where all forms of nitrogen were fully removed from the effluent before it was discharged. The investigation is based on simulations of 2017 conditions (e.g., Deltares 2022a) because results from the 2019 simulation were not yet final when these analyses were begun.

**Methods.** The scenario run is identical to the baseline 2017 run except that concentrations of all nitrogen forms (ammonium, nitrate and nitrite, dissolved organic nitrogen and detrital particulate organic nitrogen) are set to zero in the effluent. Both the baseline and scenario runs included a two-year spin-up period. Zero effluent concentrations were implemented throughout the spin-up years of the scenario run, so its results are representative of a long-term reduction in effluent nitrogen as opposed to the changes that would occur during the first year after removal of nitrogen from effluent following prior years with effluent containing nitrogen. To understand potential changes, the differences between eutrophication-related system variables (dissolved inorganic nitrogen, chlorophyll, particulate organic carbon, and oxygen) in the scenario and baseline runs are calculated and examined. Maps of the monthly-mean differences are shown at the surface, the pycnocline depth from April through September when stratification is strongest, and the seafloor. The pycnocline depth is generally about 20 m, with minor spatial variations; it is used instead of the constant 20 m depth, which would not reveal the largest changes to phytoplankton-related variables that are concentrated at the pycnocline. Monthly-mean differences are also presented on vertical slices along two transects that pass through the outfall and selected MWRA monitoring stations: one transect with roughly west-east orientation and the other with roughly north-south orientation (Figure 6-1).

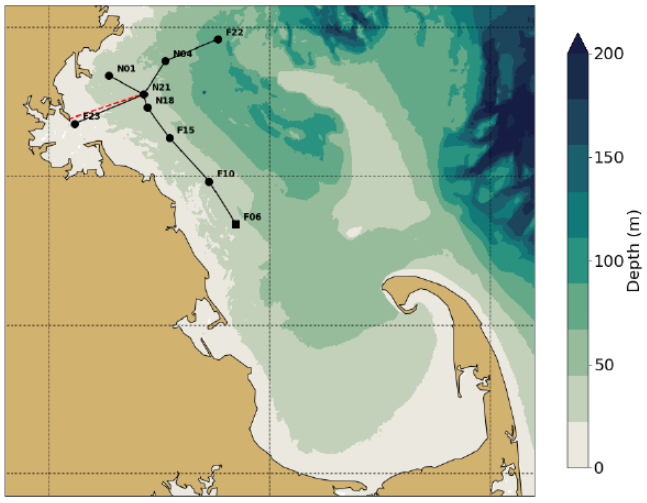


*Figure 6-1. Map showing two transects (black lines) along which vertical slices of results are shown in below figures. The west-east transect starts at F23 and ends at F22, passing through the outfall at N21. The north-south transect starts at N01 and ends at F06, also passing through the outfall. Red line is tunnel from Deer Island to the outfall.*

**Results.** We examine results for dissolved inorganic nitrogen (DIN) first because it is expected to show the largest changes; it consists of ammonium, nitrate, and nitrite, and ammonium is recognized as the best tracer of effluent (e.g. Werme et al 2021). In the baseline simulation, DIN concentrations range from highest values of about 25 uM within 10-20 km of the outfall to typical values of less than 10 uM farther away (see, for example, Figure 5-6 above, which presents model output with observations superposed).

As expected, the DIN differences between the scenario run results and the baseline run are negative (Figure 6-2, Figure 6-3). They reach maximum magnitudes of about 25 uM during the summer at the pycnocline depth and deeper, within a few km of the outfall. Generally, at several km from the outfall they have magnitude about 10-15 uM, magnitudes of up to 10 uM extend about 10-20 km from the outfall, and changes are smaller farther away. During December and January, decreases reaching

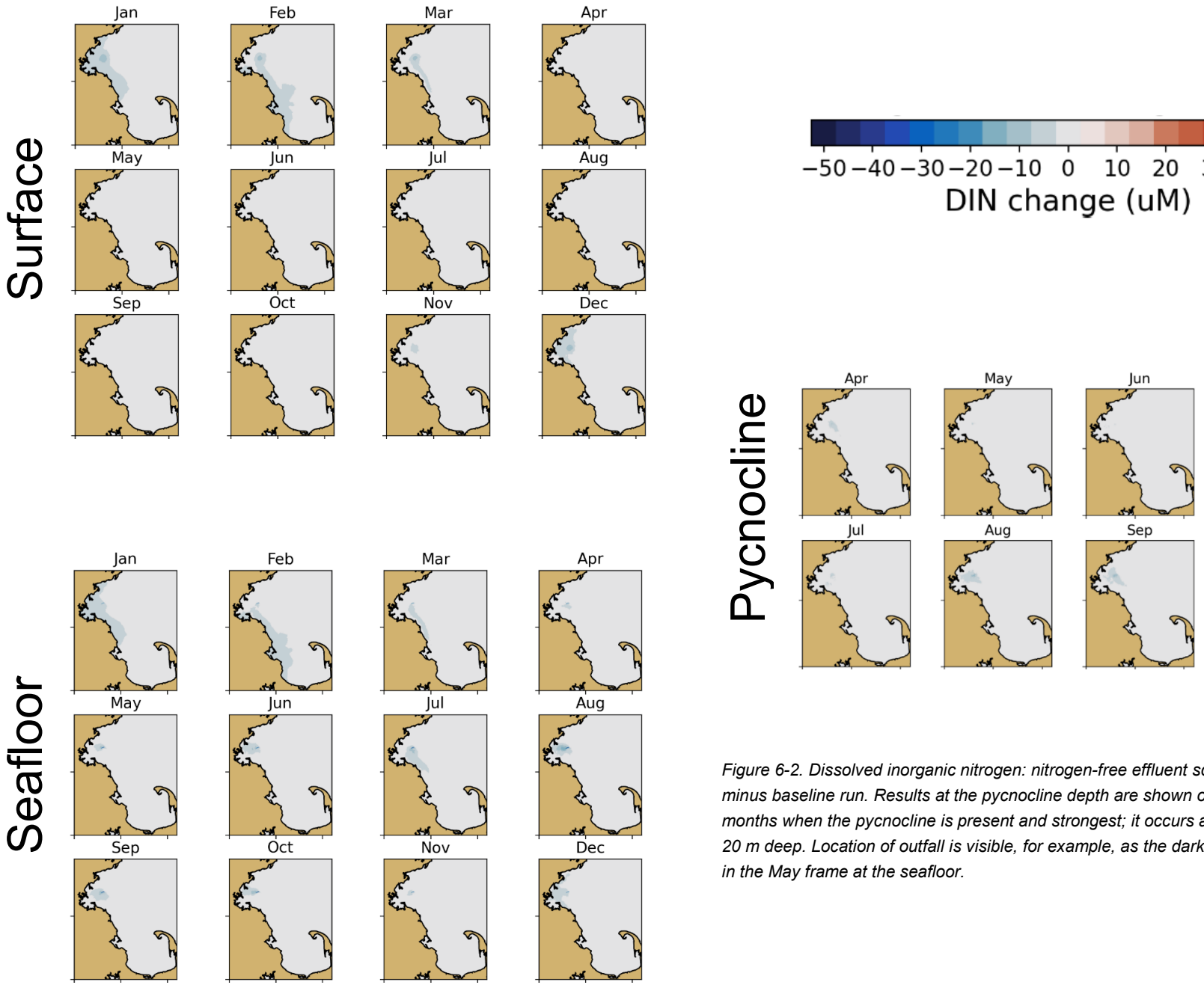


*Figure 6-2. Dissolved inorganic nitrogen: nitrogen-free effluent scenario minus baseline run. Results at the pycnocline depth are shown only for months when the pycnocline is present and strongest; it occurs at about 20 m deep. Location of outfall is visible, for example, as the darkest spot in the May frame at the seafloor.*

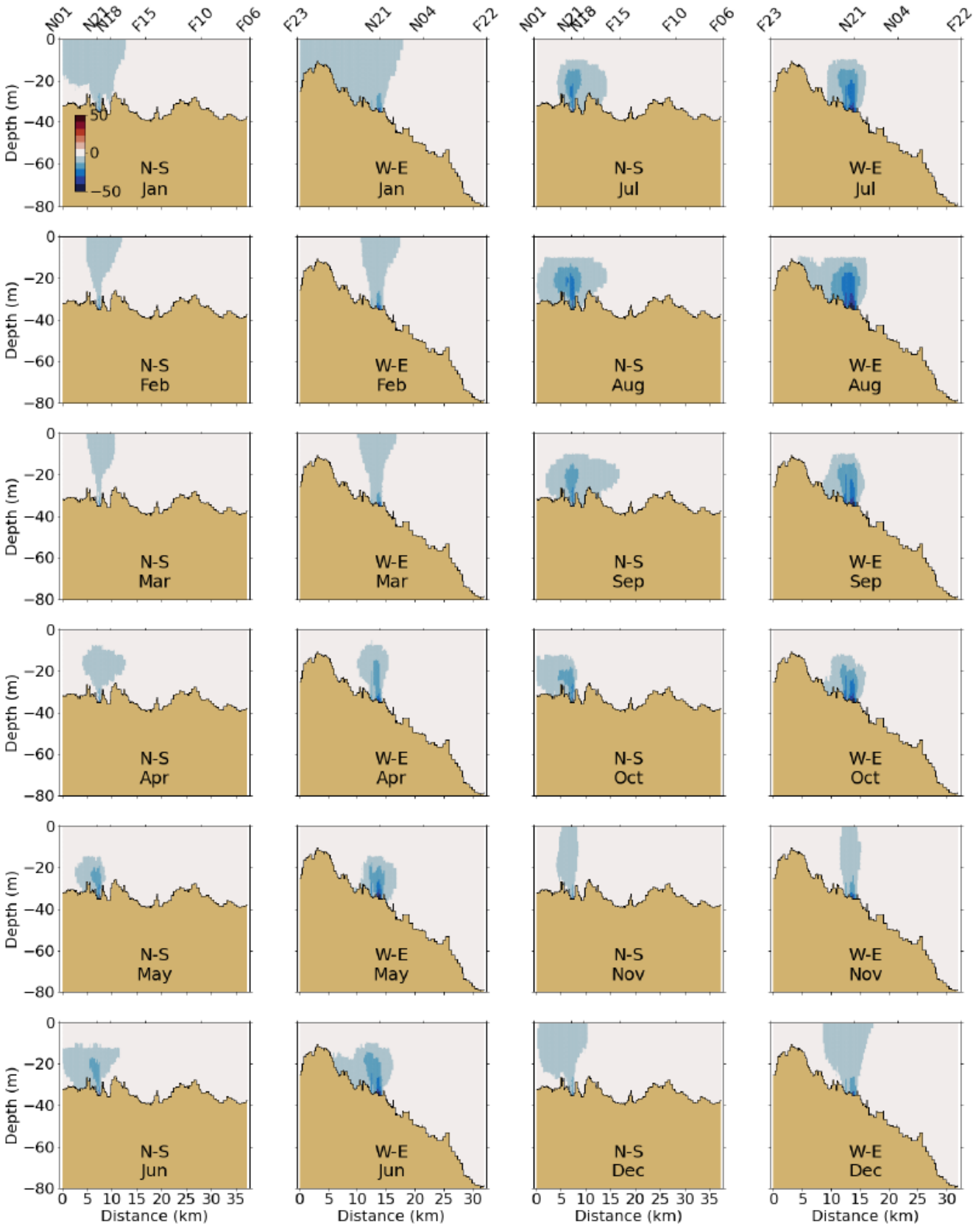


*Figure 6-3. Dissolved inorganic nitrogen: nitrogen-free effluent scenario minus baseline run. Vertical slices on transects in Fig. 6-1. Scale bar top left panel.*

magnitudes of up to 5-10 uM occur throughout Boston Harbor, and from January through April similar decreases also extend southward along the south shore and reach the northwestern corner of Cape Cod Bay. This pattern is consistent with modeled effluent dilution results (Deltares 2022b). These changes are as expected because they correspond closely with areas known to have DIN elevated over ambient levels due to effluent.

Changes to total nitrogen, which consists of DIN plus dissolved and particulate organic nitrogen, are essentially the same (not shown) as in Figures 6-2 and 6-3. This is because contributions of effluent to ambient levels of organics are smaller than its contributions to DIN. The fractional decrease to total nitrogen in the scenario run is smaller than the fractional decrease to DIN because baseline levels of total nitrogen are higher, by definition, than those of DIN.

Next, we examine changes to chlorophyll, an indicator for phytoplankton biomass. Typical base case chlorophyll concentrations (see Figure 5-9 above, which shows model output with observations superposed) reach 5-6 ug/L, vary most strongly in the vertical with higher values near the surface, and are very weakly altered within and near the effluent plume. Maps of changes to chlorophyll in the scenario run (Figure 6-4) show they generally are weak except during the stratified period when growth rates are higher. They have the largest magnitudes (reaching about 2 ug/L in small areas, and typically remaining less than about 1 ug/L) at the surface, where they are negative (that is, removing effluent nitrogen reduces chlorophyll), and at the pycnocline depth where there are some negative and some positive values. At the seafloor, the changes are small except in Boston Harbor during the summer months. The spatial extent of the decreases extends across the largest area, along the South Shore and into Cape Cod Bay, during April and October. Vertical slices (Figure 6-5) make clear a general pattern with a layer of decreases throughout most of the upper water column and a thinner layer just below, at about the pycnocline depth, with increases. The latter is most likely caused by a reduction in self-shading, due to more light reaching those depths because of the reduction in surface phytoplankton biomass at the shallower depths above.

Another indicator of phytoplankton biomass is particulate organic carbon (POC). Patterns in changes to POC in the scenario run (Figure 6-6 is an example) have many similarities to those in chlorophyll. Changes in POC occur mainly due to reduced phytoplankton biomass in the surface layers, but also due to the reduction in detrital POC near the surface and in deeper layers of the water column because there is less dead settling phytoplankton organic matter.

Finally, because reduced dissolved oxygen (DO) concentration is a potential end result for water quality degradation due to eutrophication, we examine changes to DO in the scenario run (Figure 6-7 and Figure 6-8). During the phytoplankton growing season, the change consists of reduced DO near the surface (most negative mean monthly change of ~1 mg/L in August) and slightly increased DO (~0.2 mg/L) in deeper layers. This is due to lower primary production near the surface, as noted above, and lower re-mineralization of organic matter in deeper layers because there is less settling organic matter from dead phytoplankton. A similar pattern is visible near the outfall, in and near Boston Harbor, along the South Shore and in Cape Cod Bay. In Cape Cod Bay, the change in DO at the surface is much smaller than near the outfall, while the change in DO near the seafloor is comparable. Mean monthly increases of DO reach 0.2-0.3 mg/L in August in the western part of Cape Cod Bay, most likely due to a lower accumulation and re-mineralization of detrital organic matter there.

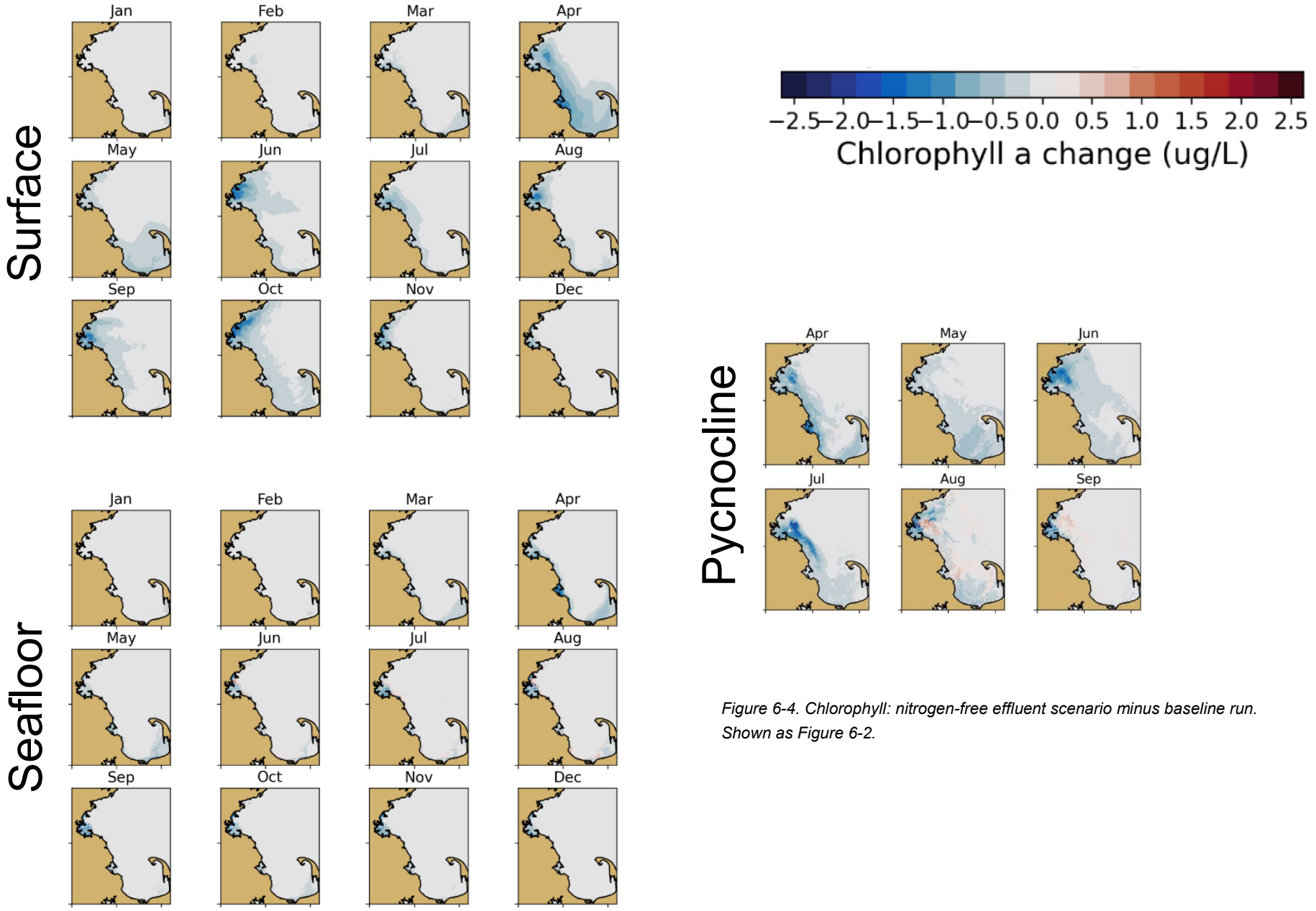


*Figure 6-4. Chlorophyll: nitrogen-free effluent scenario minus baseline run. Shown as Figure 6-2.*

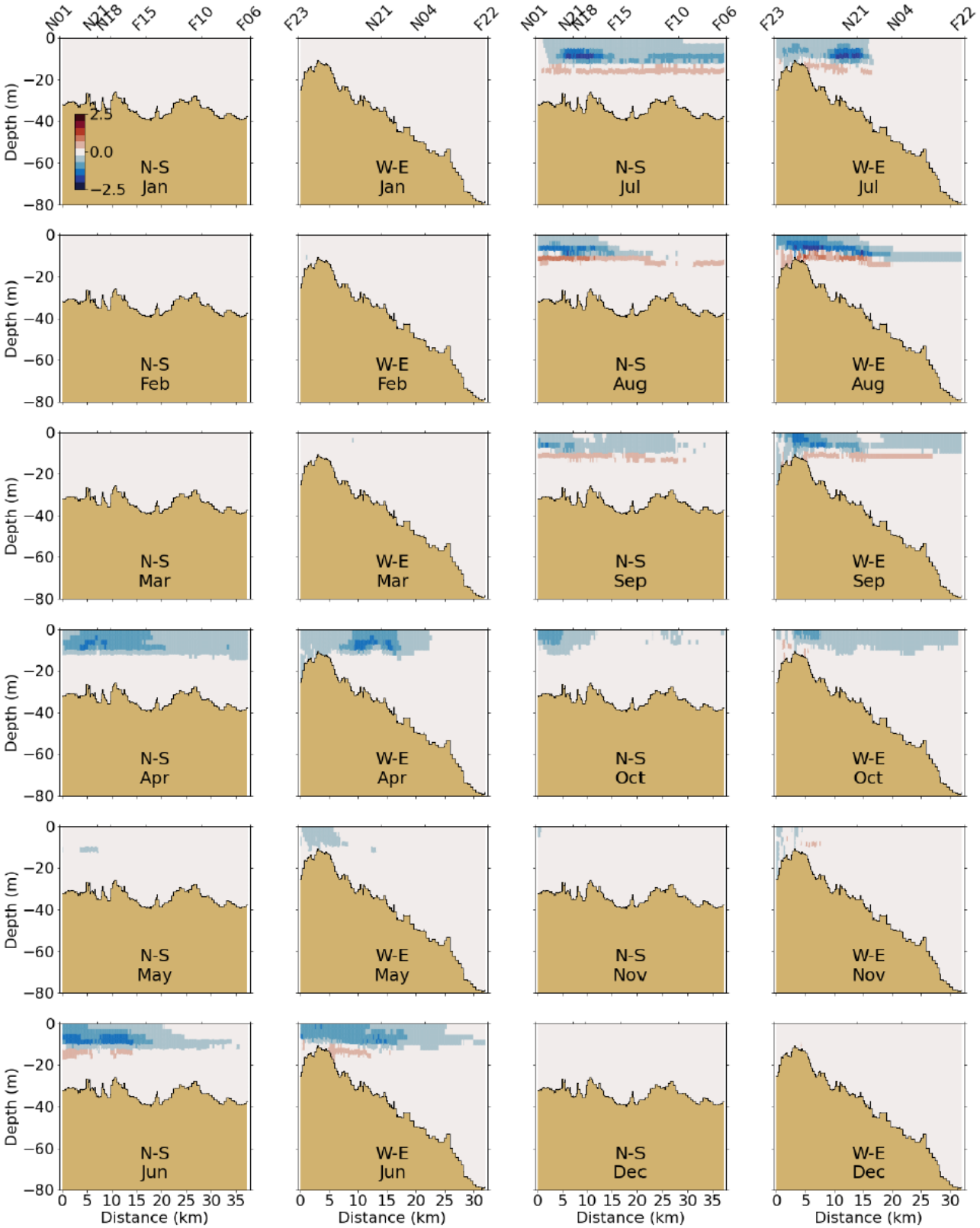


*Figure 6-5. Chlorophyll: nitrogen-free effluent scenario minus baseline run. Shown as Figure 6-3*

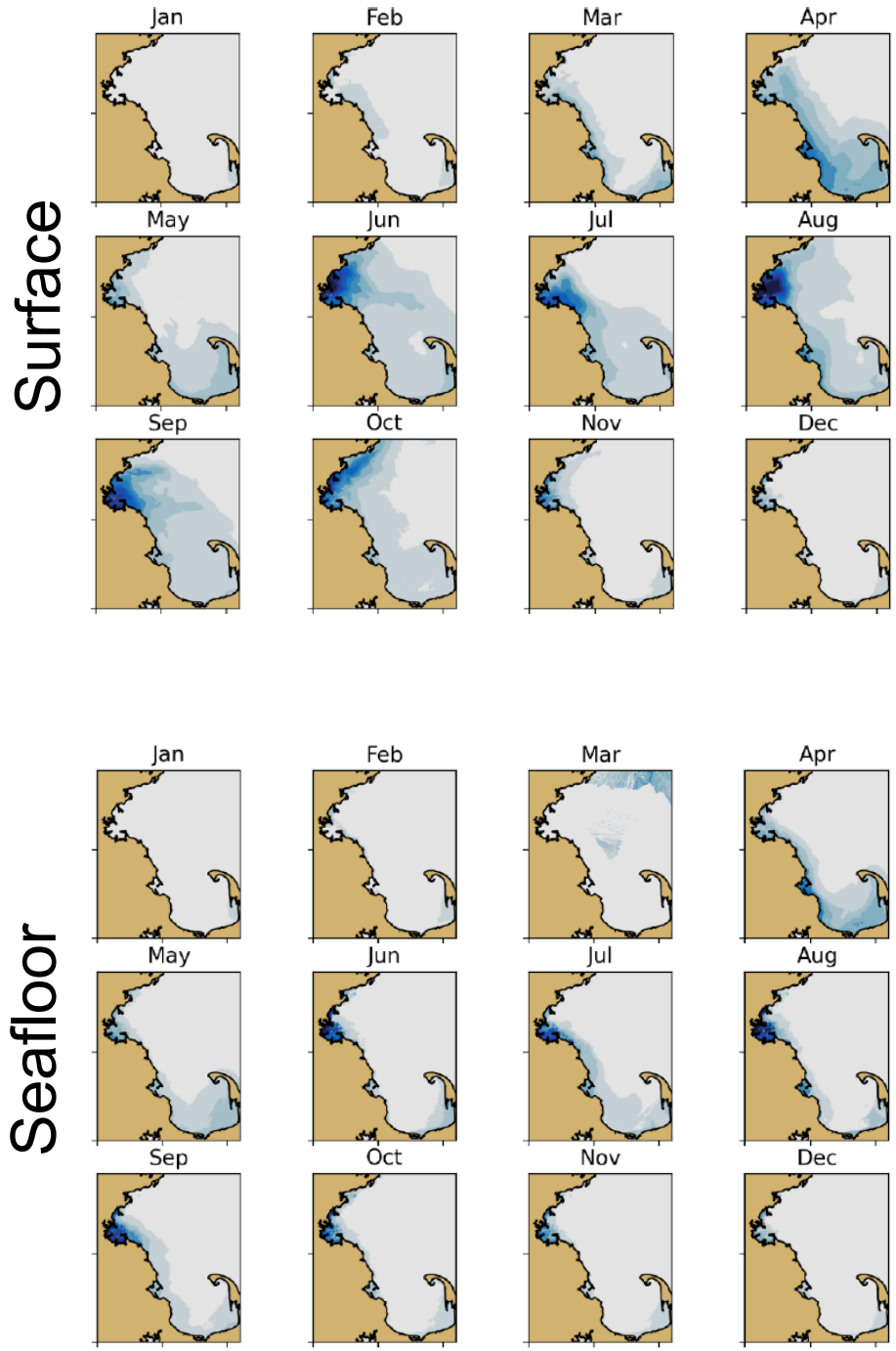


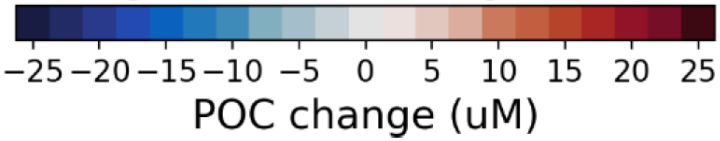


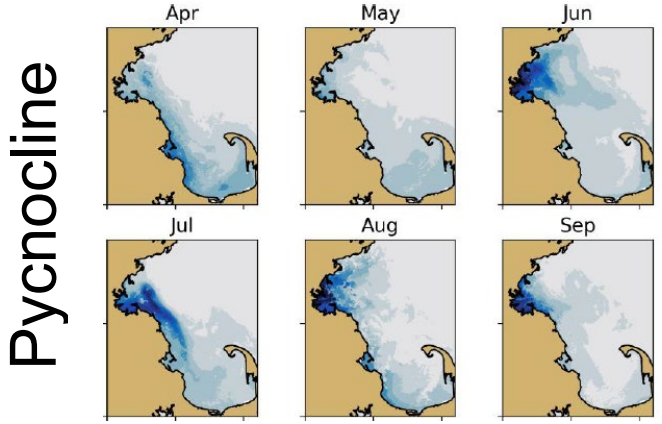


*Figure 6-6. Particulate organic carbon: nitrogen-free effluent scenario minus baseline run. Shown as Figure 6-2.*

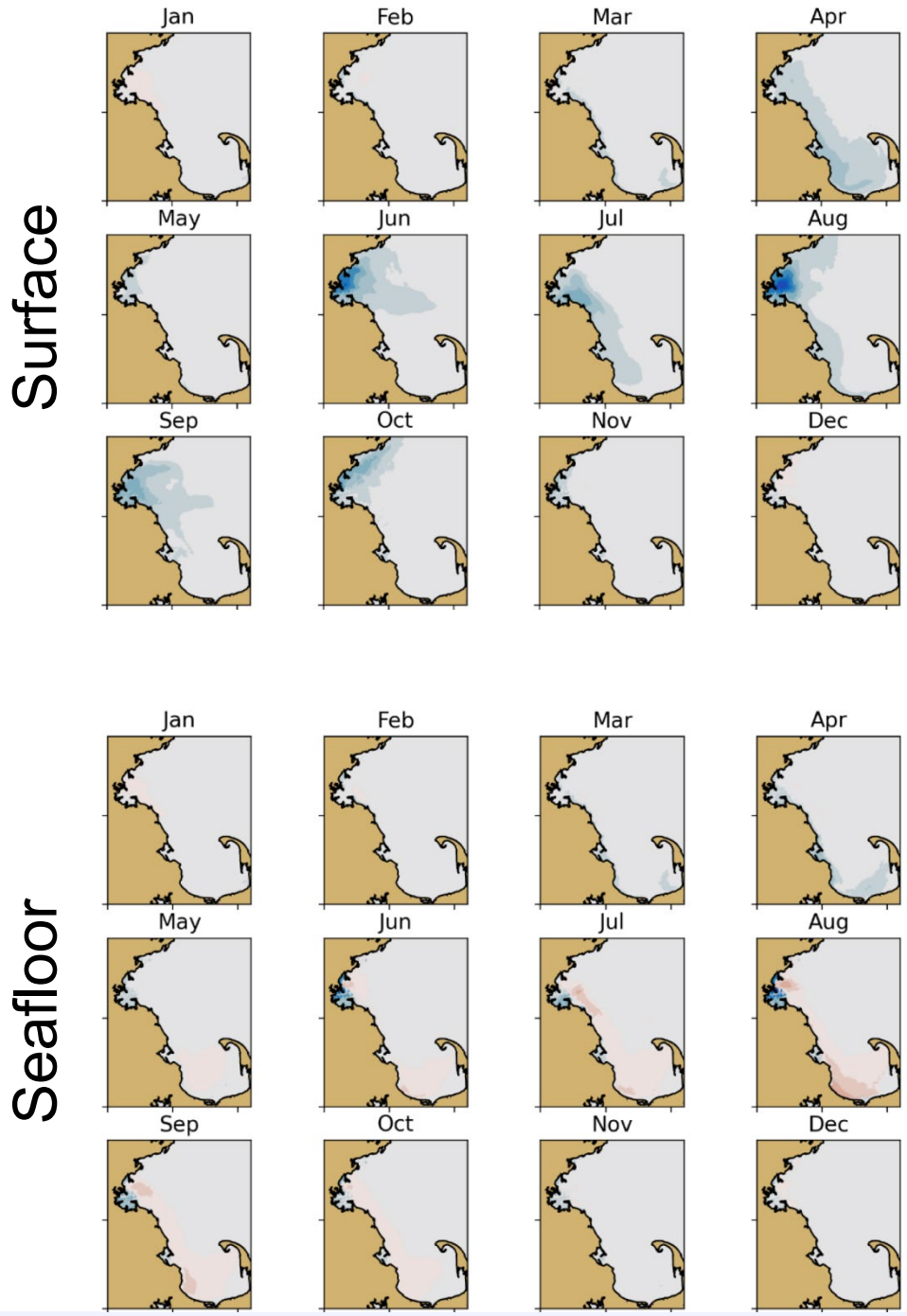


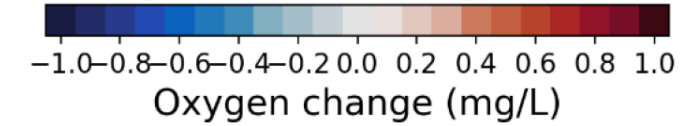


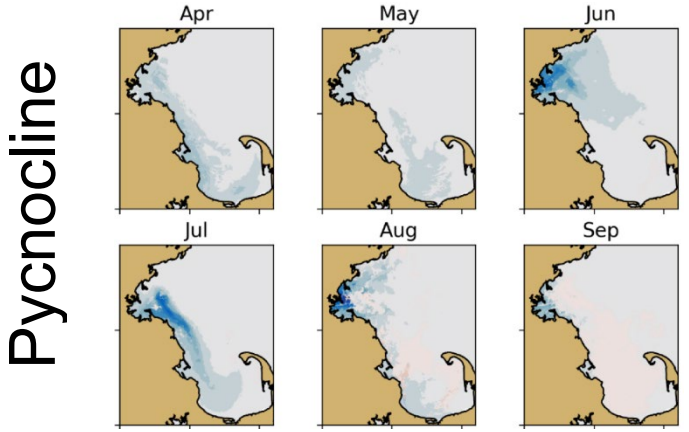


*Figure 6-7. Dissolved oxygen concentration: nitrogen-free effluent scenario minus baseline run. Shown as Figure 6-2.*

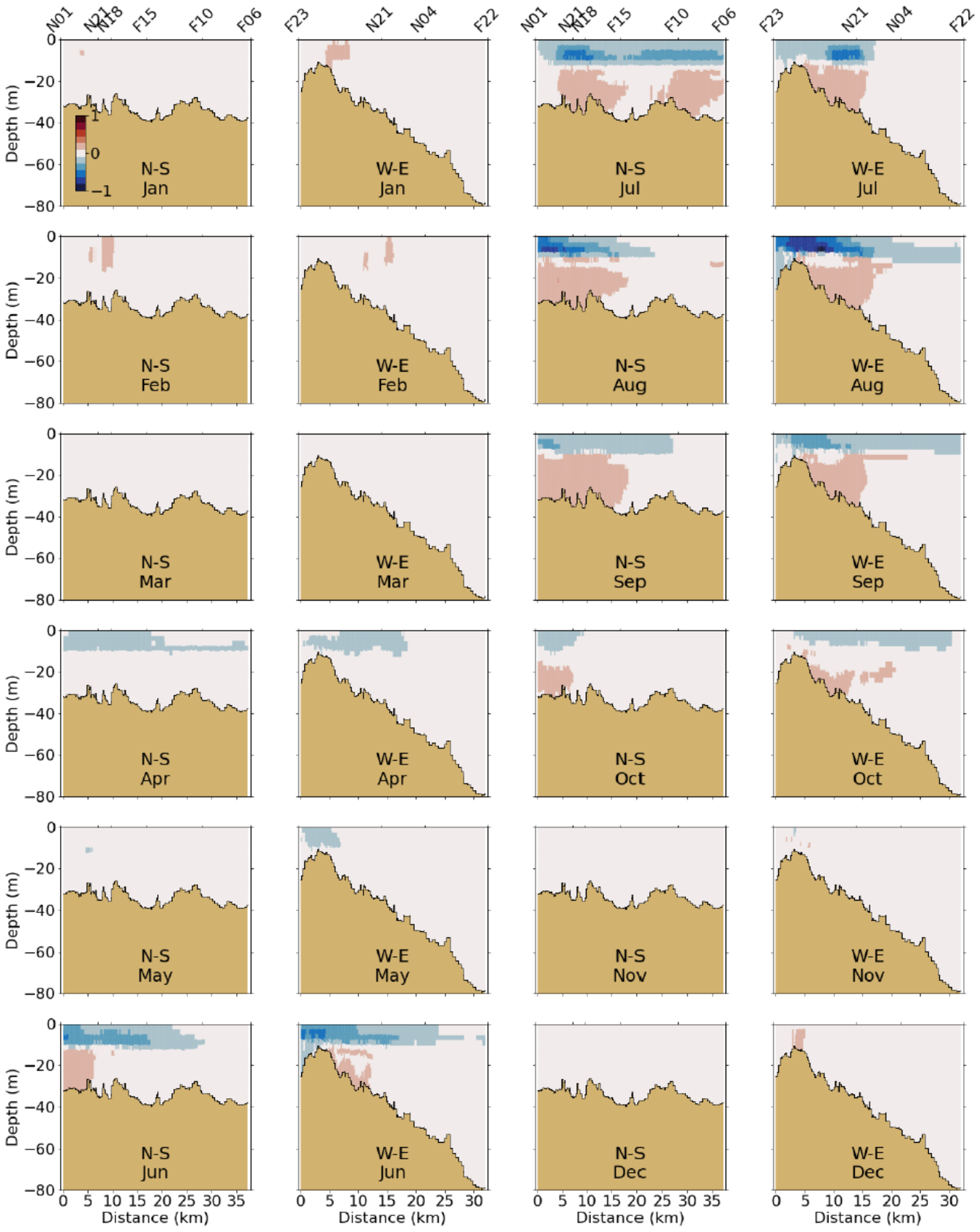


*Figure 6-8. Dissolved oxygen concentration: nitrogen-free effluent scenario minus baseline run. Shown as Figure 6-3.*

**Conclusions.** The scenario run illustrates the main effects of removing all nitrogen forms from effluent for a period of multiple years. As expected, there is a substantial reduction of DIN over seasonally varying geographic areas and depth ranges corresponding to where ammonium in effluent is known to cause higher DIN. Phytoplankton biomass (as indicated by chlorophyll and POC) is changed minimally except during the stratified growing season from about April to September, when it increases modestly near the surface and decreases in a thin deeper layer near the pycnocline due to reduced self-shading there. Similarly DO is influenced mainly during the stratified season, when there is a weak reduction near the surface due to lower generation by phytoplankton and a weaker increase at depth due to the reduction in accumulation and re-mineralization of detrital organic matter. These findings indicate that nutrients in effluent have minor influence on overall ecosystem function of the bays and are not causing eutrophication, in support of conclusions from previous observations and modeling.

# 7 Conclusion

The meteorological and hydrological forcing conditions in the year 2019 were very similar to the long-term mean over the previous 20 years. In February 2019, wind speeds fell below the long-term mean, which caused a weaker than typical upwelling, so that surface waters were warmer than typical due to the weaker cooling effect of upwelling. Furthermore, a higher than typical spring river flow caused an unusually strong spring freshet which led to much fresher surface water than in a typical year. Stratification was stronger than typical from May into September, initially due to the fresher water, then later in summer due to unusually warm surface temperatures.

The performance of the hydrodynamic model was comparable to previous years. Temperatures were reproduced accurately. Model salinity performed better than in previous years. At most stations, temperature and salinity stratification was present from mid-April until mid-October. Maximum temperature stratification occurred in July and maximum salinity stratification occurred in May, due to a large discharge from Merrimack River. Due to the storm event in mid-October, sudden mixing occurred at the shallower stations. For most stations this marked the end of the summer stratification. Sudden peaks in modeled bottom temperature (and a minor drop in surface temperature) were visible during the second half of September. Due to the very limited number of field measurements during this period, these events were not captured by the measurements.

Modeled, non-tidal current patterns were similar to observations, but the magnitudes in the top of the water column, and the temporal variability, were slightly smaller. Looking at a larger scale, the expected circulation pattern driven by the Western Maine Coastal Current was visible in the model. In general, the agreement between the hydrodynamic model and the observations was sufficient to conclude that the representation of processes was adequate to support water quality modeling.

Water quality conditions in 2019 where not exceptional compared to previous years, with respect to nutrient and oxygen concentrations and seasonal patterns. Overall, the water quality model accurately represented temporal dynamics and vertical gradients DIN, POC, DO and light conditions. Skill metrics were mostly comparable to previous years.

Extinction spatio-temporal patterns for the year 2019 were similar to previous years. The model reproduced the extinction range and variability well at most stations. Measurements were however slightly higher than for previous years, and the model appeared to slightly underestimate the highest values. The model predicted lower extinction in winter than during the rest of the year, in association with lower particulate organic carbon levels.

Seasonal variations of surface and bottom DIN concentrations in 2019 were overall similar to those observed and simulated for previous years. Surface and bottom were comparable in winter, when the water column was well mixed. Surface DIN concentrations declined in March and April and were depleted throughout the rest of spring and summer, before increasing again in fall. Bottom concentrations declined to a much lesser degree in spring and summer. The model generally reproduced these observed seasonal variations and vertical differences, because the onset of stratification was well reproduced. At some stations, bottom concentrations were however overestimated during summer (July-September), which could be related to the fact that the model underestimated a phytoplankton bloom in that period. Observed variations at intermediate depths in the water column were also generally reproduced by the model.

Seasonal variations of chlorophyll a observations in 2019 showed higher values mostly in spring and fall. Highest concentrations were observed in fall at all stations in the model-observation comparison figures. While for previous years, the largest chlorophyll a concentrations for the second half of the year usually occurred at the end of October or beginning of November, highest chlorophyll a values in 2019 were reported at the start of September. This peak was not captured by the model, which underestimated the summer dinoflagellate bloom and simulated higher chlorophyll a concentrations during the fall diatom bloom. As in the simulations for previous years, near-surface simulated concentrations were in the same range as observations (except this time for September), while the temporal variability was not always reproduced. This was to some extent related to the relatively low sampling frequency and the high temporal variability. As in the simulations for previous years, simulated chlorophyll a was underestimated at many stations near the seafloor and at intermediate depths. Simulated chlorophyll a concentrations decreased eastward from the coast between May and September. Early spring increases occurred throughout the water column as it was relatively well mixed. During the more stratified months, simulated bottom chlorophyll a remained low and highest values occurred in the subsurface. The observations tended to show that chlorophyll a concentrations were highest in April and September. In these periods, high concentrations were observed up to about 30 m deep or deeper.

Particulate organic carbon (POC) concentrations at the observation stations were extremely variable and it was difficult to identify a clear seasonal pattern. Concentrations were however slightly lower in winter than the rest of the year. POC concentrations were highest closer to the harbor, likely due to POC inputs from rivers. Concentrations were significantly lower near the bottom than at the surface. The model generally captured these POC concentration ranges, variability and vertical gradients. POC concentrations were however generally overestimated near the harbor. Peaks in POC concentrations during the September phytoplankton bloom were not captured by the model. As for chlorophyll, simulated POC concentrations increased from the coast eastward.

The 2019 seasonal patterns in measured DO concentrations were similar to previous years, with maximum concentrations observed at the end of winter or early spring and decreasing until fall before rising again. While winter concentrations at the surface and the bottom were comparable, bottom concentrations dropped lower in fall. The model overall reproduced these seasonal patterns well. As for previous years, the model reproduced minimum observed values at some stations, but not all. In May-June, differences between observed surface and seabed DO concentrations were larger than for previous years. The model did not capture this. In that period, the model slightly underestimated surface DO concentrations, while overestimating those at the bottom, simulating higher concentrations near the seabed than at the surface. The model-observation comparison at intermediate water depths showed similar behavior. For 2019, the model usually underestimated vertical gradients at intermediate depths. The North-South and West-East cross-section plots show that DO generally had weak vertical gradients. Concentrations were higher at the end of winter and beginning of spring, and decreased until fall. Higher concentrations were observed and simulated in the subsurface in periods with higher primary production (e.g. June). In periods with visible vertical gradients in DO concentrations, the model captured the depth of highest DO concentrations well; amplitudes of DO concentrations in the growing season didn’t always coincide, due to mismatches between the timing of observed and simulated blooms.

Simulated primary production was generally in the range of historical measurements for the entire year 2019. It was also quite typical in comparison to the years 2012 to 2016, with no exceptional peaks nor prolonged periods of exceptionally low production.

Simulated sediment fluxes were low in winter and peaked in the summer due to higher temperatures, favorable to biogeochemical activity (mineralization of organic matter in the sediment). Sediment fluxes were higher in the harbor area than in Massachusetts Bay, which was captured by the model. Results for the year 2019 were similar to those from the previous years. These were mostly in the range of historical measurements.

Although total phytoplankton biomass temporal dynamics differed from station to station for the year 2019, phytoplankton composition showed similar temporal patterns. Marine diatoms dominated in the winter period and were succeeded in spring by marine flagellates. Dinoflagellates clearly dominated from June to the end of October. These species successions are similar to those simulated for previous years. The proportion of *Phaeocystis* in total phytoplankton biomass in the model remained low at all stations throughout the year 2019.

According to the model results, the MWRA outfall did not have visible effects on ecosystem functioning at the Massachusetts Bay scale. The signature of the outfall in terms of DIN concentrations was visible all year round, with increased concentrations up to a distance of about 10 km. The increased DIN concentrations were trapped in the lower layers of the water column during the period of stratification (April-September). During the other months, the effluent led to an increase in surface DIN concentrations as well. These temporal patterns were similar to those observed in previous years. All year round, chlorophyll a concentrations were higher nearshore. This was most likely due to the nutrient inputs from rivers to the harbor area, promoting algal growth. Any effect of the outfall on chlorophyll a concentrations could not be detected. As for chlorophyll a, no effect of the outfall on DO concentrations was apparent.

# References


Alessi, Carol A., Beardsley, Robert C., Limeburner, Richard, Rosenfeld, Leslie K., Lentz, Steven J., Send, Uwe, Winant, Clinton D., Allen, John S., Halliwell, George R., Brown, Wendell S., Irish, James D.,1985. "CODE-2: moored array and large-scale data report", Woods Hole Oceanographic Institution Technical Report 85-35, DOI:10.1575/1912/1641. (https://hdl.handle.net/1912/1641)

Blauw AN, HFJ Los, M Bokhorst and PLA Erftemeijer, 2009. GEM: a Generic Ecological Model for estuaries and coastal waters. Hydrobiologia 618: 175-198.

Deltares, 2019a. D-Flow Flexible Mesh, Technical Reference Manual. Released for: Delft3D FM Suite 2020. Version: 1.1.0 SVN Revision: 63652. December 4, 2019.

Deltares. 2019b. Delft3D Flexible Mesh Suite, D-Flow FM in Delta Shell, User Manual, Version 1.5.0, December 5, 2019 (https://content.oss.deltares.nl/delft3d/manuals/DFlow_FM_User_Manual.pdf)

Deltares, 2021. Demonstration of the updated Bays Eutrophication Model. Boston: Massachusetts Water Resources Authority. Report 2021-02. 138 p. plus appendices. (www.mwra.com/harbor/enquad/pdf/2021-02.pdf)

Deltares, 2022a. Simulations of 2017 Hydrodynamics and Water Quality in the Massachusetts Bay System using the Bays Eutrophication Model. Boston: Massachusetts Water Resources Authority. Report 2021-12. 107 p. https://www.mwra.com/harbor/enquad/pdf/2021-12.pdf

Deltares, 2022b. Simulations of 2018 Hydrodynamics and Water Quality in the Massachusetts Bay System using the Bays Eutrophication Model. Boston: Massachusetts Water Resources Authority. Report 2022-06. 89 p. https://www.mwra.com/harbor/enquad/pdf/2022-06.pdf

Hunt CD, RK Kropp, JJ Fitzpatrick, P Yodzis, and RE Ulanowicz, 1999. A Review of Issues Related to the Development of a Food Web Model for Important Prey of Endangered Species in Massachusetts and Cape Cod Bays. Boston: Massachusetts Water Resources Authority. Report ENQUAD 99-14. 62 p. (http://www.mwra.state.ma.us/harbor/enquad/pdf/1999-14.pdf)

Keay KE, WS Leo, and PS Libby, 2012. Comparisons of Model-Predicted and Measured Productivity in Massachusetts Bay. Boston: Massachusetts Water Resources Authority. Report 2012-03. 11 p. plus Appendix. (http://www.mwra.state.ma.us/harbor/enquad/pdf/2012-03.pdf)

Libby PS, Borkman DG, Geyer WR, Turner JT, Costa AS, Taylor DI, Wang J, Codiga D. 2020. 2019 Water Column Monitoring Results. Boston: Massachusetts Water Resources Authority. Report 2020-08. 60p. https://www.mwra.com/harbor/enquad/pdf/2020-08.pdf

Scully, M.E., Geyer, W.R., Borkman, D, Pugh, T.L., Costa, A. Nichols, O.C., 2022. Unprecedented Summer Hypoxia in Southern Cape Cod Bay: An Ecological Response to Regional Climate Change? Biogeosciences Discuss., https://doi.org/10.5194/bg-2022-48, 2022

Los, FJ, 2009. Eco-hydrodynamic modeling of primary production in coastal waters and lakes using BLOOM. Ph.D. Thesis, Wageningen University, 2009.

Scully, M. E., Geyer, W. R., Borkman, D., Pugh, T. L., Costa, A., and Nichols, O. C., 2022, Unprecedented Summer Hypoxia in Southern Cape Cod Bay: An Ecological Response to Regional Climate Change?, Biogeosciences Discuss. [preprint, in review], https://doi.org/10.5194/bg-2022-48.

Tucker J, S Kelsey, and AE Giblin, 2010, 2009 benthic nutrient flux annual report. Boston: Massachusetts Water Resources Authority. Report 2010-10. 27 p. (http://www.mwra.state.ma.us/harbor/enquad/pdf/2010-10.pdf)

Werme C, Codiga DL, Libby PS, Carroll, SR, Charlestra L, Keay KE. 2021. 2020 outfall monitoring overview. Boston: Massachusetts Water Resources Authority. Report 2021-10. 55 p. https://www.mwra.com/harbor/enquad/pdf/2021-10.pdf

Xue, P, C Chen, J Qi, RC Beardsley, R Tian, L Zhao, and H Lin, 2014. Mechanism studies of seasonal variability of dissolved oxygen in Mass Bay: A multi-scale FVCOM/UG-RCA application. Journal of Marine Systems. 131, 102-119.

Zhao L, Beardsley RC, Chen C, Codiga DL, Wang L, 2017. Simulations of 2016 Hydrodynamics and Water Quality in the Massachusetts Bay System using the Bays Eutrophication Model. Boston: Massachusetts Water Resources Authority. Report 2017-13. 111p. (https://www.mwra.com/harbor/enquad/pdf/2017-13.pdf)

**Massachusetts Water Resources Authority**
**100 First Avenue • Boston, MA 02129**
**www.mwra.com**
**617-242-6000**